REMOTE SENSING OF SPRUCE BUDWORM DEFOLIATION IN QUEBEC, CANADA USING EO-1 HYPERION DATA

ZHONGWEI HUANG

September 2015

TECHNICAL REPORT
NO. 299

REMOTE SENSING OF SPRUCE BUDWORM DEFOLIATION IN QUEBEC, CANADA USING EO-1 HYPERION DATA

Zhongwei Huang

Department of Geodesy and Geomatics Engineering
University of New Brunswick
P.O. Box 4400
Fredericton, N.B.
Canada
E3B 5A3

September, 2015

PREFACE

This technical report is a reproduction of a thesis submitted in partial fulfillment of the requirements for the degree of Master of Science in Engineering in the Department of Geodesy and Geomatics Engineering, September 2015. The research was supervised by Dr. Yun Zhang, and funding was provided by the Canada Research Chairs Program.

As with any copyrighted material, permission to reprint or quote extensively from this report must be received from the author. The citation to this work should appear as follows:

Huang, Zhongwei (2015). *Remote Sensing of Spruce Budworm Defoliation in Quebec, Canada Using EO-1 Hyperion Data.* M.Sc.E. thesis, Department of Geodesy and Geomatics Engineering Technical Report No. 299, University of New Brunswick, Fredericton, New Brunswick, Canada, 137 pp.

ABSTRACT

Satellite remote sensing has special advantages for monitoring the extent of defoliation caused by insects. Remote sensing has been used to monitor spruce budworm defoliation, mostly using the data captured by multispectral sensors such as Landsat (MSS, TM, and ETM+), MODIS and SPOT. However, these images have a low spectral resolution (using 4 to 36 spectral bands each covers a broad spectral bandwidth) which limited their abilities to identify small spectral variations in individual pixels for diagnosing specific forest insect infection. As an alternative, the hyperspectral data provided by EO-1 Hyperion sensor provides a high spectral resolution using 242 spectral bands from 0.4 to 2.5 μm (each band covers a very narrow spectral bandwidth). However, little study has been conducted on using Hyperion or other satellite hyperspectral images for monitoring spruce budworm defoliation. Taking advantage of the rich spectral information, this thesis proposed methods for remotely sensing, estimating and mapping spruce budworm (SBW) defoliation using the spectral information, i.e. vegetation indices (VIs), extracted from Hyperion images. 15% of accuracy improvement in SBW defoliation estimation and mapping has been achieved by applying the developed Hyperion VIs compared with conventional multispectral VIs. Highly accurate mapping results have been generated by developing suitable feature extraction method.

ACKNOWLEDGEMENTS

I would primarily thank my supervisor Dr. Yun Zhang for his continuous support and providing me with the opportunity to conduct this research. Without the support, the research would not have been possible. In addition, I would like to thank Dr. Zhang for supervising and providing me with proper guidance to complete the research and this thesis.

I would like to thank NASA for collecting the Hyperion images of the testing areas, Dr. David MacLean and his research team for the support in field investigation, and Dr. Brigitte Leblon and her student in spectral measurements of the infected spruce and balsam branches.

I would extend my thanks to the staff at GGE, especially David Fraser and Sylvia Whitaker. They helped me out with the software and the academic procedures at UNB.

I would also like to thank all the members in the research group of Dr. Zhang for their help and friendships.

Last but not least, I would like to thank my parents for their continuous support.

TABLE OF CONTENTS

ABSTRACT ii

ACKNOWLEDGEMENTS iii

TABLE OF CONTENTS iv

LIST OF TABLES ix

LIST OF FIGURES x

LIST OF SYMBOLS AND ABBREVIATIONS xiv

1 CHAPTER 1 INTRODUCTION 1

1.1 Thesis Structure 2

1.2 Background of the Spruce Budworm Defoliation 4

1.3 Monitoring Spruce Budworm Defoliation using Remote Sensing 7

1.3.1 Studies Using Multispectral Data 8

1.3.2 Studies Using Hyperspectral Data 10

1.3.3 Research Problem 12

1.4 Research Objective 14

1.5 Proposed Methodology 15

1.6 Overview of Each Chapter 17

References 19

2 CHAPTER 2 CAN EO-1 ALI DATA ESTIMATE SPRUCE BUDWORM DEFOLIATION IN QUEBEC, CANADA? 22
2.1 Introduction 23
2.2 Materials 25
2.3 Methodology 27
2.3.1 Data Pre-processing 27
2.3.2 Vegetation Indices Construction and correlation with defoliation 28
2.3.3 Mapping SBW defoliation using VIs 29
2.4 Results and Discussion 30
2.5 Conclusions 33
Acknowledgement 33
References 34
3 CHAPTER 3 REMOTE SENSING OF SPRUCE BUDWORM DEFOLIATION USING EO-1 HYPERION HYPERSPECTRAL DATA: AN EXAMPLE IN QUEBEC, CANADA 36
3.1 Introduction 37
3.2 Study Site and Materials 40
3.2.1 Study site 40
3.2.2 Materials 42
3.3 Methodology 44

3.3.1 Data Preprocessing 44
3.3.2 Vegetation Indices Construction 46
3.3.3 VIs based Change Detection and Forest Stress Analysis 50
3.4 Results and Analysis 53
3.4.1 Hyperion Data Pre-processing 53
3.4.2 VIs based Change Detection 57
3.4.3 VIs based Forest Stress Analysis 63
3.5 Conclusion 66
Acknowledgement 66
References 67
4 CHAPTER 4 ESTIMATION AND MAPPING OF SPRUCE BUDWORM DEFOLIATION USING VEGETATION INDICES DERIVED FROM HYPERION HYPERSPECTRAL DATA 70
4.1 Introduction 71
4.2 Background 75
4.3 Study Site and Materials 78
4.3.1 Study site 78
4.3.2 Materials 79
4.4 Methodology 81
4.4.1 Data Pre-processing 81

4.4.2 Vegetation Indices Construction and correlation with defoliation 82

4.4.3 Mapping SBW defoliation using VIs 83

4.5 Results and Analysis 85

4.5.1 Hyperion Data Pre-processing 85

4.5.2 Correlation of Vegetation Indices with SBW defoliation 87

4.5.3 Mapping SBW defoliation using VIs 93

4.6 Conclusion 99

Acknowledgement 101

References 101

5 CHAPTER 5 EXPLOITING SPECTRAL AND SPATIAL INFORMATION FOR MAPPING SPRUCE BUDWORM DEFOLIATION USING HYPERION HYPERSPECTRAL DATA 105

5.1 Introduction 106

5.2 Study Site and Materials 109

5.2.1 Study site 109

5.2.2 Materials 111

5.3 Methodology 112

5.3.1 Data Pre-processing 112

5.3.2 Exploit Spectral Information 114

5.3.3 Exploit Spatial Information 117

5.3.4 Classification and mapping SBW defoliation 120
5.4 Experimental Results and Assessment 121
5.4.1 Comparison of mapping results 121
5.4.2 Parameter Adjustments 125
5.5 Conclusion 127
Acknowledgement 128
References 128
6 CHAPTER 6 CONCLUSIONS AND RECOMMENDATIONS 131
6.1 Summary of the Research 131
6.2 Contributions of the Research 133
6.3 Recommendations for Furthermore Research 135
References 137
Curriculum Vitae

LIST OF TABLES

Table 2.1 9 Vegetation indices analyzed in this study 24

Table 2.2 9 Vegetation indices derived from ALI bands 30

Table 3.1 13 Vegetation indices applied for change detection 47

Table 3.2 Change rates detected with 13 vegetation indices summarized for three defoliation regions 58

Table 4.1 12 vegetation indices analyzed in this study 74

Table 4.2 Potential Hyperion bands for 12 vegetation indices applied for SBW defoliation estimation. 88

Table 4.3 Comparison of accuracies using NDVI and CNDVI for mapping SBW defoliations 99

Table 5.1 Construction of VI bands used for spectral information extraction 116

Table 5.2 Comparison of accuracies using NDVI and CNDVI for mapping SBW defoliations 125

LIST OF FIGURES

Figure 1.1 Thesis structure 3

Figure 1.2 Total annual area infested by spruce budworm in Quebec, Canada. (Source: MFFP report 2014, Quebec) 6

Figure 2.1 Study site 26

Figure 2.2 Defoliation mapping result using NLI index of the study site. (a) A grayscale image of the testing area; (b) Ground truth map of assessment region where green blocks were light defoliated areas and red blocks were severely defoliated areas; (c) Defoliation results detected in EO-1 ALI MS image where black pixels indicate light defoliated pixels and white pixels indicate severely defoliated pixels. 32

Figure 3.1 Study site 42

Figure 3.2 MNF bands illustrate the effects of vertical stripes removal and cross track illumination correction. For the June image, (a) and (b) show the MNF band 1 and 6 before the correction, (c) and (d) show the MNF band 1 and 6 after the correction. For the August image, (e) and (f) show the MNF band 1 and 6 before the correction, (g) and (h) show the MNF band 1 and 6 after the correction. 54

Figure 3.3 Spectral profiles of one same vegetation pixel on radiance and reflectance images were displayed. (a) June radiance image, (b) June reflectance image, (c) August radiance image, (d) August reflectance image. Data value in both curves have unit μW/(cm2 * sr * nm) while the reflectance data has been multiplied by a scale factor of 1000. 55

Figure 3.4 Hyperion image captured on June 16, 2014 was shown in (a) and the one captured on August 7, 2014 was shown in (b). Band 29 (732 nm), band 20 (640 nm) and band 12 (559 nm) were used to display the natural color images. The defoliation magnitude reference map shown in (c) has three delineated defoliation levels: light (green), moderate (yellow) and severe (red). The black blocks were either uninvestigated regions or forestless regions. 56

Figure 3.5 The percentage changes between June and August were detected in two typical greenness VIs. (a) Change detection map of SR; (b) Change detection map of MRESR. 59

Figure 3.6 The percentage changes between June and August were detected in two typical canopy water content VIs. (a) Change detection map of MSI; (b) Change detection map of NDWI. 61

Figure 3.7 The percentage changes between June and August were detected in two typical Light Use Efficiency VIs. (a) Change detection map of SIPI; (b) Change detection map of RDRI. 62

Figure 3.8 Forest stress maps generated for the June image was shown in (a) and the one for the August image was shown in (b), the stress levels for both maps were shown as a colormap in (c). 64

Figure 3.9 Most stressed regions (light blue to black) extracted from stress maps were aligned with the aerial survey map as reference. The June map was shown in (a) and the August map was shown in (b). The stress levels displayed were from light blue, dark blue to black (from level 7, 8 to 9, with 9 being the most). 65

Figure 4.1 Study site 79

Figure 4.2 Original MNF band 1 and 6 were shown in (a) and (b). MNF band 1 and 6 after vertical stripes removal and cross track illumination correction were shown in (c) and (d). 86

Figure 4.3 Spectral profile of one vegetation pixel on both radiance image (a) and reflectance image (b). Data value in both curves have unit µW/(cm2 * sr * nm) while the reflectance data has been multiplied by a scale factor of 1000. 87

Figure 4.4 Plots for correlation matrix $\underline{R^2}$ (from 0 to 1) between defoliation and NDVI calculated using pairwise 162 Hyperion bands 447-2365 nm. Two bands (Band 1 and 2) were used to calculate one NDVI value and generate one correlation coefficient value in the $\underline{R^2}$ matrix. NIR bands (band 1-48) and SWIR bands (band 49-162) with high correlation values as illustrated were recommended for estimation of SBW defoliation and summarized in Table 4.2..... 89

Figure 4.5 Plots for correlation matrix $\underline{R^2}$ (from 0 to 1) between defoliation and NLI calculated using pairwise 162 Hyperion bands. For more information refer to Figure 4.4. 90

Figure 4.6 Plots for correlation matrix $\underline{R^2}$ (from 0 to 1) between defoliation and RDVI calculated using pairwise 162 Hyperion bands. For more information refer to Figure 4.4. 91

Figure 4.7 Plots for correlation matrix R^2 (from 0 to 1) between defoliation and CNDVI calculated using pairwise 162 Hyperion bands. For more information refer to Figure 4.4. 92

Figure 4.8 Defoliation mapping result using NDVI index of the study site. (a) A grayscale image of the testing area; (b) Defoliation results detected in EO-1 Hyperion image where black pixels indicate light defoliated pixels and white pixels indicate severely defoliated pixels ; (c) Ground truth map of assessment region where green blocks were light defoliated forestry and red blocks were severely defoliated areas..... 94

Figure 4.9 Defoliation mapping result using NLI index of the study site. For more information refer to Figure 4.8. 95

Figure 4.10 Defoliation mapping result using RDVI index of the study site. For more information refer to Figure 4.8. 96

Figure 4.11 Defoliation mapping result using CNDVI index of the study site. For more information refer to Figure 4.8. 97

Figure 5.1 Study site 110

Figure 5.2 Extract spectral information from original Hyperion data as shown in (a) by constructing 5 vegetation index bands as shown in (b). 115

Figure 5.3 Process of exploiting spatial information by extracting histogram vectors (b) from each VI band (a) and stacking into a single feature vector (c) for each pixel location. 119

Figure 5.4 Illustration of symmetric padding method used in neighborhood construction. The original VI band image was defined inside the black outlines. The blue and red blocks outside the black outlines were generated based on line or point symmetry based on their respective locations..... 120

Figure 5.5 MNF bands 1-5 as shown in (a)-(e) were used for comparison in mapping SBW defoliation. 122

Figure 5.6 Mapping result for SBW defoliation condition of study site. (a) Mapping result by using proposed SSM method; (b) Mapping result by using MNF; (c) Mapping result by using original Hyperion reflectance data; (d) Ground truth map of assessment region where green blocks were light defoliated areas and red blocks were severely defoliated areas. 124

Figure 5.7 Overall accuracies and Kappa coefficients with a range of neighborhood size w being used for experiments. The bin size of histograms h was set to be 12. 126

Figure 5.8 Overall accuracies and Kappa coefficients with a range of histogram bin size h being used for experiments. The neighborhood size w was set to be 15. 127

LIST OF SYMBOLS AND ABBREVIATIONS

ALI Advanced Land Imager

ARVI Atmospherically Resistant Vegetation Index

BTK Bacillus Thuringiensis var. Kurstaki

CSR Cosine Simple Ratio

CDVI Cosine Difference Vegetation Index

CNDVI Cosine Normalized Vegetation Index

DVI Difference Vegetation Index

ENVI ENvironment for Visualizing Images

EO-1 Earth Observing-1

ETM+ Enhanced Thematic Mapper Plus

EVI Enhanced Vegetation Index

EVI2 2-band Enhanced Vegetation Index

FLAASH Fast Line-of-sight Atmospheric Analysis of Spectral Hypercubes

LAI Leaf Area Index

MFFP Ministère des Forêt, de la Faune et des Parcs

MNF Minimum Noise Fraction

MNLI Modified Non-Linear Index

MODIS Moderate Resolution Imaging Spectroradiometer

MRENDVI Modified Red Edge Normalized Difference Vegetation Index

MRESR Modified Red Edge Simple Ratio

MSI Moisture Stress Index

MSR Modified Simple Ratio

NASA National Aeronautics and Space Administration

NDVI Normalized Difference Vegetation Index

NDWI Normalized Difference Water Index

NLI Non-Linear Index

NIR Near Infrared

PRI Photochemical Reflectance Index

RDRI Red Green Ratio Index

RDVI Renormalized Difference Vegetation Index

RENDVI Red Edge Normalized Difference Vegetation Index

RMSE Root Mean Square Error

SAVI Soil Adjusted Vegetation Index

SIPI Structure Insensitive Pigment Index

SMA Spectral Mixture Analysis

SPOT Système Pour l'Observation de la Terre

SBW Spruce Budworm

SR Simple Ratio

SWIR Short Wave Infrared

TM Thematic Mapper

VIs Vegetation Indices

VNIR Visible-Near Infrared

WBI Water Band Index

1 CHAPTER 1

INTRODUCTION

This thesis aims to provide a satellite remote sensing solution for estimation and mapping of the defoliation caused by spruce budworm in Quebec, Canada using satellite hyperspectral data. Many remote sensing studies have detected differences in spectral responses between forest insect defoliation using vegetation indices. Most of them were derived from broadband such as NIR (near infrared) and Red bands captured by multispectral sensors (Adelabu et al., 2012). Each of the multispectral bands usually covers a spectral span (or bandwidth) of hundreds of nanometers, whereas a typical hyperspectral band has only a bandwidth of 10 nm. Thus, less accurate spectral information can be captured by multispectral sensors, and the comparison between responses within a narrow wavelength span was unavailable. As an alternative, hyperspectral sensors operate with hundreds of narrow spectral bands, which make it possible to design suitable and specific narrowband VIs for monitoring different kinds of forest stresses.

The first paper investigate the possibility of using VIs constructed from multispectral data for estimation of spruce budworm defoliation in which correlation analysis was introduced. Then the second and third papers in this thesis attempt to estimate spruce budworm defoliation by using existing VIs and developing new VIs for hyperspectral data. The second paper presents a remote sensing approach based on existing VI construction and change detection methods and applies it to generate forest stress maps of a defoliated site. The third paper focuses on extending the correlation

analysis to find the most relevant VIs and associated bands from the 162 available Hyperion hyperspectral bands. Compared with existing VIs, the VIs developed in this paper achieved, on average, 15% accuracy improvement in SBW defoliation estimation and mapping.

The classification of damage degree or defoliation intensity has been considered a challenging research task. Building on top of the VIs study, the fourth paper in this thesis attempts to find an effective way for mapping the spruce budworm defoliation. With proposed feature extraction method, a highly accurate classification result for different defoliation intensities has been achieved.

1.1 Thesis Structure

The structure of the thesis was presented in Figure 1.1 below.

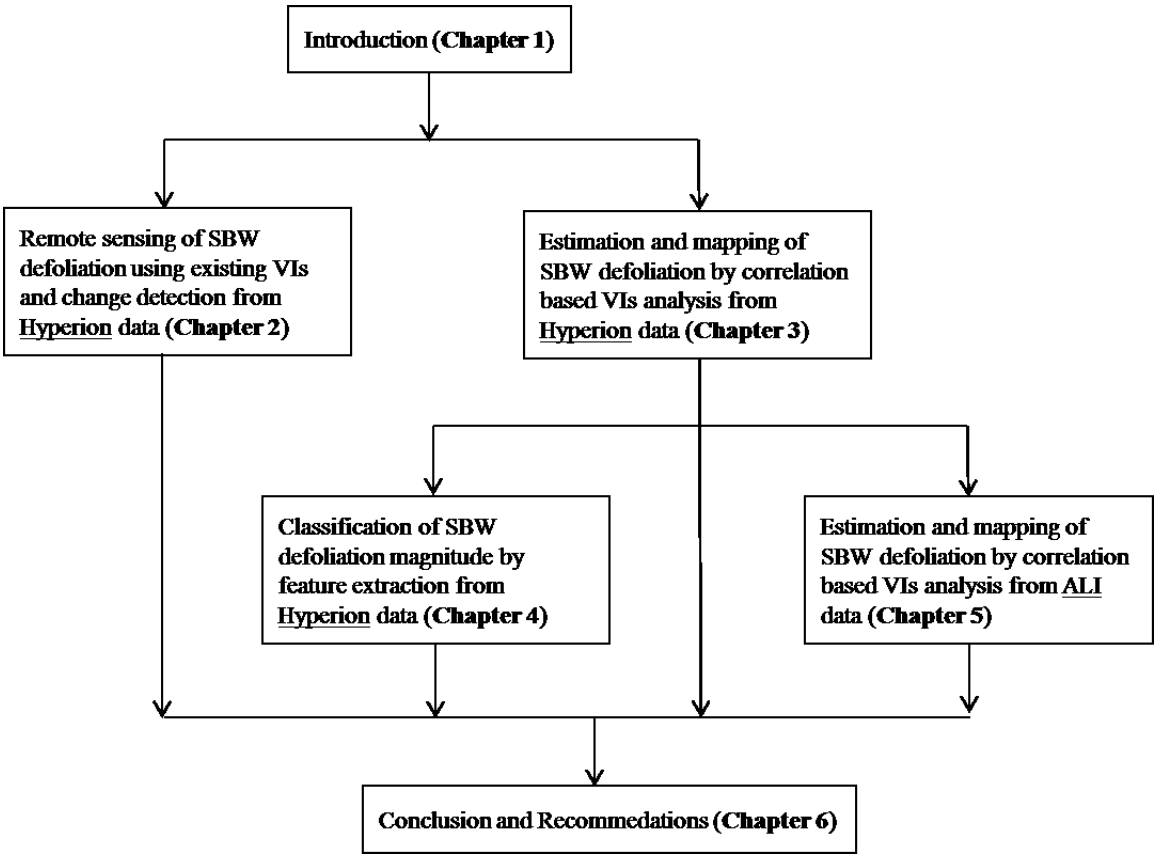

Figure 1.1 Thesis structure

1.2 Background of the Spruce Budworm Defoliation

The spruce budworm was arguably one of the most damaging native insects affecting spruces and true fir in Canada, causing severely defoliation of tens of millions of hectares of trees during a major outbreak. The fir and white spruce were the main host species of SBW, black spruce were also increasingly affected (Fan, 2006).

Spruce budworm population cycles were characterized by epidemic and endemic phases, and outbreaks occur every 30 to 40 years. The causes of outbreaks were still debated. Suitable climatic factors, such as consecutive warm, dry springs, and biotic factors such as homogeneous stands of host trees and changes in natural enemy abundance, were possible reasons for the onset of outbreaks. Population collapse was attributed to resource depletion, disease and an increase in the impact of natural enemies (Boulanger & Arseneault, 2004).

In eastern North America, the spruce budworm damage appears in May, when third instar larvae begin to feed. Evidence of a spruce budworm infestation includes defoliation of current-year shoots and the presence of larval nests and excrement. Defoliation begins at the top of the tree and quickly progresses downwards. Needles were partially or completely consumed. Spruce budworm larvae also feed on male (pollen) flowers and cones. During outbreaks, the larvae may destroy all of the cones. Severely affected stands turn a rust color as a result of dried-out needles held by strands of silk spun by the larvae. In the fall, most dead needles fall off. Defoliated stands take on a greyish appearance (Boulanger & Arseneault, 2004).

Quebec was one of the provinces in Canada with most areas suffered from moderate to severe spruce budworm (SBW) defoliation (Boulanger & Arseneault, 2004). In 1994, the Quebec government adopted a Forest Protection Strategy in which some approaches (prevention, direct control and recovery) were proposed to counter the negative effects of outbreaks of spruce budworm. Prevention measures were integrated in the planning of forest management. Direct control by aerial spraying of Bacillus thuringiensis var. kurstaki (Btk) was sometimes the only effective way to mitigate the socio-economic impact of spruce budworm outbreaks in vulnerable forests. However due to high cost in finance and manpower, it was only performed on a small proportion of defoliated forests. Finally, when the accessibility of the terrain permits, harvesting of dying or recently dead trees can reduce timber losses. To be able to apply the approaches of the Strategy, air surveys were conducted in the province to detect and delineate the areas affected by this pest (MFFP, 2014).

The aerial survey of the damage caused by major forest pests was carried out annually since 1967 by the Directorate for the Protection of the Ministry of Forests, Fauna and Parks (Ministère des Forêt, de la Faune et des Parcs, MFFP). It measures the intensity and the extent of damage caused by insects. The aerial survey was conducted in regions previously determined according to the damage of the previous year and the results of forecasting inventories of populations of the insect (MFFP, 2014).

They concluded that in 2014, the areas affected by SBW continue to rise significantly in the province. In 2014, they totaled 4,275,065 hectares compared to 3,200,348 hectares in 2013 (MFFP, 2014). Infested areas (hectares) by SBW in Quebec since the beginning of the epidemic in 1992 in shown in Figure 1.2 below. The data were provided by MFFP aerial survey report in 2014. The infested regions were divided into three categories based on their difference in defoliation intensities, namely, light (loss of foliage in the upper third of the tops of some trees), moderate (loss of foliage in the upper half of the top of most trees) and severe (loss of foliage on the entire length of the top of most trees).

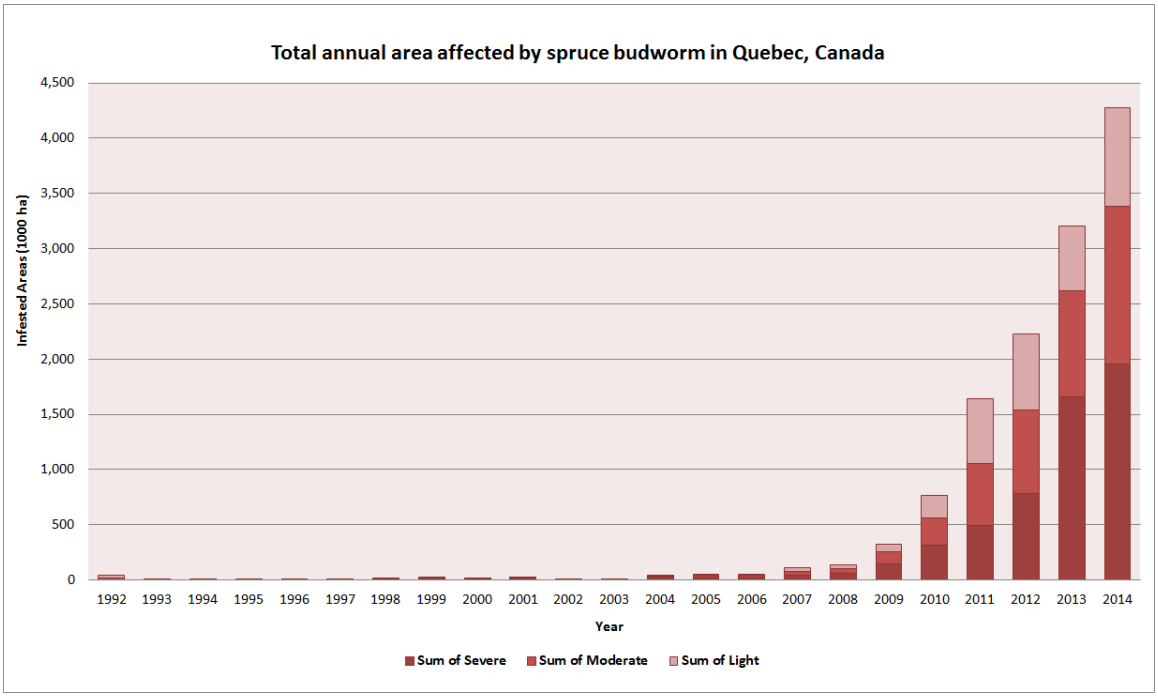

Figure 1.2 Total annual area infested by spruce budworm in Quebec, Canada. (Source: MFFP report 2014, Quebec)

A sharp increasing of the infested area can be identified from the chart start from 2009, which suggest an epidemic period of spruce budworm activity. Early intervention to prevent the spread of spruce budworm in Atlantic Canada and Quebec will protect the region from losing valuable forest resources to the severe defoliation that would be caused by a major outbreak.

According to the study of Dr. Taylor and Dr. MacLean in 2008 (Taylor & MacLean, 2008), from 1985 to 1993, 85% of 332 cases were correctly classified by aerial estimate. They concluded that aerial surveys provide a reasonable estimate of defoliation.

1.3 Monitoring Spruce Budworm Defoliation using Remote Sensing

Even though the aerial survey was considered an option to provide relative accurate mapping as investigator has a relatively close look at the trees when flight height was adjusted accordingly, the operation calls for considerable involvement of man-power and was meanwhile time-consuming. Alternatively, remote sensing techniques, especially the utilization of satellite images, provides wide spatial coverage, high temporal repeatability and increasing spatial resolutions make them suitable for such investigations (Adelabu et al., 2012).

Satellite remote sensing technology has a great potential for addressing the issue. First of all, it has the advantage of monitoring inaccessible and large areas of forest fields. Furthermore, the wide range of spectral wavelengths used in imaging sensors makes it possible to capture information beyond human eyes. Especially the reflectance in infrared regions can be vital in analysis of forest health (Rullan-Silva et al., 2013). As

a matter of fact, considerable efforts and studies can be found using remote sensing technologies for investigation of defoliation and forest stress analysis (Foody, 2003; Fuller, 2006; Pax-Lenney et al., 2001; Woodcock et al., 2001).

Remote sensing technologies have also been used to monitor defoliation caused by insects. However, many problems and limitations still exist. This section reviews the previous studies in order to identify the research gaps. They can be divided into two categories: multispectral data based approach and hyperspectral data based approach.

1.3.1 Studies Using Multispectral Data

Several studies were conducted on using multispectral images for monitoring spruce budworm defoliation. Fan, (2006) conducted studies on evaluating the sensitivity of multi-temporal Landsat-5 TM data and a single date SPOT4 HRVIR Image to cumulative SBW defoliation in the Prince Albert National Park, Saskatchewan, Canada. He concluded that the highest correlation with the defoliation was obtained when using one vegetation index calculated from SPOT4. He also concluded the Leaf Area Index (LAI) relationships between vegetation indices did not perform as well as those between defoliation and vegetation indices. Leckie et al. (1992) found a close relationship between spectral features extracted from MEIS imagery and tree defoliation caused by spruce budworm.

There were considerable studies where remotely sensed multispectral data were applied to detect, map and monitor forest insect damage in the past decades. For instance, Townsend et al., (2012) used Landsat data to predict defoliation severity caused by the

Gypsy Moth (*Lymantria dispar*) in deciduous forests. Eklundh et al., (2009) assessed defoliation by European pine sawfly (*Neodiprion sertifer*) in pine forests using Moderate Resolution Imaging Spectroradiometer (MODIS) time-series data. K.M. de Beurs and Townsend, (2008) used data from the same sensor to estimate the magnitude of defoliation caused by a gypsy moth outbreak that occurred in the US.

In order to quantity the insect defoliation using images, the construction of vegetation indices was applied by many researchers in their studies (Adelabu et al., 2012). The vegetation indices (VIs) derived from remote sensing has been widely applied to estimate vegetation health and greenness. Generally, healthy vegetation will absorb most of the visible light that falls on it, and reflects a large portion of the near-infrared light. The defoliated forest, in form of unhealthy or sparse vegetation, reflects more visible light and less near-infrared light. Existing multispectral sensors were usually configured to include reflectance from these two spectral ranges, namely, one Red band and one NIR band. For instance, the Band 3 and 4 in Landsat 5 TM, Band 2 and 3 in SPOT4 HRVIR (Fan, 2006) and Band 1 and 2 in MODIS (de Beurs and Townsend, 2008).

Making use of more spectral bands, studies have been conducted on mapping the magnitude of defoliation using more VIs constructed from multispectral images (Rullan-Silva et al., 2013). Two types of broad-band VIs were compared for measuring different types of forest damage in USA (Vogelmann, 1990). In order to map the magnitude of defoliation, Vogelmann (1990) tested three VIs that use the R, NIR, SWIR and mid-infrared (MIR) bands, and found that SWIR reflectance was very sensitive to the amount

of water in the vegetation, increasing when leaf water content decreases, a symptom of vegetation stress due to pest defoliators. De Beurs and Townsend (2008) further concluded that two VIs using SWIR band had better performances for mapping insect defoliation in their site when compared with conventional NDVI.

Change detection based on multi-temporal images was also widely applied in their studies using multispectral images. For example, (Thomas et al., 2007) developed a Landsat multi-temporal change detection approach for aspen and spruce budworm defoliation in two sites in the province of Alberta and one site in Saskatchewan, Canada. Multispectral vegetation indices and transformations have also been used extensively as data inputs in forest change detection studies. For instance, (de Beurs and Townsend, 2008) developed a MODIS defoliation index based on the difference between the VIs calculated before defoliation (with the highest values) and the ones during the defoliation (with lowest values).

1.3.2 Studies Using Hyperspectral Data

As hundreds of narrow spectral bands were operated by hyperspectral sensors, they can be more suitable and efficient at detecting subtle biophysical changes in foliage canopy during the insect defoliation. A few researchers, such as Santos et al., (2010) and Adelabu et al., (2012) have addressed the need of using hyperspectral sensors for monitoring forest defoliation. The finer spectral resolution was considered the most critical advantage of hyperspectral data. Because of the continuous spectrum provided by hyperspectral data, more sophisticated spectrum analysis can be applicable to diagnose

the reflectance at certain narrow spectral regions. For instance, Zhang et al., (2010) highlighted the advantage of hyperspectral data over multispectral data in analyzing the "red edge" position, to detect subtle changes in forest health. In addition, studies have been conducted for narrowband VIs construction using hyperspectral bands. For instance, Gong et al., (2003) investigated the potential of Vegetation Indices derived from Hyperion hyperspectral data for estimation of forest leaf area index. All available 168 Hyperion bands were involved in their experiments of VIs construction and resulted in more specific information on the correlation between the spectral data and forest biophysical properties.

Studies in insect defoliation using hyperspectral data appear to be in an early stage and less in number compared with studies using multispectral data. Most of them were conducted in the field or in an aircraft close to ground. Pontius et al., (2008) examine the capability of a commercially available sensor (SpecTIR VNIR) to map ash decline due to exotic emerald ash borer (EAB) infestations in Michigan and Ohio. The sensor was carried by a fixed wing aircraft. They applied a linear regression equation based on known stress- and chlorophyll sensitive indices to predict decline on a continuous 0- to 10 scale. Adelabu et al., (2014) examined the possibility of using ground based hyperspectral data to discriminate between three levels of mopane worm defoliation severity. Field reflectance was measured and spectral discrimination was conducted by applying a Random Forest algorithm.

Lyytikäinen-Saarenmaa et al., (2008) attempted to detect pine sawfly defoliation using remotely sensed EO-1 Hyperion data and GIS technology. They claimed their study

to be s the first attempt to analyze and classify insect defoliation with hyperspectral imagery. (Somers et al., 2010) investigated the potential of spectral mixture analysis (SMA) for defoliation monitoring in Australian mixed-aged Eucalyptus plantations using multispectral Landsat 5-TM and hyperspectral EO-1 Hyperion satellite data. However they failed to find improvement by using hyperspectral data than multispectral data by applying their method.

No publications yieled in the literature review using airborne or satellite hyperspectral data for monitoring spruce budworm defoliation.

1.3.3 Research Problem

As mentioned above, previous studies that used multispectral data with less spectral information can be less accurate for estimating or mapping spruce budworm defoliation. Especially, the VIs constructed using multispectral data can only provide broadband information, which can be insufficient for quantified analysis of forest health (Adelabu et al., 2012).

In terms of using hyperspectral data to monitor insect defoliation, the most applied ground and airborne based commercial sensors can be costly. It was also less efficient to apply them for investigation of larger regions, which was usually the case of spruce budworm defoliation. Until now, there was little evidence of aerial or satellite hyerspectral images identifying spruce budworm defoliation. Furthermore, few studies were designed to take advantage of the finer spectral resolution provided by hyperspectral sensors.

The EO-1 Hyperion sensor, operated by NASA, was the only spaceborne hyperspectral sensor. It was also provided free of charge. However, its spatial resolution was only 30 m × 30 m, which indicates a single pixel of the imagery captured from the spruce or fir forest covers considerable number of trees. Therefore, the estimation and mapping of the defoliation need accurate and specific information in order to discriminate defoliated forest pixels.

Even though a number of VIs were designed for monitoring forest health, including broadband and narrowband VIs, questions remain considering on the suitability of the VIs constructed from multispectral and hyperspectral data for investigating certain forest phenomenon, in our case, the defoliation caused by spruce budworm in Quebec, Canada. Thus the first answer needed concerns whether or not the existing VIs derived from multispectral data can be suitable for estimating SBW defoliation. If not, we turn to consider the potiential of using hyperspectral data in which more spectral information can be utilized. Then the second problem was on the potiential of the existing hyperspectral narrowband VIs for esitmation of SBW defoliation. In addition, we want to know if the current VIs can be extended to better estimating SBW defoliation when hyperspectral data were applied, which constitutes our third problem. For example, the Normalized Difference Vegetation Index (NDVI) was widely applied to estimate forest health (Vogelmann, 1990). For commonly applied multispectral data, the Red and NIR band for constructing NDVI were usually limitted if not unique, without room for exploration. However, when hyperspectral data were applied for VIs construction, it was reasonable to wonder what the most relevant bands to calculate in favor of estimating the defoliation

were. Finally, classification or discrimination from different damage degrees in forest defoliation caused by insects was long considered challenge remain to solve and has never been done with satellite hyperspectral images. This was thus the fourth major research problem of this thesis.

1.4 **Research Objective**

As mentioned above, the thesis aims at solving the four major problems exist in monitoring SBW defoliation using satellite multispectral and hyperspectral images.

To investigate the potential of multispectral VIs for estimation of SBW defoliation, we applied a statistics based correlation analysis which involves all the available multispectral bands for VIs construction.

To investigate the potential of hyperspectral VIs for estimation of SBW defoliation, first of all, the research aims to design a remote sensing method for SBW defoliation. It should:

- incorporate existing VIs constructed using hyperspectral data;
- apply suitable method, e.g. change detection to investigate the potential of each VI;
- investigate the potential of synthesizing information provided by existing VIs for estimating SBW defoliation.

Secondly, we needed to design a thorough hyperspectral based VIs construction method should be designed to further take advantage of the spectral information provided

by hyperspectral sensor, which was extended from the correlation analysis used in multispectral study. The method should:

- apply narrowband VIs construction using all available Hyperion bands;
- couple with reference data from ground-based assessments and ancillary information;
- select relevant VIs and associated bands for estimation and mapping of SBW defoliation.

Finally, a mapping method that can accurately classify defoliation intensities should be designed. It should:

- requires no pre-labeled endmembers;
- applicable with existing unsupervised classifiers;
- computationally efficient;
- be able to detect severe defoliation accurately without using multitemporal images.

1.5 Proposed Methodology

This section provided a brief description of the research conducted for accomplishing the objectives of this study. The satellite data used in this research, i.e., EO-1 Hyperion hyperspectral (30 m ground resolution), was obtained with the assistance of NASA Goddard Space Flight Center. The data targeting and acquisition were free of charge. The data pre- and post-processing were implemented mainly using ENVI/IDL.

In Chapter 2, in order to investigate the first problem mentioned in research objectives – whether or not the multispectral data can be suitable for estimating SBW defoliation – the VIs based correlation analysis was applied on multispectral EO-1 ALI image to investigate the possibility of using multispectral images for estimation of SBW defoliation. The ALI image was acquired at the same time with the Hyperion image used in Chapters 4 and 5.

In Chapter 3, in order to investigate the second problem mentioned in research objectives – whether or not the existing narrowband hypersepctral VIs can be suitable for estimating SBW defoliation – the experiments aimed at analyzing the defoliated condition in a forested region in the province of Quebec, Canada by integrating the information from VIs that focused at different aspects of overall health and vigor in forested areas. Two Hyperion images applied in this study were acquired on June and August, 2014 respectively from NASA. The VIs based change detection was applied in this study to quantize the change of different VIs between multi-temporal Hyperion images acquired from June and August respectively over the study site. VIs from four difference categories were investigated to find the VIs with most significant changes in response to the increasing defoliation from June to August. Finally, spatial maps of forest stress were generated for two images respectively using the selected VIs.

In Chapter 4, in order to investigate the third problem mentioned in research objectives – if the current VIs can be extended to better estimating SBW defoliation when hyperspectral data were applied – the potential of 9 conventional and 3 developed vegetation indices using Hyperion data in estimation of defoliation caused by spruce

budworm in Quebec region, Canada was investigated. The method used in our study for constructing VIs was based on the form of conventional VIs while examine the performance of them using spectral bands among 162 available Hyperion hyperspectral bands. The VIs include linear, nonlinear as well as soil adjusted models. The assessments on the performance of all tested 12 VIs were based on their correlation with defoliation data provided by airborne survey on the same site and mapping results.

In Chapter 5, in order to investigate the fourth problem mentioned in research objectives – classification or discrimination from different damage degrees in forest defoliation caused by SBW – a spectral-spatial based method for mapping the defoliation caused by spruce budworm in a study site in Quebec, Canada using Hyperion hyperspectral data was proposed. The spectral information was derived from vegetation index bands. Those bands were proven to be most relevant to defoliation status (Huang, 2015). As only 5 bands were used, the proposed method can be considered a new approach for hyperspectral dimensional reduction. Moreover, the proposed method integrates the spatial information from used VI bands by extracting histograms from neighborhood of each incident pixel. Thus spectral-spatial features can be extracted from hyperspectral data. The efficiency of constructed feature was examined in mapping experiments.

1.6 Overview of Each Chapter

This thesis was organized into six chapters. Chapter 1 introduces briefly the spruce budworm and the defoliation caused by it in Quebec, Canada and reviews previous

studies on remote sensing for monitoring SBW defoliation. The identified research gaps were used to determine the research objective of this thesis. The general methodological design and the thesis structure were also introduced.

Chapter 2 investigates the potentials of using multispectral vegetation indices derived using EO-1 ALI bands for estimating and mapping the SBW defoliation.

Chapter 3 and 4 investigate the potentials of using existing vegetation indices and vegetation indices developed using Hyperion bands for estimating and mapping the SBW defoliation. In Chapter 5, a spectral-spatial based mapping method was developed for accurately classification of SBW defoliation intensities in the study site.

The final Chapter, Chapter 6, summarizes and concludes the research presented in this thesis, and highlighted the contributions of this thesis towards the research objective. Then, recommendations for further research were presented.

References

Adelabu, S., Mutanga, O., Adam, E., & Sebego, R. (2014). Spectral discrimination of insect defoliation levels in mopane woodland using hyperspectral data. *IEEE Journal of Selected Topics in Applied Earth Observations and Remote Sensing*, *7*(1), 177–186. doi:10.1109/JSTARS.2013.2258329

Adelabu, S., Mutanga, O., & Azong, M. (2012). A review of remote sensing of insect defoliation and its implications for the detection and mapping of imbrasia belina defoliation of mopane woodland. *The African Journal of Plant Science and Biotechnology,* 6(1):1-13. 2011.12.

Boulanger, Y., Arseneault, D., Morin, H., Jardon, Y., Bertrand, P., & Dagneau, C. (2012). Dendrochronological reconstruction of spruce budworm (Choristoneura fumiferana) outbreaks in southern Quebec for the last 400 years. Canadian Journal of Forest Research, 42, 1264–1276. doi:10.1139/X2012-069

De Beurs, K. M., & Townsend, P. A. (2008). Estimating the effect of gypsy moth defoliation using MODIS. *Remote Sensing of Environment*, *112*, 3983–3990. doi:10.1016/j.rse.2008.07.008

Eklundh, L., Johansson, T., & Solberg, S. (2009). Mapping insect defoliation in Scots pine with MODIS time-series data. *Remote Sensing of Environment*, *113*(7), 1566–1573. doi:10.1016/j.rse.2009.03.008

Fan, H. (2006). Satellite remote sensing of cumulative spruce budworm defoliation in Prince Albert National Park. *University of Saskatchewan Electronic Theses and Dissertations*.

Foody, G. M. (2003). Remote sensing of tropical forest environments: towards the monitoring of environmental resources for sustainable development. International journal of remote sensing, 24(20), 4035-4046.

Fuller, D. O. (2006). Tropical forest monitoring and remote sensing: A new era of transparency in forest governance? *Singapore Journal of Tropical Geography*, *27*, 15–29. doi:10.1111/j.1467-9493.2006.00237.x

Gong, P., Pu, R., Biging, G. S., & Larrieu, M. R. (2003). Estimation of forest leaf area index using vegetation indices derived from Hyperion hyperspectral data. *Geoscience and Remote Sensing, IEEE Transactions on*, *41*(6), 1355–1362.

Lyytikäinen-Saarenmaa, P., Holopainen, Mar., Ilvesniemi, S., & Haapanen, R. (2008). Detecting pine sawfly defoliation by means of remote sensing and GIS. *Forstschutz Aktuell*, *44*, 14–15.

Ministère des Forêt, de la Faune et des Parcs (MFFP). (2014). Aires infestées par la tordeuse des bourgeons de l'épinette au Québec en 2014. Version 1.0 [Online] September 2014: http://www.mffp.gouv.qc.ca/publications/forets/fimaq/insectes/tordeuse/TBE_2014_P.pdf

Taylor, S. L., & MacLean, D. A. (2008). Validation of spruce budworm outbreak history developed from aerial sketch mapping of defoliation in New Brunswick. Northern Journal of Applied Forestry, 25(3), 139-145.

Leckie, D. G., Yuan, X., Ostaff, D. P., Piene, H., & MacLean, D. A. (1992). Analysis of high resolution multispectral MEIS imagery for spruce budworm damage assessment on a single tree basis. Remote Sensing of Environment,40(2), 125-136.

Pax-Lenney, M., Woodcock, C. E., Macomber, S. A., Gopal, S., & Song, C. (2001). Forest mapping with a generalized classifier and Landsat TM data. *Remote Sensing of Environment*, *77*, 241–250. doi:10.1016/S0034-4257(01)00208-5

Pontius, J., Martin, M., Plourde, L., & Hallett, R. (2008). Ash decline assessment in emerald ash borer-infested regions: A test of tree-level, hyperspectral technologies. *Remote Sensing of Environment*, *112*, 2665–2676. doi:10.1016/j.rse.2007.12.011

Rullan-Silva, C. D., Olthoff, a. E., Delgado De la Mata, J. A., & Pajares-Alonso, J. A. (2013). Remote monitoring of forest insect defoliation. A review. *Instituto National de Investigacion Y Tecnologia Agraria Y Alimentaria (INIA)*, *22*(3), 377–391. doi:10.5424/fs/2013223-04417

Santos, M. J., Greenberg, J. A., & Ustin, S. L. (2010). Using hyperspectral remote sensing to detect and quantify southeastern pine senescence effects in red-cockaded woodpecker (Picoides borealis) habitat. *Remote Sensing of Environment*, *114*(6), 1242–1250. doi:10.1016/j.rse.2010.01.009

Somers, B., Verbesselt, J., Ampe, E. M., Sims, N., Verstraeten, W. W., & Coppin, P. (2015). Spectral mixture analysis to monitor defoliation in mixed-aged Eucalyptus globulus Labill plantations in southern Australia using Landsat 5-TM and EO-1 Hyperion data. *ITC Journal*. doi:10.1016/j.jag.2010.03.005

Taylor, S. L., & MacLean, D. A. (2008). Validation of spruce budworm outbreak history developed from aerial sketch mapping of defoliation in New Brunswick. Northern Journal of Applied Forestry, 25(3), 139-145.

Thomas, S. J., Deschamps, A., Landry, R., van der Sanden, J. J., & Hall, R. J. (2007). Mapping insect defoliation using multi-temporal Landsat data. Proceedings: Our common borders–safety, security, and the environment through remote sensing, October 28–November 1, Ottawa, Ontario, Canada.

Townsend, P. A., Singh, A., Foster, J. R., Rehberg, N. J., Kingdon, C. C., Eshleman, K. N., & Seagle, S. W. (2012). A general Landsat model to predict canopy defoliation in broadleaf deciduous forests. *Remote Sensing of Environment*, *119*, 255–265. doi:10.1016/j.rse.2011.12.023

Vogelmann, J. E. (1990). Comparison between two vegetation indices for measuring different types of forest damage in the north-eastern United States. *Remote Sensing*, *11*(12), 2281–2297.

Woodcock, C. E., Macomber, S. A., Pax-Lenney, M., & Cohen, W. B. (2001). Monitoring large areas for forest change using Landsat: Generalization across space, time and Landsat sensors. *Remote Sensing of Environment*, *78*, 194–203. doi:10.1016/S0034-4257(01)00259-0

Zhang, T., Liu, H., & Pei, X. (2010). Application of remote sensing technology in monitoring forest diseases and pests. *Plant Diseases and Pests*, *1*, 57–62.

2 CHAPTER 2

CAN EO-1 ALI DATA ESTIMATE SPRUCE BUDWORM DEFOLIATION IN QUEBEC, CANADA?

Abstract

Timely and accurate estimation of the spruce budworm defoliation will provide crucial support to mitigate the socio-economic impact on vulnerable forests. Remotely sensed satellite images make the investigation of infested regions available and convenient. A common approach of interpreting the images and get relevant information about the forests was to derive vegetation indices (VIs) from the remote sensing images. Multispectral data and VIs derived from multispectral images were widely applied for estimation of forest properties. In comparison to the hyperspectral data, moderate spatial resolution multispectral satellite imagery was easier to obtain and to process. Especially, the VIs derived from multispectral imageries have been applied for mapping insect defoliation. Therefore, this study attempted to apply a statistics based correlation analysis using VIs derived from moderate spatial resolution EO-1 Advanced Land Imager (ALI) multispectral imagery to investigate its ability of estimating and mapping spruce budworm defoliation. It suggested that the ALI data could not produce reliable estimation of the SBW defoliation in Quebec, Canada.

Keywords: EO-1 Advanced Land Imager (ALI), multispectral data, spruce budworm defoliation, vegetation index.

2.1 Introduction

Spruce budworm causes severe damages to spruce and fir in Eastern Canada in each of their outbreaks. Finding the location of defoliation caused by spruce budworm was one of the primary as well as difficult tasks for forest experts and relevant government agencies. The considerable size of forest regions makes it extremely time-consuming for field investigations. Even though remote sensing provides an alternative indirect investigation method, the SBW defoliation can be hard to identify from a satellite image since the difference between defoliated forest pixels and healthy forest pixels can be subtle.

With the recent surge in the availability of spectral imaging sensors, the technology of remote sensing offers a potential way to estimate and map insect caused defoliations (e.g., Adelabu, Mutanga, Adam, & Sebego, 2014; Adelabu, Mutanga, & Azong, 2012; de Beurs & Townsend, 2008; Eklundh, Johansson, & Solberg, 2009; Fan, 2006). However, remote sensing of insect defoliation was still a big challenge because it was often hard to find effective way to relate the image data to the defoliation magnitude. A common way was to use the vegetation indices (VIs) derived from remote sensing to estimate vegetation health and greenness and thus estimate the defoliation.

Generally, healthy vegetation will absorb most of the visible light that falls on it, and reflects a large portion of the near-infrared light. The defoliated forest, in form of

unhealthy or sparse vegetation, reflects more visible light and less near-infrared light. Making use of these two spectral bands conventional pairwise VIs can be constructed. A list of investigated VIs can be found in Table 2.1. The widely applied broad-band indices were usually constructed with near-infrared (NIR) and red (R) bands, use average spectral information over broad bandwidths (Blackburn, 1998).

Table 2.1 9 Vegetation indices analyzed in this study

Abbreviation	Formula	Vegetation Index Name	References
SR	ρ_2 / ρ_1	Simple Ratio.	(Qi, Chehbouni, Huete, Kerr, and Sorooshian, 1994), (Birth and McVey, 1968)
DVI	$\rho_2 - \rho_1$	Difference Vegetation Index	(Tucker, 1979)
NDVI	$(\rho_2 - \rho_1)/(\rho_2 + \rho_1)$	Normalized Difference Vegetation Index	(Griffin, May-Hsu, Burke, Orloff, and Upham, 2005)
EVI2	$2.5*(\rho_2 - \rho_1)/(\rho_2 + 2.4*\rho_1)$	2-band Enhanced Vegetation Index	(Jiang et al., 2008)
SAVI	$(\rho_2 - \rho_1)*(1+L)/(\rho_2 + \rho_1 + L)$	Soil Adjusted Vegetation Index	(Huete, 1988)
NLI	$(\rho_2^2 - \rho_1)/(\rho_2^2 + \rho_1)$	Non-Linear Index	(Goel and Qin, 1994; Gong et al., 2003)
MNLI	$(\rho_2^2 - \rho_1)*(1+L)/(\rho_2^2 + \rho_1 + L)$	Modified Non-Linear Index	(Gong et al., 2003)
MSR	$\frac{\rho_2 / \rho_1 - 1}{\sqrt{\rho_2 / \rho_1} + 1}$	Modified Simple Ratio	(Chen, 1996)
RDVI	$(\rho_2 - \rho_1)/\sqrt{\rho_2 + \rho_1}$	Renormalized Difference Vegetation Index	(Roujean and Breon, 1995)

Note that ρ_1 and ρ_2 represent red and NIR wavelengths respectively for constructing traditional vegetation indices but in this study they were extended to all spectral wavelengths provided by 9 available ALI bands.

Gong et al. designed a method for correlating Leaf Area Index (LAI) with VIs constructed using Hyperion data which demonstrate the advantage of across bands VIs construction in modeling biophysical parameters (Gong et al., 2003). To inherit their method, we overlapped the EO-1 ALI multispectral imagery with the ground truth map provided by the Quebec government report (MFFP, 2014). Correlation analysis was applied between the VIs and defoliation measurements. Multispectral bands with high correlation coefficients were examined.

2.2 Study Site and Materials

A set of EO-1 Hyperion and ALI images was acquired from NASA free of charge from June to August, 2014 on a selected site centered at 48°09'54''S/67 °19'21''W near the Causapscal city, across the Bas-Saint-Laurent region which located along the south shore of the lower Saint Lawrence River in the Quebec Province, Canada. It was a relatively homogeneous rural area mostly covered by spruce and fir forests. The two tree species were alike in appearance, both served as preferred habitats for SBW and mixed in the forests in the study site. The high density of trees in the forestry regions makes them vulnerable to spruce budworms and the defoliated regions can be formed as large blocks. According to the aerial survey report "Infested areas of spruce budworm in Quebec in 2014" (Quebec, November 2014), the Bas-Saint-Laurent region was one of the most dominant infested areas by spruce budworm in Quebec, totaled 316,103 hectares. The area affected by SBW continues to rise significantly in the province. In 2014, they totaled 4,275,065 hectares compared to 3,200,348 hectares in 2013. Part of the ALI imagery was

selected as study site (Figure 2.1) to match with the Interpretation ground truth of SBW infested fields provided by the Quebec government report (MFFP, 2014).

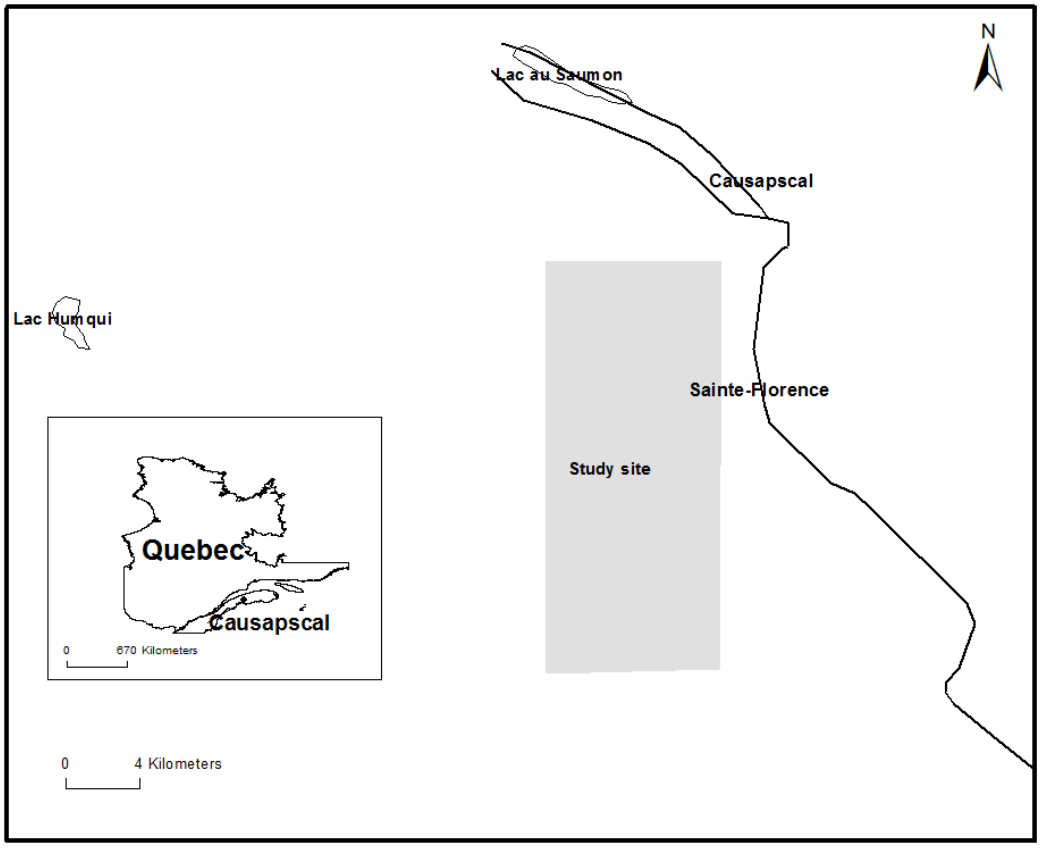

Figure 2.1 Study site

The selection of imagery was determined by both the image quality which heavily affected by the cloud condition and the acquisition date which should reflect most infested areas. An EO-1 ALI multispectral image over the study site acquired on July 19, 2014, around 10:20 A.M. local time for this study. All nine of the ALI image's 30 m resolution multispectral bands were used to apply vegetation indices analysis in this

study. The image was processed to Standard Terrain Correction (Level 1T) before being downloaded from the USGS website. Since the imagery was ortho-rectified, only the ground truth map needs georefferencing in order to match both of them.

Interpretation ground truth of SBW infested fields was provided by the Quebec government report (MFFP, 2014). The aerial survey of damage caused by major forest pests was carried out annually by the Ministry of Forests, Fauna and Parks (Ministère des Forêt, de la Faune et des Parcs, MFFP). The SBW defoliation magnitude levels were provided by the aerial survey report (MFFP, 2014) and one thematic map covering our study site has been used. The report classifies defoliation into three classes: slight (loss of foliage in the upper third of the tops of some trees), moderate (loss of foliage in the upper half of the top of most trees) and severe (loss of foliage on the entire length of the top of most trees). In order for further process, the three classes were quantified into three percentage levels: 33.3% for slight level, 50% for moderate level and 100% for severe level.

According to the study of Dr. Taylor and Dr. MacLean in 2008 (Taylor & MacLean, 2008), from 1985 to 1993, 85% of 332 cases were correctly classified by aerial estimate. They concluded that aerial surveys provide a reasonable estimate of defoliation.

2.3 Methodology

2.3.1 Data Pre-processing

The pre-processing of ALI data was different from that of Hyperion data. The digital numbers were converted into radiance values by using the multiplicative factors

and the additive factors of each band (Chander et al., 2009). Radiance of all nine multispectral bands was input into the Fast Line-of-sight Atmospheric Analysis of Spectral Hypercubes (FLAASH), an atmospheric correction module implemented in the ENVI software (ITT Visual Information Solutions, Boulder, CO, USA) to calibrate the at-sensor radiance data to land surface reflectance. The FLAASH model was run following the "ENVI FLAASH Module User's Guide" (ITT Visual Information Systems, 2006). As ALI level L1T data were in units of W/(m2 sr μm) while the FLAASH atmospheric correction software uses units of μW/(cm2 sr nm), the scale factors 10 were used when running the FLAASH model. The projection of the ALI L1T data was UTM 19N, datum WGS 84. In order to match the ground truth map with the ALI L1T imagery, geometric correction was conducted on the ground truth map provided by (MFFP, 2014) using the ENVI software.

2.3.2 Vegetation Indices Construction and correlation with defoliation

After overlapping the EO-1 ALI imagery with the ground truth map, 30 sample pixels were selected as we retrieve reflectance values from the calibrated ALI images with correspondence with the defoliation. Note that the spatial resolution of ALI data was 30 meters which makes each pixel a mixture of a large number of trees. So the 30 points were all selected within homogeneous forests areas by examining the ALI image. In addition, the ground truth map was roughly delineated that not available for pixel-by-pixel match with our image. So in order to make sure selected samples contain relatively accurate defoliation magnitude, we avoid regions near the boundaries of different classes on the map. This gives us 30 observations of defoliation magnitude which constitute a

defoliation variable. Furthermore, we need 30 observations of VI which constitute a VI variable. In this study, we use 9 available EO-1 ALI bands to construct 9 two-band VIs, so that will end up with 9x9x9 different VI variables that will be ran through our correlation test.

In this study, we use the correlation method developed in (Gong et al., 2003). For each of the 9 VIs, a linear correlation coefficient R^2 was calculated between the VI and defoliation measurement (30 samples). Since each VI in Table 2.1 could be constructed from any pair among the possible 9 bands, a linear correlation coefficient R^2 matrix could be constructed. From the correlation matrices, ALI bands with high correlation coefficients were examined.

2.3.3 Mapping SBW defoliation using VIs

Based on the correlation results, the most relevant VIs and associated bands in terms of defoliation estimation would be selected for mapping SBW defoliation. The mapping results were assessed at a selected region in which two pieces of forests were clearly separated by their defoliation levels: severe and light as shown in Figure 2.2(b). The subset image of the assessment region was extracted. Then a histogram equalization was applied on each VI image followed by a global image threshold using Otsu's method (Smith et al., 1979). So the classification result will become a binary image with white pixels representing severe defoliation areas while black pixels representing light defoliation areas, as shown in Figure 2.2(c). Finally, the assessments were conducted by comparing the mapping results with the ground truth map pixel-by-pixel.

2.4 Results and Discussion

Based on the highest correlation values for all 9 VIs used in this study, the associated ALI spectral band pairs, wavelengths, bandwidths and spectral regions were summarized respectively in Table 2.2.

Table 2.2 9 Vegetation indices derived from ALI bands

Index	R^2	ALI spectral bands ρ_1 / ρ_2	Wavelength (nm) ρ_1 / ρ_2	Bandwidth(nm) ρ_1 / ρ_2	Spectral Region ρ_1 / ρ_2
NDVI	0.21	7 / 1p	2226 / 442	272 / 19	SWIR / VNIR(blue)
DVI	0.23	5 / 1p	1640 / 442	171 / 442	SWIR / VNIR(blue)
EVI2	0.22		Similar to DVI's		
SR	0.11	4p / 2	866 / 567	44 / 70	VNIR / VNIR(green)
SAVI	0.21		Similar to NDVI's		
NLI	0.28	5 / 1p	1640 / 442	171 / 442	SWIR / VNIR(blue)
MNLI	0.28		Similar to NLI's		
MSR	0.11	4 / 2	790 /567	31 / 70	VNIR / VNIR(green)
RDVI	0.22		Similar to NDVI's		

For each of the 9 VIs, the highest correlation values yielded were summarized in second column. From the third to sixth column, the applied ALI spectral band pairs, their respective wavelengths, bandwidths and spectral regions were summarized.

As shown in the table, all VIs constructed with ALI fail to provide a reliable correlation with the defoliation data (with a highest of 0.28 among all obtained), in other

words, the VIs constructed from EO-1 ALI multispectral data could not estimate spruce budworm defoliation in the study site of Quebec, Canada.

The accuracy assessment was done pixel by pixel to quantify how well ALI VIs can map the spruce budworm defoliation. The NLI which generated the highest correlation value among the ALI VIs was used as a mapping example. As shown in Figure 2.2, the extract binary image (b) from NLI image (a) fails to differentiate the light defoliation level from the severe level as marked by the ground truth (b), as most of the vegetation pixels were considered as light defoliated. Similar results stay for the change of threshold applied for converting the index image to binary image.

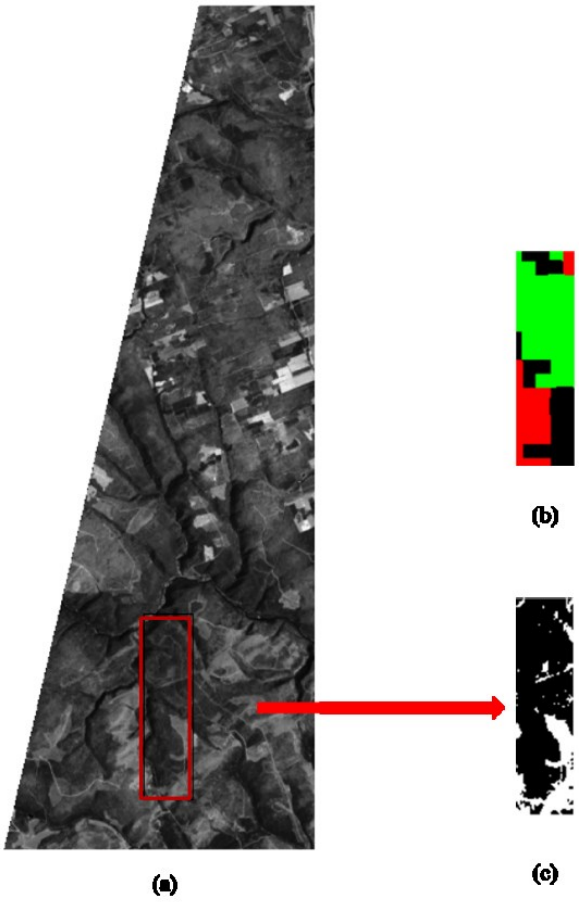

Figure 2.2 Defoliation mapping result using NLI index of the study site. (a) A grayscale image of the testing area; (b) Ground truth map of assessment region where green blocks were light defoliated areas and red blocks were severely defoliated areas; (c) Defoliation results detected in EO-1 ALI MS image where black pixels indicate light defoliated pixels and white pixels indicate severely defoliated pixels.

Poor results also reflect on accuracy assessment, for light/severe level, the mapping result from NLI provided User's accuracy of 22% / 54% and Producer's accuracy of 99% / 0% with an overall accuracy of 32%. As anticipated, the performance was poorer than by chance, which in our specific case was 50% / 50% for either level. Thus the kappa coefficient -0.24 was negative.

The mapping result and the correlation results consistently suggest the incapability of moderate resolution multispectral satellite images in terms of estimation of the SBW defoliation in our study site. Even though the multispectral images were easier to obtain as well as process, the lack of spectral information could lead to its failure of monitoring certain phenomenon of interest. This result stimulates us to investigate if it was possible to improve the results by using hyperspectral images.

2.5 Conclusions

This study investigated if moderate spatial resolution EO-1 ALI multispectral imagery could estimate and map spruce budworm defoliation in a study area located in Quebec, Canada. VIs based correlation analysis were applied. By correlating the VIs derived from EO-1 ALI data, the results suggest all of the VIs fail to estimate the defoliation information derived from our ground truth map. The low accuracies further demonstrated the incapability of multispectral ALI data in mapping SBW defoliation in Quebec. Thus, moderate spatial resolution multispectral imagery was not recommended for mapping the defoliation caused by spruce budworm in sites similar to our study site.

Acknowledgement

This research was funded by the Canada Research Chair Program. The authors would like to thank NASA for collecting the ALI images of the testing areas.

References

Adelabu, S., Mutanga, O., Adam, E., & Sebego, R. (2014). spectral discrimination of insect defoliation levels in mopane woodland using hyperspectral data. IEEE Journal of Selected Topics in Applied Earth Observations and Remote Sensing, 7(1), 177–186. doi:10.1109/JSTARS.2013.2258329

Adelabu, S., Mutanga, O., & Azong, M. (2012). A review of remote sensing of insect defoliation and its implications for the detection and mapping of imbrasia belina defoliation of mopane woodland. The African Journal of Plant Science and Biotechnology, 6(1):1-13. 2011.12.

Blackburn, G. A. (1998). Quantifying chlorophylls and caroteniods at leaf and canopy scales. Remote Sensing of Environment, 66(98), 273–285. doi:10.1016/S0034-4257(98)00059-5

Chander, G., Markham, B. L., & Helder, D. L. (2009). Summary of current radiometric calibration coefficients for Landsat MSS, TM, ETM+, and EO-1 ALI sensors. Remote sensing of environment, 113(5), 893-903.

De Beurs, K. M., & Townsend, P. A. (2008). Estimating the effect of gypsy moth defoliation using MODIS. Remote Sensing of Environment, 112, 3983–3990. doi:10.1016/j.rse.2008.07.008

Eklundh, L., Johansson, T., & Solberg, S. (2009). Mapping insect defoliation in Scots pine with MODIS time-series data. Remote Sensing of Environment, 113(7), 1566–1573. doi:10.1016/j.rse.2009.03.008

Fan, H. (2006). Satellite remote sensing of cumulative spruce budworm defoliation in Prince Albert National Park. University of Saskatchewan Electronic Theses and Dissertations.

Gong, P., Pu, R., Biging, G. S., & Larrieu, M. R. (2003). Estimation of forest leaf area index using vegetation indices derived from Hyperion hyperspectral data. Geoscience and Remote Sensing, IEEE Transactions on, 41(6), 1355–1362.

ITT Visual Information Systems (2006). "ENVI FLAASH Module User's Guide (2006 Edition)." [Online] September 21, 2012: ftp://popo.jpl.nasa.gov/pub/ENVI_Installers/ENVI_Documentation/docs/FLAASH_Module.pdf.

Ministère des Forêt, de la Faune et des Parcs (MFFP). (2014). Aires infestées par la tordeuse des bourgeons de l'épinette au Québec en 2014. Version 1.0 [Online] September 2014:

http://www.mffp.gouv.qc.ca/publications/forets/fimaq/insectes/tordeuse/TBE_2014_P.pdf

Smith, P., Reid, D. B., Environment, C., Palo, L., Alto, P., & Smith, P. L. (1979). A Threshold Selection Method from Gray-Level Histograms. IEEE Transactions on Systems, Man, and Cybernetics, 9(1), 62–66. doi:10.1109/TSMC.1979.4310076

Taylor, S. L., & MacLean, D. A. (2008). Validation of spruce budworm outbreak history developed from aerial sketch mapping of defoliation in New Brunswick. Northern Journal of Applied Forestry, 25(3), 139-145.

3 CHAPTER 3

REMOTE SENSING OF SPRUCE BUDWORM DEFOLIATION USING EO-1 HYPERION HYPERSPECTRAL DATA: AN EXAMPLE IN QUEBEC, CANADA

Abstract

Each year, the spruce budworm (SBW) causes severe, widespread damage to spruces and true fir in east coast Canada. Early estimation of the defoliation will provide crucial support to mitigate the socio-economic impact on vulnerable forests. Remote sensing techniques were more suitable to investigate the affected region usually consists of large and inaccessible forestry areas. Derived from satellite images, surface reflectance at two or more wavelengths were combined to generate vegetation indices (VIs) which indicate relative abundance of features of interest. Forest health analysis based on VIs was considered as one of the primary information sources for monitoring vegetation conditions. Especially the spectral resolution of Hyperion hyperspectral imagery used in this study, allows for examination of the red-NIR spectrum in more detail, which helps to identify areas of stressed vegetation. Several existing narrowband vegetation indices were used to indicate the overall amount and quality of photosynthetic material and moisture content in vegetation. By integrating the information from VIs that focused at different aspects of overall health and vigor in forested areas, the study aims at investigating the defoliation in a forested region in the province of Quebec, Canada. Two Hyperion images

applied in this study were acquired on June and August, 2014 respectively from NASA. The changes of health and vigor were observed and quantitatively compared as remote sensing images from different time were applied. The experimental results suggest the narrowband VIs based forest health analysis has potential for estimation of SBW defoliation in the study site.

Keywords: Hyperion, hyperspectral data, spruce budworm defoliation, vegetation index.

3.1 Introduction

The spruce budworm was arguably the most damaging insect of North America's forest and, in Canada, it occurs throughout most of the range of spruce and balsam fir (Gray, 2008). Defoliation begins at the top of the tree and quickly progresses to the periphery of the crown from the top downwards. Current-year needles were partially or completely consumed. Spruce budworm larvae also feed on staminate (male) flowers and cones. During epidemics, the larvae may destroy all of the cones (Boulanger et al., 2012). In the province of Quebec, Canada, the government conducted survey and released reports annually on the SBW defoliation. They concluded that in 2014, the areas affected by SBW continue to rise significantly in the province. In 2014, they totaled 4,275,065 hectares compared to 3,200,348 hectares in 2013 (MFFP, 2014). Conventional Strategies to eliminate or slow the spread of these destructive pests such like pesticide spraying can be costly, time consuming and less effective when accurate estimation of defoliated regions was not available. The sizes and locations of defoliated regions make field

investigation difficult. Aerial survey was considered an option to provide relative accurate mapping as investigator has a relatively close look at the trees when flight height was accordingly adjusted. This kind of operation has been conducted in Quebec, Canada directed by Ministry of Forests, Fauna and Parks (Ministère des Forêt, de la Faune et des Parcs, MFFP), Government of Quebec, to provide defoliation mapping results across the province. However, the operation calls for considerable involvement of man-power and was meanwhile time-consuming. Alternatively, remote sensing techniques, especially the utilize of satellite images, provide wide spatial coverage, high temporal repeatability and increasing spatial resolutions make them suitable for such investigations.

There were many studies where remote sensing techniques have been applied to detect, map and monitor forest insect damage in the past decades. For instance, Townsend et al. (2012) used Landsat data to predict defoliation severity caused by *Lymantria dispar* in deciduous forests. Eklundh et al. (2009) assessed defoliation by the European pine sawfly in pine forests using Moderate Resolution Imaging Spectroradiometer (MODIS) time-series data. Data from the same sensor have been also applied to estimate the magnitude of defoliation caused by a gypsy moth outbreak that occurred in the US. Study was also conducted on evaluating the sensitivity of multi-temporal Landsat-5 TM data and a single date SPOT4 HRVIR Image to cumulative SBW defoliation in the Prince Albert National Park, Saskatchewan, Canada (Han et al., 2002).

To facilitate their investigation, most of abovementioned research involves with construction of vegetation indices from the remote sensing data, which have been successfully applied on estimating and mapping field forest ecosystem variables or

properties (Gong et al., 2003; Rullan-Silva et al., 2013). Detection of vegetation stress by remote sensing techniques was based on the assumption that stress factors interfere with photosynthesis or the physical structure of the vegetation and affect the absorption of light energy and thus alter the reflectance spectrum of vegetation (Riley, 1989; Pinter and Hatfield, 2003). The vegetation indices (VIs) derived from remote sensing were generally used to estimate vegetation health and greenness (Rullan-Silva et al., 2013). Healthy vegetation will absorb most of the visible light that falls on it, and reflects a large portion of the near-infrared light. The defoliated forest, in form of unhealthy or sparse vegetation, reflects more visible light and less near-infrared light. The widely applied broad-band indices were thus usually constructed with near-infrared (NIR) and red (R) bands, use average spectral information over broad bandwidths (Blackburn, 1998).

However, the broad-band VIs have limited spectral information concerning the significance of response at different spectral wavelengths. As an alternative, more refined VIs can be constructed through the use of distinct narrow bands from hyperspectral images. Instead of indicating general health or greenness, the narrow-band VIs provide more specific information regarding the overall amount and quality of photosynthetic material and moisture content in vegetation. Thus they have advantage over broad-band VIs in quantifying different biophysical characteristics of vegetation (Gong et al., 2003). It was also believed that the hyperspectral data can be useful in early stress detection as spectral differences can be identified from only certain wavelengths while existing remote sensing studies on SBW defoliation use mostly broadband VIs or limited narrow

bands VIs (Rullan-Silva et al., 2013). However, little evidence has been found on mapping SBW defoliation using hyperspectral VIs (Rullan-Silva et al., 2013).

The hyperspectral data from the Hyperion sensor on the Earth Observing-1 Mission (EO-1) satellite was used in this study. Unlike expensive high-resolution multispectral images, the Hyperion hyperspectral images were provided by NASA free of charge. Despite their coarse spatial resolution (30m), they provide a 10 nm spectral resolution across spectral bands from 0.4 to 2.5 μm (Ungar et al., 2003). The fine spectral resolution increases the capability to distinguish structures and objects in the image scene (Curran, 1989). Furthermore, access to multi-temporal images captured by the same hyperspectral sensor allows for assessment of changes occurred during the period of time, when SBW activities continuously accumulate. This measurement was carried out by observing the spectral changes on hyperspectral images by means of VIs. Seven VIs derived from the Hyperion images representing different bio-physical properties were used to measure the change during SBW defoliation. Three different VIs were combined to assess the forest health for estimation of SBW defoliation magnitudes. The aerial survey map provided by MFFP was used as reference.

3.2 Study Site and Materials

3.2.1 Study site

Several EO-1 campaigns were established during June, July and August, 2014 on a selected site centered at 48°14'32.69"S/ 67°25'45.77"W to the east of the Sainte-Florence village, west of Lac Humqui, at the southern part of the Bas-Saint-Laurent region which

located along the south shore of the lower Saint Lawrence River in the Quebec Province, Canada (Figure 3.1). It was a relatively homogeneous rural area mostly covered by spruce and fir forests. The two tree species were alike in appearance, both served as preferred habitats for SBW and mixed in the forests in the study site. The high density of trees in the forestry regions makes them vulnerable to spruce budworms and the defoliated regions can be formed as large blocks. According to the aerial survey report "Infested areas of spruce budworm in Quebec in 2014" (Quebec, November 2014), the Bas-Saint-Laurent region was one of the most dominant infested areas by spruce budworm in Quebec, totaled 316,103 hectares. The area affected by SBW continues to rise significantly in the province. In 2014, they totaled 4,275,065 hectares compared to

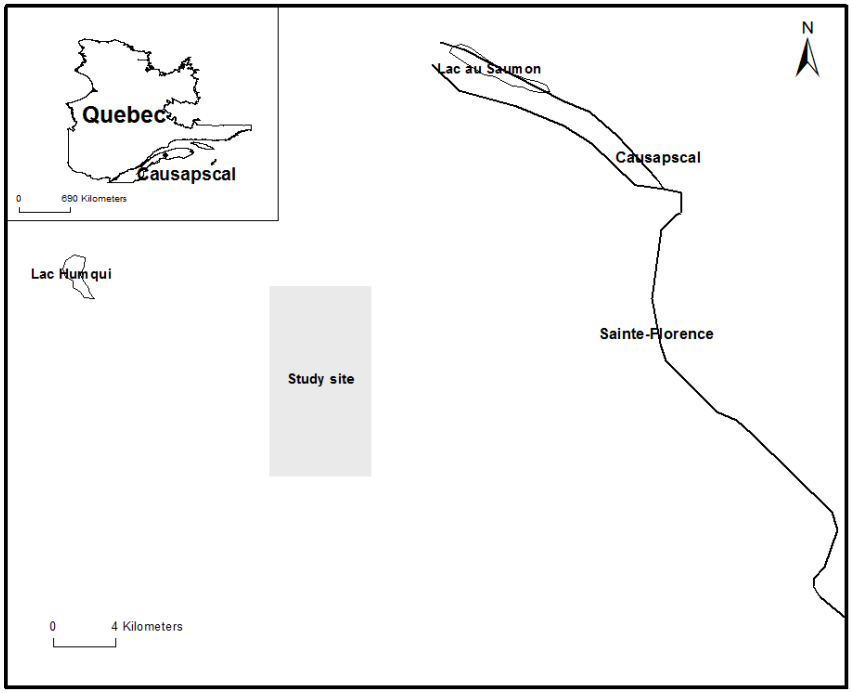

Figure 3.1 Study site

3,200,348 hectares in 2013.

3.2.2 Materials

Interpretation reference of SBW infested fields was provided by the Quebec government report (MFFP, 2014). The aerial survey of damage caused by major forest pests was carried out annually by the Ministry of Forests, Fauna and Parks (Ministère des Forêt, de la Faune et des Parcs, MFFP), Government of Quebec. The aerial survey scans natural disturbances observed from the air in real time. The observations digital rendering was done to the screen with a stylus. To facilitate the work of the observer, a topographic map was displayed on the screen depending on the route of the aircraft. These geo-

referenced data was then processed and analyzed using geographic information system (GIS) software. The aerial survey scans natural disturbances observed from the air in real time. The aircraft flies at an altitude of about 240 meters, at a speed of 160 km / h, keeping a distance of 4.5 kilometers between flight lines. The survey reports three levels of defoliation in Quebec, namely slight, moderate and serious, containing the study site mentioned above.

The SBW defoliation magnitude levels were provided by the aerial survey report (MFFP, 2014) and one thematic map covering our study site has been used. The report classifies defoliation into three classes: slight (loss of foliage in the upper third of the tops of some trees), moderate (loss of foliage in the upper half of the top of most trees) and severe (loss of foliage on the entire length of the top of most trees). In order for further process, the three classes were quantified into three percentage levels: 33.3% for slight level, 50% for moderate level and 100% for severe level.

According to the study of Dr. Taylor and Dr. MacLean in 2008 (Taylor & MacLean, 2008), from 1985 to 1993, 85% of 332 cases were correctly classified by aerial estimate. They concluded that aerial surveys provide a reasonable estimate of defoliation.

A set of EO-1 Hyperion images was acquired from NASA free of charge from June to August, 2014. They were targeted to cover the abovementioned study site in order to investigate the defoliation magnitude. The selection of imagery was determined by both the image quality which heavily affected by the cloud condition and the acquisition date which should reflect most infested areas. Two EO-1 Hyperion hyperspectral images were

acquired over the study site. The first one were captured on June 16, 2014, around 10:20 A.M. local time and the second one were captured on August 7, 2014, around 10:30 A.M. local time. The image was at level L1R processing, meaning that it was only radiometrically corrected and with no geometrically correction applied (Beck, 2003).

3.3 Methodology

To process acquired image data for SBW defoliation analysis, the method used in this study consists of two major parts: data preprocessing and VIs based change detection. The pre-processing of Hyperion data includes: band selection, abnormal pixels removal, vertical stripe removal, smile effect correction, atmospheric correction, and geometric correction. The VIs based change detection includes: construction of individual VIs from multi-temporal images, change detection based on each VI images, synthesize several VIs to generate forest health map and change detection based on the health map.

3.3.1 Data Preprocessing

Since Hyperion operates from a space platform with consequently modest surface signal levels and full-column atmospheric effects, its data demand careful processing to manage sensor and processing noise (Datt et al., 2003). The approach taken here involves band selection which only keeps necessary and useful spectral bands for further analysis, noise removal including abnormal pixels and vertical striping noise that existed in visible near-infrared (VNIR 400–1000 nm) and shortwave infrared (SWIR 900–2500 nm) arrays, "smile effect" removal that adjust the wavelength centers and radiometric and

atmospheric correction to apparent surface reflectance. Finally, the reflectance image will be geometrically corrected by georeferencing to common geographic coordinates.

The Hyperion sensor acquire image data with 242 bands in total, including 70 visible-near-infrared (VNIR) bands, and 172 shortwave-infrared (SWIR) bands. Among them, 44 bands were intentionally not illuminated or correspond to areas of low sensitivity of the spectrometer materials. In addition, two more zero bands were identified in our data of use, which were band 80 and 81. Among the other 196 bands, only 194 bands were unique (NIR bands 8-57, 427-925 nm and SWIR bands 79-224, 912-2395 nm) because there were four bands in the overlap between the two spectrometers of VNIR and SWIR. In addition, atmospheric water vapor bands which absorb almost the entire incident and reflected solar radiation and the bands that have very severe vertical stripping were identified by visual inspection of the image data (Datt et al., 2003). Thus, the subset of 162 selected bands (bands 10-57, 77-79, 82-119, 134-165, and 181-221 within 447-2365 nm) were applied in this study.

Abnormal pixels that have lower DN values as compared to their neighboring pixels were corrected by replacing their DN values with the average DN values of their immediate left and right neighboring pixels (Han et al., 2002). Vertical stripes were removed using the “SPEAR Vertical Stripe Removal” in the ENVI software (ITT Visual Information Systems, 2006) (Datt et al., 2003). The "smile effects" that refer to an across-track wavelength shift from center wavelength due to the change of dispersion angle with field position (Goodenough et al., 2003) were removed using the procedure of "Cross-Track Illumination Correction" (Jupp et al., 2003) in the ENVI software (ITT Visual

Information Systems, 2006). This study uses the Fast Line-of-sight Atmospheric Analysis of Spectral Hypercubes (FLAASH), an atmospheric correction module implemented in the ENVI to calibrate the at-sensor radiance data to land surface reflectance (Beck, 2003).

Both Hyperion images from June and August were geometrically corrected using the ENVI "Image to Map Registration" process. They were first projected to datum WGS 84 and the "Geographic lat/lon" projection was selected. The latitude and longitude of selected ground control points were matched on Google Earth. An overall root mean square error (RMSE) of 0.37 pixel and 0.28 pixel were achieved respectively for both images. The defoliation map used as reference was also georeferenced using the same setting.

3.3.2 Vegetation Indices Construction

Presence and condition of leaf foliage were reliable indicators of tree health, similarly as canopy foliage was of the forest stand. Research on forest VIs was aimed to the spectral identification, detection and quantification of forest health (Rullan-Silva et al., 2013). Water, pigments, nutrients, and carbon were each expressed in the reflected optical spectrum from 400 nm to 2500 nm, with often overlapping, but spectrally distinct, reflectance behaviors. These known signatures allow scientists to combine reflectance measurements at different wavelengths to enhance specific vegetation characteristics by defining VIs. In order to measure the change of forestry bio-physical properties during the SBW defoliation, 13 VIs of 3 major different categories (vegetation greenness, Canopy Water Content and Light Use Efficiency) concerning different aspects of forest

health were calculated using ENVI, as shown in Table 3.1.

Table 3.1 13 Vegetation indices applied for change detection

Abbreviation	Formula	Vegetation Index Name	Category
SR	$\frac{NIR}{RED}$	Simple Ratio.	Broadband Greenness
NDVI	$\frac{NIR - RED}{NIR + RED}$	Normalized Difference Vegetation Index	
EVI	$2.5 * \frac{NIR - RED}{NIR + 6 * RED - 7.5 * BLUE + 1}$	Enhanced Vegetation Index	
ARVI	$\frac{NIR - [RED - \gamma(BLUE - RED)]}{NIR + [RED - \gamma(BLUE - RED)]}$	Atmospherically Resistant Vegetation Index	
RENDVI	$\frac{\rho_{750} - \rho_{705}}{\rho_{750} + \rho_{705}}$	Red Edge Normalized Difference Vegetation Index	Narrowband Greenness
MRESR	$\frac{\rho_{750} - \rho_{445}}{\rho_{750} + \rho_{445}}$	Modified Red Edge Simple Ratio	
MRENDVI	$\frac{\rho_{750} - \rho_{705}}{\rho_{750} + \rho_{705} - 2 * \rho_{445}}$	Modified Red Edge Normalized Difference Vegetation Index	
MSI	$\frac{\rho_{1599}}{\rho_{819}}$	Moisture Stress Index	Canopy Water Content
WBI	$\frac{\rho_{970}}{\rho_{900}}$	Water Band Index	
NDWI	$\frac{\rho_{857} - \rho_{1241}}{\rho_{857} + \rho_{1241}}$	Normalized Difference Water Index	
PRI	$\frac{\rho_{531} - \rho_{570}}{\rho_{531} + \rho_{570}}$	Photochemical Reflectance Index	Light Use Efficiency
SIPI	$\frac{\rho_{800} - \rho_{445}}{\rho_{800} + \rho_{680}}$	Structure Insensitive Pigment Index	
RDRI	$\frac{\sum_{i=600}^{699} R_i}{\sum_{i=500}^{599} R_j}$	Red Green Ratio Index	

The vegetation greenness was further divided into broadband greenness and narrowband greenness VIs. The broadband greenness VIs were most commonly used as they can be derived from broadband multispectral sensors, such as AVHRR, Landsat TM, and QuickBird. As long as the sensor provides image data covering near infrared and visible regions, the VIs can be constructed without very precise spectral resolution. In Table 2.1, NIR stands for a near infrared band and Red stands for a Red band. NDVI was the most widely used broadband VIs. Note that as Hyperion hyperspectral data with finer spectral resolution than multispectral images, the NDVI as well as other broadband VIs listed above derived from Hyperion image was not technically broad as that derived from multispectral images. For calculation, it chooses the band nearest 650 nm for the Red term and the band nearest 860 nm for the NIR term. SR and NDVI were considered the simplest measures of the general quantity and vigor of green vegetation. Both of them were combinations of reflectance measurements that were sensitive to the combined effects of foliage chlorophyll concentration, canopy leaf area, foliage clumping, and canopy architecture. These VIs were designed to provide a measure of the overall amount and quality of photosynthetic material in vegetation, which was essential for understanding the state of vegetation for any purpose. Both EVI and ARVI attempt to reduce the atmospheric influence on NDVI, ARVI uses blue reflectance to correct red reflectance for atmospheric scattering (the adjustment parameter γ was set to be 1 as default) while EVI uses the blue reflectance region to correct for soil background signals.

Narrowband reflectance measurements take advantage of finer spectral resolution of hyperspectral sensors. Specifically, the spectra of incident vegetation pixels were used

to locate a so-called “red edge” in order to enhance the performance of original VIs. Red edge was defined as the steeply sloped region of the vegetation reflectance curve between 690 nm and 740 nm that was caused by the transition from chlorophyll absorption and near-infrared leaf scattering. Increased chlorophyll concentration broadens the absorption feature and moves the red edge to longer wavelengths. It was believed that making narrowband measurements in the red edge allows these indices to be more sensitive to smaller changes in vegetation health than the broadband greenness VIs, particularly in conditions of dense vegetation where the broadband measures can saturate.

The canopy water content VIs provide a measure of the amount of water contained in the foliage canopy. Water content was an important quantity of vegetation because higher water content indicates healthier vegetation that was likely to grow faster and be more fire-resistant. Canopy water content VIs use reflectance measurements in the near-infrared and shortwave infrared regions to take advantage of known absorption features of water and the penetration depth of light in the near-infrared region to make integrated measurements of total column water content. Several relevant wavelengths were discovered and applied to construct VIs to represent water content. As the absorption around 1599 nm increases with the increasing of water content in canopies while absorption around 819 nm stays stable, MSI was constructed by taking advantage of these two wavelengths. Two reflectance values at 857 nm in NIR region and 1241 nm in SWIR region respectively were used to calculate NDWI, a measurement of their relative difference was sensitive to changes in vegetation canopy water content. Similarly, reflectance at 970 nm and 900 nm were used to calculate WBI.

The light use efficiency VIs provide a measure of the efficiency with which vegetation can use incident light for photosynthesis. Light use efficiency was highly related to carbon uptake efficiency and vegetative growth rates. Thus the light use efficiency VIs provide measurements of the efficiency with which vegetation can use incident light for photosynthesis. It was also an important indicator of forest health and SBW defoliation, as defoliated forests will suffer from a decreased ability of light use. Most reflectance measurements within visible region were applied to construct light use efficiency VIs. Photochemical Reflectance Index (PRI) was designed to be sensitive to changes in carotenoid pigments in live foliage. Carotenoid pigments were indicative of photosynthetic light use efficiency, or the rate of carbon dioxide uptake by foliage per unit energy absorbed. Structure Insensitive Pigment Index (SIPI) was designed to maximize the sensitivity of the index to the ratio of bulk carotenoids (for example, alpha-carotene and beta-carotene) to chlorophyll while decreasing sensitivity to variation in canopy structure (for example, leaf area index). Increases in SIPI were thought to indicate increased canopy stress (carotenoid pigment). The Red Green Ratio Index (RGRI) on the other hand, has been used to estimate the course of foliage development in canopies. It was an indicator of leaf production and stress, and it may also indicate flowering in some canopies. The SBW has the potential of interfering with growth of spruce and fir, specifically during the summer season.

3.3.3 VIs based Change Detection and Forest Stress Analysis

High resolution Landsat imagery has been widely used in change detection of insect defoliation. A normal approach was using one image before the defoliation and one

immediately after the defoliation. However, this kind of analysis can be less applicable when one of the images were not available, especially the image that capturing the healthy forests prior to defoliation. Moreover, it was still difficult to determine such a pre-defoliation image, if existed, has such desirable condition, as defoliation from previous years can be involved (de Beurs and Townsend, 2008). Finally, the long period between two captures can result in the occurrences of forest disturbance other than the one of particular interest. It was also a difficult task to differentiate forest stress from insect defoliation from natural factors like rainfall, temperature, climate changes, etc. Thus, this study focuses on the investigation of spread of defoliation in our study site during the summer within the year of 2014. The image data were captured on June and August respectively at the study site during the significant SBW defoliation.

In eastern North America, the spruce budworm damage appears in May, when third instar larvae begin to feed. Moths emerge from pupal cases usually in late July or early August. In late June, feeding terminates showing the damage to host trees as rust brown due to the accumulation of frass, chewed desiccated needles, dead buds and silken webbing. The damage continues in the summer and accumulates defoliation for current year. The damage reaches the peak approximately in August, and then SBW becomes less active as temperature drops in the fall. Thus in this study we aim at monitoring SBW defoliation in June and August in order to compare and analysis its spread and accumulation in the study site.

The strategy of using VIs in this study was to find most relevant VIs in each category as described and use them to carry out forest stress analysis. In order to find

those specific VIs out of their alternatives, change detections were applied using acquired Hyperion images. After suitable pre-processing and alignment of the images, we will be able to monitor the changes of VIs values in pixel level. This will allow for quantitative analysis on the influence of SBW defoliation on different aspects of forest health. Pixel level change detection will be applied for each VIs image derived from two multi-temporal images. The relative difference of VIs (de Beurs and Townsend, 2008) was applied to calculate individual change detection for each VIs image:

$$\text{Change Rate}(\%) = \frac{\text{VI}_{\text{before}} - \text{VI}_{\text{during}}}{\text{VI}_{\text{before}}} \times 100,$$

where $\text{VI}_{\text{before}}$ was the value of a vegetation index at the high point before defoliation and $\text{VI}_{\text{during}}$ was the value of the vegetation index at the low point during the defoliation event. In this study, $\text{VI}_{\text{before}}$ was derived from the June image whereas $\text{VI}_{\text{during}}$ was derived from the August image. In order to make the change detection of other VIs more efficient and accurate, the NDVI values derived from both images were used as masks. To be specific, a NDVI value of 0.2 was used to delineate only vegetation pixels on which change detections will be conducted. The change rate of each VI was also summarized in a region level. Using the aerial survey map as a reference, the change rates at each defoliation magnitude level (light, moderate and severe) were averaged from pixels within each region.

Furthermore, three selected VIs were synthesized to analyze forest health in order to estimate the spread of defoliation. This was done using “Forest Health Tool” provided by ENVI software (ITT Visual Information Systems, 2006). A spatial map was generated

to show the overall health and vigor of a forested region. Forest health mapping was useful for detecting pest and blight conditions in a forest, and it was useful in assessing areas of timber harvest. A forest exhibiting low stress conditions was usually made up of healthy vegetation, whereas a forest under high stress conditions shows signs of dry or dying plant material, very dense or sparse canopy, and inefficient light use. The spatial maps generated for two multi-temporal images will then be aligned with aerial survey map for comparison.

3.4 Results and Analysis

3.4.1 Hyperion Data Pre-processing

The resultant radiance image from vertical stripes removal and cross track illumination correction was examined via MNF transformation (Datt et al., 2003). The MNF technique responds to interactions between the spatial structure of the data and that of the noise when the noise has strong spatial structure. As shown in Figure 3.2, the first and sixth MNF bands were generated from MNF transformation on original and output radiance data. Specifically "smile effect" can lead to a brightness gradient appearing in the first MNF band as shown in Figure 3.2(a) and (e). Stripes can be illustrated in subsequent MNF bands as shown in Figure 3.2(b) and (f). The brightness gradient was removed after the correction as shown in MNF band 1 in Figure 3.2 (c) and (g). The stripes were removed as shown in MNF band 6 in Figure 3.2 (d) and (h).

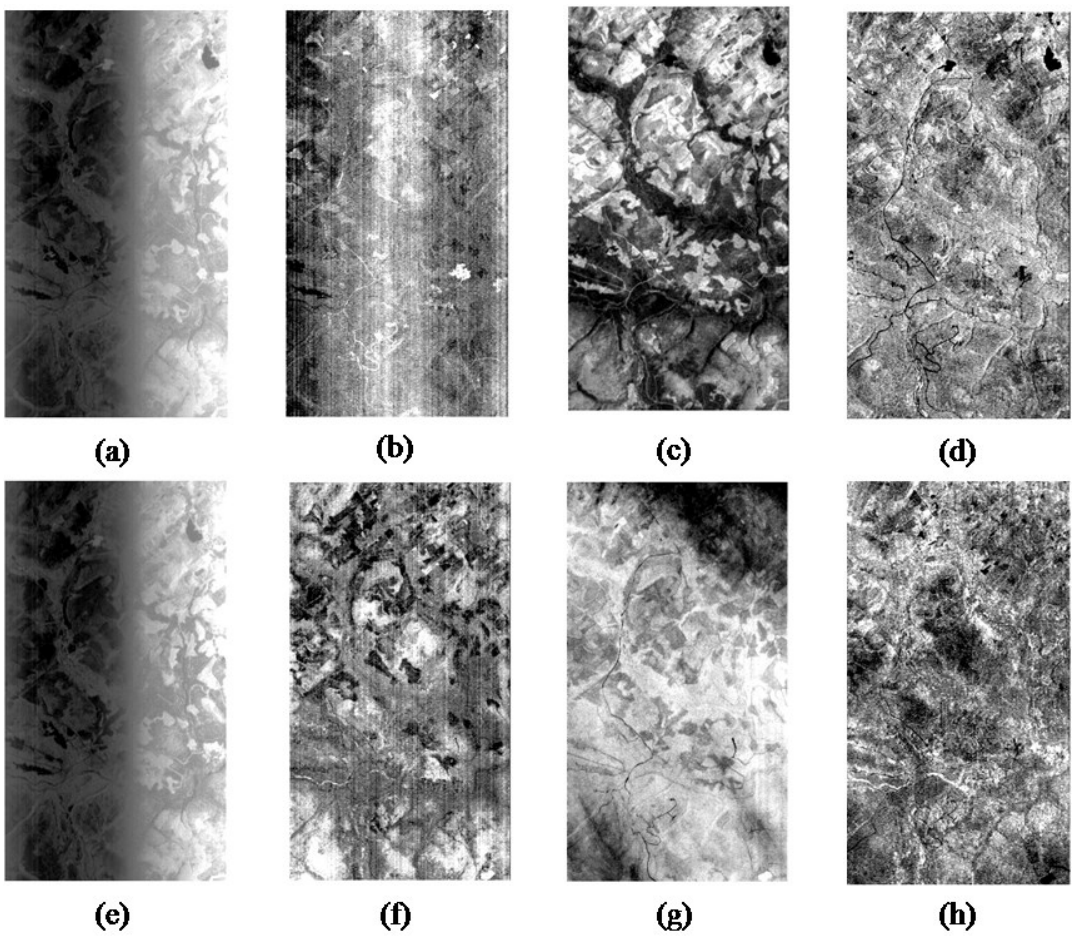

Figure 3.2 MNF bands illustrate the effects of vertical stripes removal and cross track illumination correction. For the June image, (a) and (b) show the MNF band 1 and 6 before the correction, (c) and (d) show the MNF band 1 and 6 after the correction. For the August image, (e) and (f) show the MNF band 1 and 6 before the correction, (g) and (h) show the MNF band 1 and 6 after the correction.

The resultant radiance image from spatial corrections was then input to derive reflectance image through atmospheric correction. The spectra of one vegetation pixel on both radiance image and reflectance image were shown in Figure 3.3. A pixel was located

at both the June and August images. The spectra of that location on radiance and reflectance images were displayed for both images.

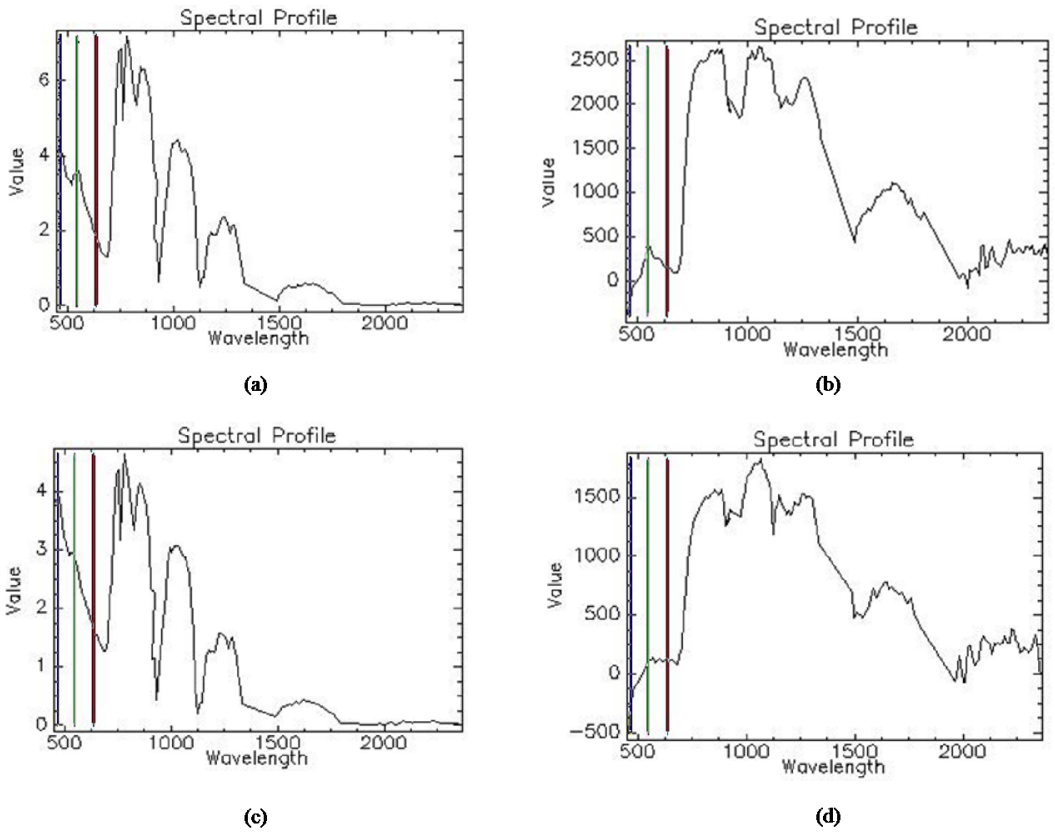

Figure 3.3 Spectral profiles of one same vegetation pixel on radiance and reflectance images were displayed. (a) June radiance image, (b) June reflectance image, (c) August radiance image, (d) August reflectance image. Data value in both curves have unit μW/(cm2 * sr * nm) while the reflectance data has been multiplied by a scale factor of 1000.

The reflectance curves in Figure 3.3 (b) and (d) provide spectral profile as typical vegetation spectral reflectance with significant low responses in visible region and high responses in the near infrared region. It can be noticed that both reflectance spectrum

were identical from a visual perspective, this also explains why quantified analysis was necessary for the change detection study.

After geometric correction, both images were overlapped and cropped to generate the final reflectance images for further analysis. The images were shown in Figure 3.4(a) and (b) respectively. The aerial survey map used as reference in this study was also georeferenced in order to match the Hyperion images. Because of rough quality of the map, it has been delineated to clearly show regions with different defoliation magnitude. The reference map was shown in Figure 3.4(c).

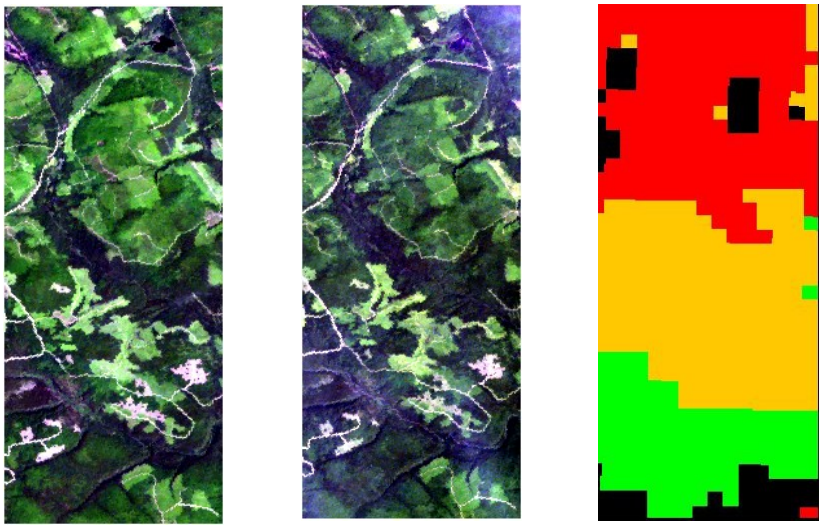

(a) (b) (c)

Figure 3.4 Hyperion image captured on June 16, 2014 was shown in (a) and the one captured on August 7, 2014 was shown in (b). Band 29 (732 nm), band 20 (640 nm) and band 12 (559 nm) were used to display the natural color images. The defoliation magnitude reference map shown in (c) has three delineated defoliation levels: light

(green), moderate (yellow) and severe (red). The black blocks were either uninvestigated regions or forestless regions.

3.4.2 VIs based Change Detection

The VIs based change detection results were based on the four VIs images derived from June and August images respectively. The pixel-level changes in percentages were calculated for each VI. The change rates for different defoliation magnitude regions were summarized in Table 3.2.

Table 3.2 Change rates detected with 13 vegetation indices summarized for three defoliation regions

VI	Light	Moderate	Severe
SR	25%	23%	24%
NDVI	4.4%	4.1%	3.7%
EVI	19%	18%	19%
ARVI	23%	20%	17%
RENDVI	5.6%	6.3%	5.7%
MRESR	16%	16%	17%
MRENDVI	12%	12%	11%
MSI	13%	14%	13%
WBI	8.8%	8.2%	7.6%
NDWI	9.3%	7.5%	13%
PRI	6.0%	4.8%	3.2%
SIPI	8.8%	8.0%	7.2%
RDRI	43%	41%	43%

The change rates for 13 applied VIs varied from one another. Some suggest slight changes, less than 10%, from June to August images, such like NDVI and PRI, while some suggest significant changes, more than 20%, such like SR and RDRI. It was noticeable that for VIs within the same category, the change rates also have spectacular

differences. Among the broadband greenness VIs, slightest changes were identified with NDVI, while its extended version, EVI and ARVI both have a noticeable changes between the measurements on two images. In general, NDVI was used as an identifier of vigor vegetation. However, the distance from which the satellite images were taken compensates the density of the forests that were supposedly diminished by the budworms. This was also why a diversity of VIs should be involved in this study. The other simple index SR suggests the sharpest changes in all three defoliation levels with respectively 25%, 23% and 24%. The distribution of changes detection with SR was shown in Figure 3.5(a).

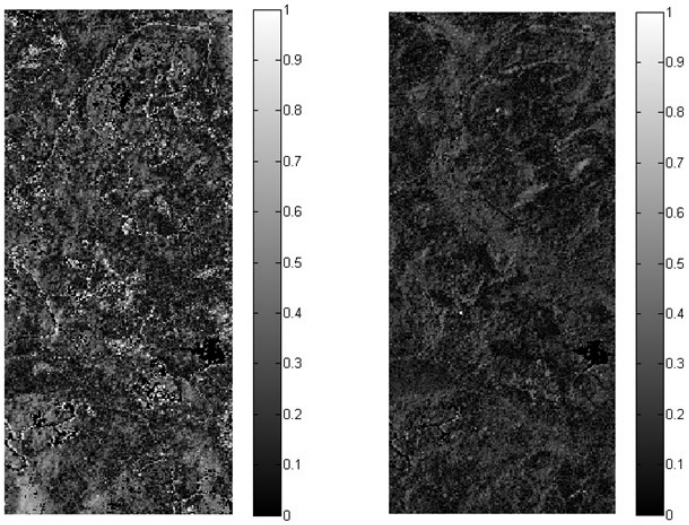

Figure 3.5 The percentage changes between June and August were detected in two typical greenness VIs. (a) Change detection map of SR; (b) Change detection map of MRESR.

The distribution of SR change rates in the study site appear to be homogenous with most

identifiable changes located at lower left corner as well as small clusters near the center of the scene.

For red-edge involved narrowband greenness VIs, similar change rates with their original version NDVI and SR were detected within the defoliation regions. The MRESR has the highest change rates among the three with bands within red edges used in its construction. The distribution of changes of MRESR was shown in Figure 3.5(b). The change rates have a similar pattern with SR while fewer individual sharp bright points were presented.

For the VIs concerning canopy water content, with WBI generates slighter changes, the rest two VIs MSI and NDWI have similar change rates for the study site. Their respective distributions of changes were shown in Figure 3.6(a) and (b).

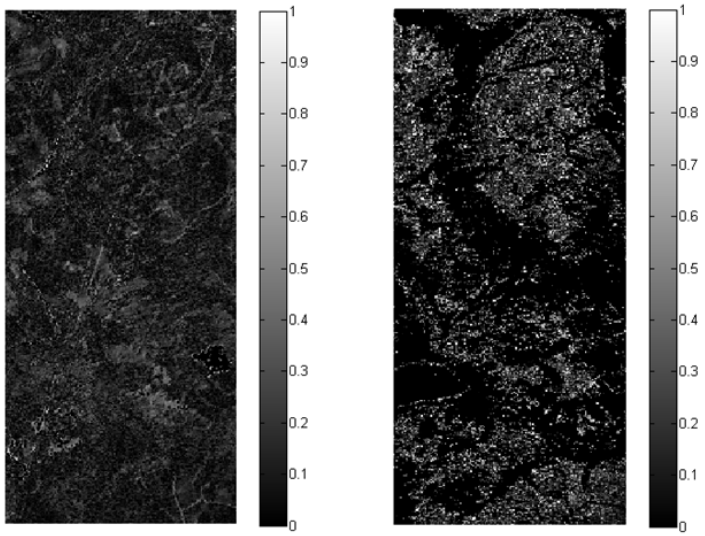

Figure 3.6 The percentage changes between June and August were detected in two typical canopy water content VIs. (a) Change detection map of MSI; (b) Change detection map of NDWI.

The distributions of changes in these two VIs, however, suggest noticeable difference. The changes in MSI appear to be more homogenous while the NDWI change map presents clusters of high brightness with contrast to low ones. Despite the first impression of such obvious difference, one can still identify similar patterns from MSI map that has been highlighted in the map of NDWI. In order for further analysis, NDWI was selected as more contrast in terms of different regions can be used for analysis.

Light Use Efficiency VIs have considerable differences in terms of their changes detection between the two images. The RDRI which incorporates more bands within red and green spectral regions generate a highest change rates among the three as well as among all 13 investigated VIs. The SIPI has a slight higher change rates than PRI within

three defoliation regions. The distributions of changes in RDRI and SIPI were shown in Figure 3.7(a) and (b).

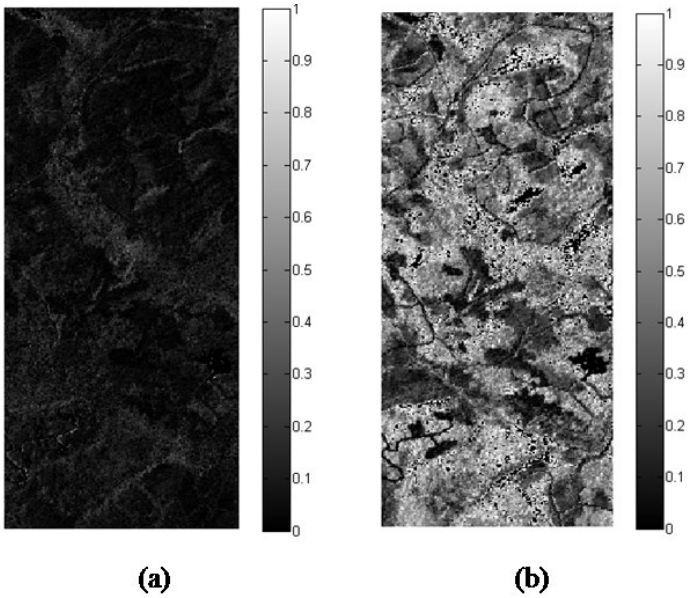

Figure 3.7 The percentage changes between June and August were detected in two typical Light Use Efficiency VIs. (a) Change detection map of SIPI; (b) Change detection map of RDRI.

The RDRI has a very high change rate between June and August in the study site, with more than 40% within each defoliation regions. The SIPI has relatively low change rate while its clusters of relatively high change regions were also identifiable in RDRI map. RDRI was selected for further analysis of forest stress because of its distinctness.

3.4.3 VIs based Forest Stress Analysis

As mentioned above, we use the "Agricultural Stress Vegetation Analysis" tool provided by ENVI to synthesize the VIs and generate a spatial map showing the distribution of the forest stress in the study site. In addition to the hyperspectral image, the tool takes in three VIs from different categories as input, namely Greenness Index, Canopy Water or Nitrogen Index and Light Use Efficiency or Leaf Pigment Index. In our case, SR, NDWI and RDRI were used for these three inputs. The VIs from June and August Hyperion images were respectively used to implement the stress analysis. The results from both images were aligned with the aerial survey map for comparison. The Agricultural Stress Tool divides the input scene into nine classes, from lowest stress to highest stress. The resultant spatial maps generated for June and August image were shown in Figure 3.8(a) and (b).

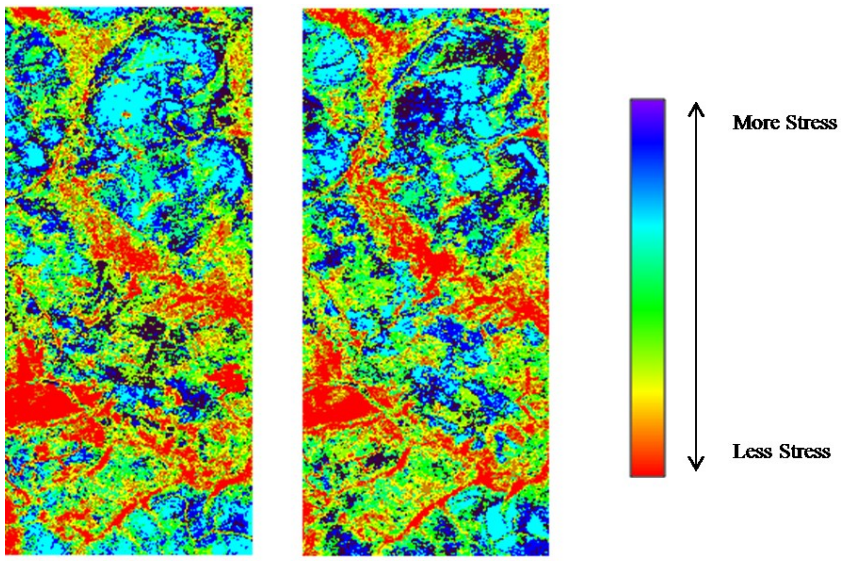

Figure 3.8 Forest stress maps generated for the June image was shown in (a) and the one for the August image was shown in (b), the stress levels for both maps were shown as a colormap in (c).

Most stressed pixels were from light blue, dark blue to black. In order to better illustrate their distribution and compare the two maps, we extract only these three levels and aligned with the aerial survey map. The new maps were shown in Figure 3.9(a) and

(b).

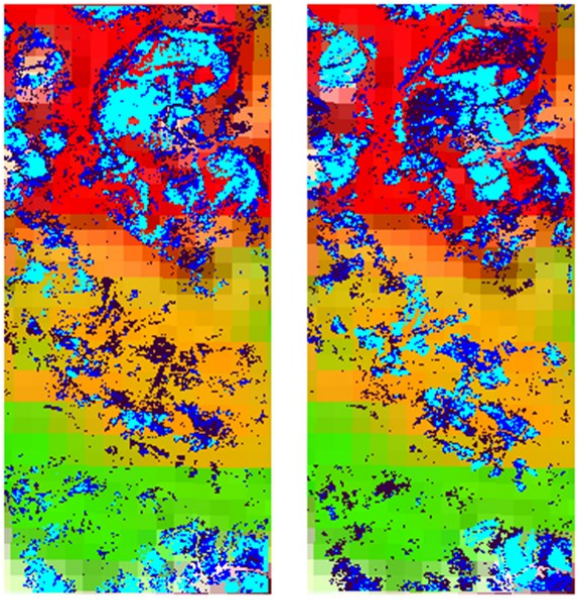

Figure 3.9 Most stressed regions (light blue to black) extracted from stress maps were aligned with the aerial survey map as reference. The June map was shown in (a) and the August map was shown in (b). The stress levels displayed were from light blue, dark blue to black (from level 7, 8 to 9, with 9 being the most).

It was noticeable that from June to August, the severe defoliated (red) region and light defoliated (green) region, more light blue blocks transferred to black or dark blue color, suggesting the stress level getting higher. In the moderate defoliated region (yellow), it appears that less highly stressed pixels were identified in August image than in June image. However, it also appears that the stressed regions have expanded, as some isolated stressed pixels in June image tend to form clusters in August. As a result, the

forest stress map generated from VIs generally matched the aerial survey result for defoliation.

3.5 Conclusion

In this study, we investigated the potential of using remote sensing and vegetation indices derived from Hyperion hyperspectral images to analyze the defoliation caused by spruce budworm in Quebec region, Canada. The VIs based change detection was applied in this study to quantize the change of different VIs between multi-temporal Hyperion images acquired from June and August respectively over the study site.

We investigate the VIs from four difference categories with the aim to find the VIs with most significant changes in response to the increasing defoliation from June to August. The change rates of different VIs generated from these two images were calculated, the VIs with high change rates were then considered as more relevant to the SBW defoliation. Finally, spatial maps of forest stress were generated for two images respectively using the selected VIs. The result suggest the forest stress distribution generated using remotely sensed hyperspectral images and VIs have potential for estimating SBW defoliation, in terms of its spread and severity.

Acknowledgement

This research was funded by the Canada Research Chair Program. The authors would like to thank NASA for collecting the Hyperion images of the testing areas.

References

Beck, R. (2003). EO-1 User Guide v. 2.3, 74. Retrieved from http://eo1.usgs.gov/documents/EO1userguidev2pt320030715UC.pdf

Blackburn, G. A. (1998). Quantifying chlorophylls and caroteniods at leaf and canopy scales. Remote Sensing of Environment, 66(98), 273–285. doi:10.1016/S0034-4257(98)00059-5

Boulanger, Y., Arseneault, D., Morin, H., Jardon, Y., Bertrand, P., & Dagneau, C. (2012). Dendrochronological reconstruction of spruce budworm (Choristoneura fumiferana) outbreaks in southern Quebec for the last 400 years. Canadian Journal of Forest Research, 42, 1264–1276. doi:10.1139/X2012-069

Curran, P. J. (1989). Remote sensing of foliar chemistry, 278, 271–278. doi:10.1016/0034-4257(89)90069-2

Datt, B., McVicar, T. R., Van Niel, T. G., Jupp, D. L. B., & Pearlman, J. S. (2003). Preprocessing EO-1 Hyperion hyperspectral data to support the application of agricultural indexes. IEEE Transactions on Geoscience and Remote Sensing, 41(6), 1246–1259. doi:10.1109/TGRS.2003.813206

De Beurs, K. M., & Townsend, P. A. (2008). Estimating the effect of gypsy moth defoliation using MODIS. Remote Sensing of Environment, 112, 3983–3990. doi:10.1016/j.rse.2008.07.008

Eklundh, L., Johansson, T., & Solberg, S. (2009). Mapping insect defoliation in Scots pine with MODIS time-series data. Remote sensing of environment, 113(7), 1566-1573.

Gong, P., Pu, R., Biging, G. S., & Larrieu, M. R. (2003). Estimation of forest leaf area index using vegetation indices derived from Hyperion hyperspectral data. Geoscience and Remote Sensing, IEEE Transactions on, 41(6), 1355–1362.

Goodenough, D. G., Dyk, A., Niemann, K. O., Pearlman, J. S., Chen, H., Han, T., … West, C. (2003). Processing Hyperion and ALI for forest classification. IEEE Transactions on Geoscience and Remote Sensing, 41(6), 1321–1331. doi:10.1109/TGRS.2003.813214

Gray, D. R. (2008). The relationship between climate and outbreak characteristics of the spruce budworm in eastern Canada. Climatic Change, 87(October), 361–383. doi:10.1007/s10584-007-9317-5

Han, T., Goodenough, D. G., Dyk, a., & Love, J. (2002). Detection and correction of abnormal pixels in Hyperion images. IEEE International Geoscience and Remote Sensing Symposium, 3(C), 1327–1330. doi:10.1109/IGARSS.2002.1026105

ITT Visual Information Systems (2006). "ENVI FLAASH Module User's Guide (2006 Edition)." [Online] September 21, 2012: ftp://popo.jpl.nasa.gov/pub/ENVI_Installers/ENVI_Documentation/docs/FLAASH_Module.pdf.

Jupp, D.L.B., Datt, B., McVicar, T.R., Van Niel, T.G., Pearlman, J.S., Lovell, J.L. and King, E. A. (2003). Improving the Analysis of Hyperion Red-Edge Index from an Agricultural area. Image Processing and Pattern Recognition in Remote Sensing, 4898(October 2002), 1–15. doi:10.1117/12.472696

Ministère des Forêt, de la Faune et des Parcs (MFFP). (2014). Aires infestées par la tordeuse des bourgeons de l'épinette au Québec en 2014. Version 1.0 [Online] September 2014: http://www.mffp.gouv.qc.ca/publications/forets/fimaq/insectes/tordeuse/TBE_2014_P.pdf

Pinter Jr, P. J., Hatfield, J. L., Schepers, J. S., Barnes, E. M., Moran, M. S., Daughtry, C. S., & Upchurch, D. R. (2003). Remote sensing for crop management. Photogrammetric Engineering & Remote Sensing, 69(6), 647-664.

Rullan-Silva, C. D., Olthoff, a. E., Delgado De la Mata, J. A., & Pajares-Alonso, J. A. (2013). Remote monitoring of forest insect defoliation. A review. Instituto National de Investigacion Y Tecnologia Agraria Y Alimentaria (INIA), 22(3), 377–391. doi:10.5424/fs/2013223-04417

Riley, J. R. (1989). Remote sensing in entomology. Annual review of entomology, 34(1), 247-271.

Taylor, S. L., & MacLean, D. A. (2008). Validation of spruce budworm outbreak history developed from aerial sketch mapping of defoliation in New Brunswick. Northern Journal of Applied Forestry, 25(3), 139-145.

Townsend, P. A., Singh, A., Foster, J. R., Rehberg, N. J., Kingdon, C. C., Eshleman, K. N., & Seagle, S. W. (2012). A general Landsat model to predict canopy defoliation in broadleaf deciduous forests. Remote Sensing of Environment, 119, 255-265.

Ungar, S. G., Pearlman, J. S., Mendenhall, J. A., & Reuter, D. (2003). Overview of the Earth Observing One (EO-1) mission. IEEE Transactions on Geoscience and Remote Sensing, 41(6), 1149–1159. doi:10.1109/TGRS.2003.815999

4 CHAPTER 4

ESTIMATION AND MAPPING OF SPRUCE BUDWORM DEFOLIATION USING VEGETATION INDICES DERIVED FROM HYPERION HYPERSPECTRAL DATA

Abstract

Defoliation during spruce budworm (SBW) outbreaks causes severe, widespread damage to spruce and balsam fir forests in eastern Canada. Early estimation of the defoliation will provide crucial support to mitigate the socio-economic impact on vulnerable forests. Vegetation indices (VIs) from remote sensing images can be used for estimation of forestry biophysics characteristics such as defoliation. However, traditional VIs constructed from broad multispectral bands provide insufficient spectral information which limits the potential in defoliation investigation. In this paper, narrowband VIs were constructed using 162 available Hyperion hyperspectral bands, in order to find the most relevant spectral bands that capture the defoliation characteristics. The VIs were calculated by pairing bands from the all 162 bands. Most relevant VIs and associated bands were selected for mapping based on their correlation with the defoliation magnitude provided by the ground truth. Nine existing two-band vegetation indices (VIs) were explored and three new non-linear two-band VIs were developed for a study site in the province of Quebec, Canada. The experimental results indicate that most important hyperspectral bands with high correlations to defoliation ground truth were mostly in the

near-infrared (NIR) region and some in shortwave infrared (SWIR) region. The correlation coefficients generated using those Hyperion hyperspectral bands were considerably higher than that generated using ALI multispectral bands. The mapping results also demonstrate that the new non-linear VIs have achieved, on average, 15% of accuracy improvement in SBW defoliation estimation and mapping over the existing VIs.

Keywords: Hyperion, hyperspectral data, spruce budworm defoliation, vegetation index.

4.1 Introduction

The spruce budworm (SBW) was one of the most damaging native insects of spruce and fir forests in Quebec, Canada. During a major outbreak, tens of millions of hectares of trees can be severely defoliated by the insect (Gray and Re, 2000). An outbreak may last for several years, and cumulative defoliation can cause significant levels of mortality and growth loss in mature softwood forests. According to the annual report released by Quebec Government in 2014 (MFFP, 2014), the areas affected by SBW continue to rise significantly. In 2014, they totaled 4,275,065 hectares compared to 3,200,348 hectares in 2013. Conventional Strategies to eliminate or slow the spread of these destructive pests such like pesticide spraying can be costly, time consuming and less effective when accurate estimation of defoliated regions was not available. The sizes and locations of defoliated regions make field investigation difficult. Alternatively, remote sensing techniques, especially the utilize of satellite images, provide spatially unlimited and wide coverage for investigation. Researches have been conducted on

estimating and mapping field forest ecosystem variables or properties using remote sensing data (Gong et al., 2003; Rullan-Silva et al., 2013). The vegetation indices (VIs) derived from remote sensing has been widely applied to estimate vegetation health and greenness (Rullan-Silva et al., 2013). Generally, healthy vegetation will absorb most of the visible light that falls on it, and reflects a large portion of the near-infrared light. The defoliated forest, in form of unhealthy or sparse vegetation, reflects more visible light and less near-infrared light. Making use of these two spectral bands existing pairwise VIs can be constructed. A list of investigated VIs can be found in Table 4.1. The widely applied broad-band indices were usually constructed with near-infrared (NIR) and red (R) bands, use average spectral information over broad bandwidths (Blackburn, 1998).

Studies have been conducted on mapping the magnitude of defoliation using VIs constructed from multispectral images (Rullan-Silva et al., 2013). Those VIs were broad-band VIs which indicates only one or two reflectance values at investigated spectral wavelength region (e.g. NIR or SWIR) will be applied. Two types of broad-band VIs were compared for measuring different types of forest damage in USA (Vogelmann, 1990). In order to map the magnitude of defoliation, three VIs that use the R, NIR, SWIR and mid-infrared (MIR) bands were tested, suggesting that SWIR reflectance was very sensitive to the amount of water in the vegetation, increasing when leaf water content decreases, as happens in vegetation stressed by pest defoliators. They further concluded that two VIs using SWIR band had better performances for mapping insect defoliation in their site when compared with conventional NDVI (de Beurs and Townsend, 2008).

However, the broad-band VIs have limited spectral information concerning the significance of response at different spectral wavelengths. As an alternative, more refined VIs can be constructed through the use of distinct narrow bands from hyperspectral images. Narrow bands can be crucial for providing additional information over broad bands in quantifying biophysical characteristics of vegetation (Gong et al., 2003). It was also believed that the hyperspectral data can be useful in early stress detection as spectral differences can be identified from only certain wavelengths while existing remote sensing studies on SBW defoliation use mostly broadband VIs or limited narrowband VIs (Rullan-Silva et al., 2013). Moreover, little evidence has been found on mapping SBW defoliation using hyperspectral VIs (Rullan-Silva et al., 2013). Thus in our study, narrow-band VIs were constructed using hyperspectral data. The aim was to find the most important spectral bands in measuring SBW defoliation by means of VIs construction. The hyperspectral data from the Hyperion sensor on the Earth Observing-1 Mission (EO-1) satellite was used in this study. It provides a 10 nm spectral resolution provide spectral bands from 0.4 to 2.5 μm (Ungar et al., 2003). The fine spectral resolution increases the capability to distinguish structures and objects in the image scene (Curran, 1989). So investigations on spectral bands by means of VIs construction can provide more specific information for quantifying SBW defoliation. In this study, 12 two-band VIs were constructed using reflectance from all 162 available Hyperion bands. Most relevant VIs and associated

Table 4.1 12 vegetation indices analyzed in this study

Abbreviation	Formula	Vegetation Index Name	References
SR	ρ_2 / ρ_1	Simple Ratio.	(Qi, Chehbouni, Huete, Kerr, and Sorooshian, 1994), (Birth and McVey, 1968)
DVI	$\rho_2 - \rho_1$	Difference Vegetation Index	(Tucker, 1979)
NDVI	$(\rho_2 - \rho_1)/(\rho_2 + \rho_1)$	Normalized Difference Vegetation Index	(Griffin, May-Hsu, Burke, Orloff, and Upham, 2005)
EVI2	$2.5*(\rho_2 - \rho_1)/(\rho_2 + 2.4*\rho_1)$	2-band Enhanced Vegetation Index	(Jiang et al., 2008)
SAVI	$(\rho_2 - \rho_1)*(1+L)/(\rho_2 + \rho_1 + L)$	Soil Adjusted Vegetation Index	(Huete, 1988)
NLI	$(\rho_2^2 - \rho_1)/(\rho_2^2 + \rho_1)$	Non-Linear Index	(Goel and Qin, 1994; Gong et al., 2003)
MNLI	$(\rho_2^2 - \rho_1)*(1+L)/(\rho_2^2 + \rho_1 + L)$	Modified Non-Linear Index	(Gong et al., 2003)
MSR	$\frac{\rho_2 / \rho_1 - 1}{\sqrt{\rho_2 / \rho_1} + 1}$	Modified Simple Ratio	(Chen, 1996)
RDVI	$(\rho_2 - \rho_1)/\sqrt{\rho_2 + \rho_1}$	Renormalized Difference Vegetation Index	(Roujean and Breon, 1995)
CSR	$\cos(\rho_2 / \rho_1)$	Cosine Simple Ratio	Developed in this paper
CDVI	$\cos(\rho_2 - \rho_1)$	Cosine Difference Vegetation Index	Developed in this paper
CNDVI	$\cos\frac{\rho_2 - \rho_1}{\rho_2 + \rho_1}$	Cosine Normalized Vegetation Index	Developed in this paper

Note that ρ_1 and ρ_2 represent red and NIR wavelengths respectively for constructing traditional vegetation indices but in this study they were extended to all spectral wavelengths provided by 162 available Hyperion bands.

bands were found by correlation with defoliation magnitude levels reported by airborne survey (MFFP, 2014).

4.2 Background

Research on VIs aims at the spectral identification, detection and quantification of forest health. They have been correlated with a variety of forest ecosystem variables, suggesting a strong indicator of field vegetation conditions (Thenkabail et al., 2000). With observation on reflectance of plants across the electromagnetic spectrum, we can derive information by focusing on the satellite bands that were most sensitive to vegetation information (near-infrared and red). Different responses on these two spectral regions can be used to distinguish between soil and vegetation and further diagnose external disturbance on vegetation amount and health. Constructed with this concept, the Difference Vegetation Index (DVI) (Tucker, 1979), the ratio-based NDVI (Datt et al., 2003; Gong et al., 2003) and Simple Ratio (SR) (Chen, 1996; Gong et al., 2003) were most commonly applied VIs (Table 4.1). An enhanced vegetation index (EVI) was designed in order to enhance the vegetation signal with improved sensitivity in high biomass regions and improved vegetation monitoring through a de-coupling of the canopy background signal and a reduction in atmosphere influences (Alfredo Huete et al., 1999). However, the necessity of a blue band in this index weaken its usage as blue band always carries with poor signal to noise ratio (SNR) and blue band was unavailable in certain cases. So a two-band EVI (EVI2) was developed attempting to maintain the merit of EVI without a blue band (Jiang et al., 2008). Several VIs were proposed by attempting to reduce the sensitivity to optical properties of the soil ground. The widely applied

methods to account for this background influence were implemented by introducing correction factors to original NDVI. The soil-adjusted vegetation index (SAVI) attempts to correct for the influence of soil brightness when vegetative cover was low (Huete, 1988). The SAVI was structured similar to the NDVI but with the addition of a soil brightness correction factor, L. The value of factor L varies by the amount of vegetation coverage: in vegetation regions with highest density, L equals to zero which makes it equivalent to NDVI; whereas for lowest vegetation regions L equals to zero. It was also suggested an L=0.5 works well in most situations and was the default value used.

Traditional VIs use a linear model of NIR and red bands while it was observed that the relationship between VIs and biophysical parameters was not necessarily linear. In order to stimulate this nonlinear relationship, several nonlinear vegetation indices have been proposed, including the nonlinear vegetation index (NLI) (Goel and Qin, 1994), the renormalized difference vegetation index (RDVI) (Roujean and Breon, 1995), and the modified simple ratio vegetation index (MSR) (Chen, 1996). The soil brightness correction from SAVI has been integrated into NLI in order to make it resist to variety in soil condition, this approach generate the Modified Non-Linear Index (MNLI) (Gong et al., 2003). In this study, in order to find better modeling of VIs for correlating the forest defoliation magnitude levels, the tradition SR, DVI and NDVI were modeled using cosine functions. We expect that some new two-band VIs, constructed from the 162 bands, may be found that produce higher correlations with forest defoliation than currently used VIs.

The advent of hyperspectral sensor allows for narrowband VIs construction and provides more concrete information when the VIs was correlated with biophysical parameters. The study for correlating Leaf Area Index (LAI) with VIs constructed using Hyperion data demonstrate the advantage of across bands VIs construction in modeling biophysical parameters (Gong et al., 2003). It was also suggested that the SWIR spectral region (1.0–2.5 μm) and middle-infrared (MIR) (1.55–1.75 μm), though neglected in traditional VIs construction, were proven to perform better in modeling the LAI. In the study of mapping the magnitude of defoliation in a largely broadleaved and oak-dominated forest area in the USA, it was suggested that Normalized Difference Infrared Index bands 6 and 7 (NDIIb6 and NDIIb7, both using the SWIR band) performed significantly better than NDVI (Spruce et al., 2011). However, existing remote sensing studies on SBW defoliation use mostly broadband VIs or limited narrowband VIs (Rullan-Silva et al., 2013). This was because the images originated from multispectral sensors fails to provide a fine spectral resolution and combining SWIR with NIR can be especially difficult when both bands have different spatial resolution. In this study, we focus on the evaluation performance of 12 two-band VIs, as listed in Table 4.1, in estimating the spruce budworm defoliation. By taking advantage of the wider wavelength coverage and finer spectral resolution provided by Hyperion data, we construct those VIs using all 162 available bands after selection. Note that because of our approach, ρ_1 and ρ_2 in Table 4.1 represent any Hyperion spectral band though we use ρ_1 as RED band and ρ_2 as NIR band in traditional VIs. By correlating all the VIs generated, our study aims to provide recommendation on not only the suitable VIs for estimating SBW

defoliation but also the spectral bands at specific wavelengths that were used for constructing these VIs.

4.3 Study Site and Materials

4.3.1 Study site

Several EO-1 campaigns were established during June, July and August, 2014 on a selected site centered at 48°09’54’’S/67 °19’21’’W near the Causapscal city, across the Bas-Saint-Laurent region which located along the south shore of the lower Saint Lawrence River in the Quebec Province, Canada (Figure 4.1). It was a relatively homogeneous rural area mostly covered by spruce and fir forests. The two tree species were alike in appearance, both served as preferred habitats for SBW and mixed in the forests in the study site. The high density of trees in the forestry regions makes them vulnerable to spruce budworms and the defoliated regions can be formed as large blocks. According to the aerial survey report “Infested areas of spruce budworm in Quebec in 2014” (Quebec, November 2014), the Bas-Saint-Laurent region was one of the most dominant infested areas by spruce budworm in Quebec, totaled 316,103 hectares. The area affected by SBW continues to rise significantly in the province. In 2014, they totaled 4,275,065 hectares compared to

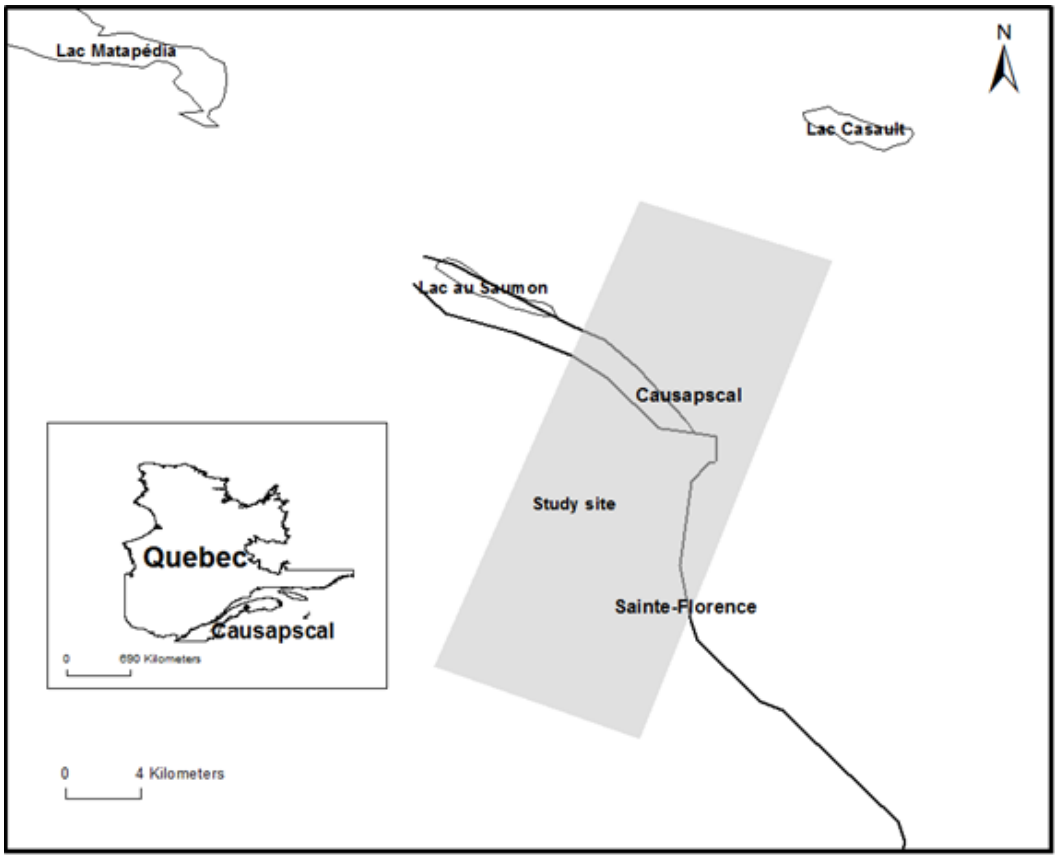

Figure 4.1 Study site

3,200,348 hectares in 2013.

4.3.2 Materials

Interpretation ground truth of SBW infested fields was provided by the Quebec government report (MFFP, 2014). The aerial survey of damage caused by major forest pests was carried out annually by the Ministry of Forests, Fauna and Parks (Ministère des Forêt, de la Faune et des Parcs, MFFP). The aerial survey scans natural disturbances observed from the air in real time. The observations digital rendering was done to the screen with a stylus. To facilitate the work of the observer, a topographic map was displayed on the screen depending on the route of the aircraft. These geo-referenced data

was then processed and analyzed using geographic information system (GIS) software. The aerial survey scans natural disturbances observed from the air in real time. The aircraft flies at an altitude of about 240 meters, at a speed of 160 km / h, keeping a distance of 4.5 kilometers between flight lines. The survey reports three levels of defoliation in Quebec, namely slight, moderate and serious, containing the study site mentioned above.

The SBW defoliation magnitude levels were provided by the aerial survey report (MFFP, 2014) and one thematic map covering our study site has been used. The report classifies defoliation into three classes: slight (loss of foliage in the upper third of the tops of some trees), moderate (loss of foliage in the upper half of the top of most trees) and severe (loss of foliage on the entire length of the top of most trees). In order for further process, the three classes were quantified into three percentage levels: 33.3% for slight level, 50% for moderate level and 100% for severe level.

According to the study of Dr. Taylor and Dr. MacLean in 2008 (Taylor & MacLean, 2008), from 1985 to 1993, 85% of 332 cases were correctly classified by aerial estimate. They concluded that aerial surveys provide a reasonable estimate of defoliation.

A set of EO-1 Hyperion images was acquired from NASA free of charge from June to August, 2014. They were targeted at the abovementioned study site in order to investigate the defoliation magnitude. The selection of imagery was determined by both the image quality which heavily affected by the cloud condition and the acquisition date which should reflect most infested areas. An EO-1 Hyperion hyperspectral image over

the study site acquired on July 19, 2014, around 10:20 A.M. local time for this study, it was captured together with the EO-1 ALI image used in Chapter 2. The image was at level L1R processing, meaning that it was only radiometrically corrected and with no geometrically correction applied (Beck, 2003).

4.4 Methodology

4.4.1 Data Pre-processing

The Hyperion sensor has 242 bands in total, including 70 visible-near-infrared (VNIR) bands, and 172 shortwave-infrared (SWIR) bands. Among them, 44 bands were intentionally not illuminated or correspond to areas of low sensitivity of the spectrometer materials (Datt et al., 2003). In addition, two more zero bands were identified in our data of use, which were band 80 and 81. Among the other 196 bands, only 194 bands were unique (NIR bands 8-57, 427-925 nm and SWIR bands 79-224, 912-2395 nm) because there were four bands in the overlap between the two spectrometers of VNIR and SWIR (Datt et al., 2003). In addition, atmospheric water vapor bands which absorb almost the entire incident and reflected solar radiation and the bands that have very severe vertical stripping were identified by visual inspection of the image data . Thus, the subset of 162 selected bands (bands 10-57, 77-79, 82-119, 134-165, and 181-221 within 447-2365 nm) were applied in this study.

Abnormal pixels that have lower DN values as compared to their neighboring pixels were corrected by replacing their DN values with the average DN values of their immediate left and right neighboring pixels (Han et al., 2002). Vertical stripes were

removed using the “SPEAR Vertical Stripe Removal” in the ENVI software (ITT Visual Information Systems, 2006) (Datt et al., 2003). The "smile effects" that refer to an across-track wavelength shift from center wavelength due to the change of dispersion angle with field position (Goodenough et al., 2003) were removed using the procedure of "Cross-Track Illumination Correction" (Jupp et al., 2003) in the ENVI software (ITT Visual Information Systems, 2006). This study uses the Fast Line-of-sight Atmospheric Analysis of Spectral Hypercubes (FLAASH), an atmospheric correction module implemented in the ENVI to calibrate the at-sensor radiance data to land surface reflectance (Beck, 2003).

Both the ground truth map and the Hyperion data were geometrically corrected using the ENVI “Image to Map Registration” process. They were first projected to datum WGS 84 and the “Geographic lat/lon” projection was selected. The latitude and longitude of selected ground control points were matched on Google Earth. An overall root mean square error (RMSE) of 0.39 pixel was achieved.

4.4.2 Vegetation Indices Construction and correlation with defoliation

After overlapping the Hyperion imagery with the ground truth map, 30 sample pixels were selected as we retrieve reflectance spectra from the calibrated Hyperion images. Note that the spatial resolution of Hyperion data was 30 meters which makes each pixel a mixture of a large number of trees. So the 30 points were all selected within homogeneous forests areas by examining the Hyperion image. In addition, the ground truth map was roughly delineated that not available for pixel-by-pixel match with our image. So in order to make sure selected samples contain relatively accurate defoliation

magnitude, we avoid regions near the boundaries of different classes on the map. This gives us 30 observations of defoliation magnitude which constitute a defoliation variable. Furthermore, we need 30 observations of VI which constitute a VI variable. Note that we use 162 available Hyperion bands to construct 12 two-band VIs, so that will end up with 162x162x12 different VI variables that will be ran through our correlation test.

In this study, three new nonlinear VIs were developed in this paper attempting to maximize the merit of nonlinear VIs. The three VIs were adapted from NDVI, DVI and NLI while using a Cosine function to project the outputs. We analyze the potential of different VIs for estimating SBW defoliation by constructing them from all the 162 available Hyperion bands. After overlapping the Hyperion imagery with the ground truth map, 30 sample pixels were selected as we retrieve reflectance spectra from the calibrated Hyperion images. We use the correlation method developed in (Gong et al., 2003). For each of the 12 VIs, a linear correlation coefficient R^2 was calculated between the VI and defoliation measurement (30 samples). Since each VI in Table 4.1 could be constructed from any pair among the possible 162 bands, a linear correlation coefficient R^2 matrix could be constructed. From the correlation matrices, hyperspectral bands with high correlation coefficients were examined.

4.4.3 Mapping SBW defoliation using VIs

Based on the correlation results, VIs will be constructed using the most relevant bands from the georeferenced reflectance image for mapping SBW defoliation. First, the VIs were derived from reflectance data using band pairs recommended in correlation

results. The band pairs with highest correlations with defoliation were used for mapping respectively. So a VI map can be generated by using two associated spectral bands to calculate VI for all pixels. Then same process were managed to generate a class image from each VI, here we used NDVI, NLI, RDVI and CNDVI for comparison. The reflectance at wavelengths 1568 and 691 nm were used for constructing NDVI for mapping SBW defoliation, 488 nm and 1568 nm for NLI, 2254 nm and 448 nm for RDVI, 702 nm and 752nm were used for CNDVI. For accuracy assessment, one region on the upper left corner of the study site was selected as shown in Figure 4.8(a). The airborne survey provides cross province defoliation report but the map was very coarse in resolution. Thus the mapping results were assessed at a selected region in which two pieces of forests were clearly separated by manmade and nature land cover. The upper half was covered by light defoliated or relative healthy forestry pixels while the lower half was covered with severe ones. The ground truth for this region was delineated by taking only vegetation pixels into account using the aerial report (MFFP, 2014) as a reference. The severely defoliated regions were delineated as red color while light defoliated regions were delineated as green color, as shown in Figure 4.8(c). In order to generate binary image to classify original image into specified bi-level map, the subset image of the assessment region was extracted for further process. A histogram equalization was applied on each VI image followed by a global image threshold using Otsu's method (Smith et al., 1979). So the classification result will become a binary image with white pixels representing severe defoliation areas while black pixels representing light defoliation areas, as shown in Figure 4.8(b). Finally, the assessments

were conducted by comparing the mapping results with the ground truth map pixel-by-pixel.

4.5 Results and Analysis

4.5.1 Hyperion Data Pre-processing

The resultant radiance image from vertical stripes removal and cross track illumination correction was examined via MNF transformation (Datt et al., 2003). The MNF technique responds to interactions between the spatial structure of the data and that of the noise when the noise has strong spatial structure. As shown in Figure 4.2, the first and sixth MNF bands were generated from MNF transformation on original and output radiance data. Specifically "smile effect" can lead to a brightness gradient appearing in the first MNF band as shown in Figure 4.2(a) and stripes can be illustrated in subsequent MNF bands as shown in Figure 4.2(b).

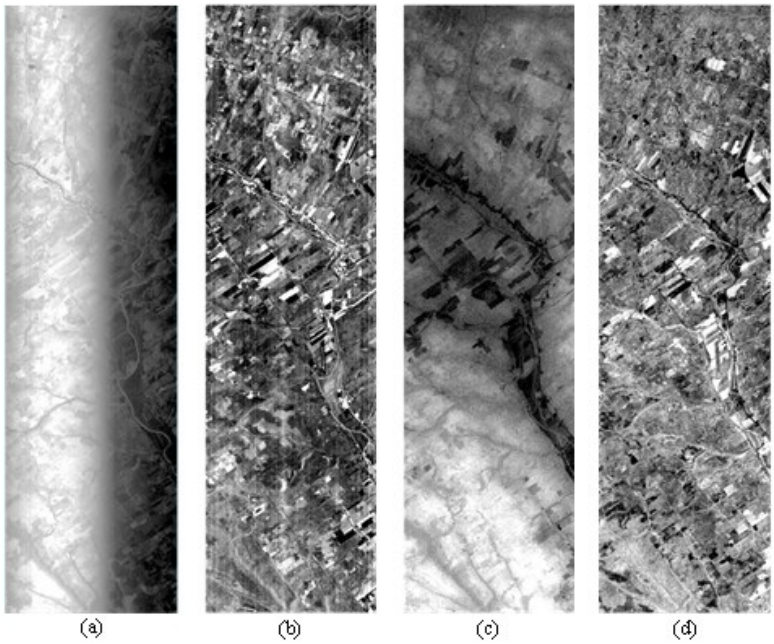

Figure 4.2 Original MNF band 1 and 6 were shown in (a) and (b). MNF band 1 and 6 after vertical stripes removal and cross track illumination correction were shown in (c) and (d).

The resultant radiance image from spatial corrections was then input to derive reflectance image through atmospheric correction. The spectra of one vegetation pixel on both radiance image and reflectance image were shown in Figure 4.3(a) and Figure 4.3(b). The reflectance curve in Figure 4.3(b) provides spectral profile as typical vegetation spectral reflectance with significant low responses in visible region and high responses in the

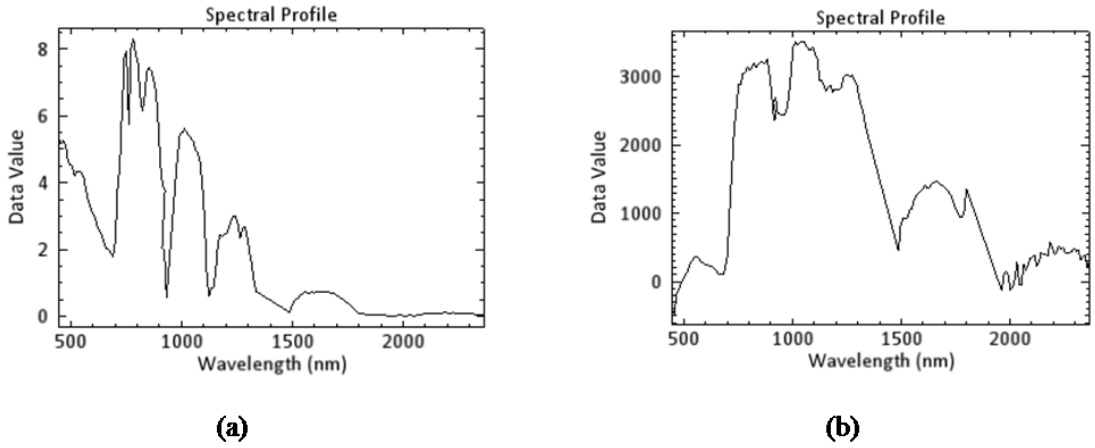

Figure 4.3 Spectral profile of one vegetation pixel on both radiance image (a) and reflectance image (b). Data value in both curves have unit μW/(cm2 * sr * nm) while the reflectance data has been multiplied by a scale factor of 1000.

near infrared region.

4.5.2 Correlation of Vegetation Indices with SBW defoliation

Based on the correlation values, the bands recommended for estimating defoliation were summarized for each VI in Table 4.2 by means of wavelengths and Full width at half maximum (FWHM).

Table 4.2 Potential Hyperion bands for 12 vegetation indices applied for SBW defoliation estimation.

Index	R^2	Band Center (nm) ρ_1 / ρ_2	FWHM (nm) ρ_1 / ρ_2	Spectral Region ρ_1 / ρ_2
NDVI	0.55	1568 / 691 1770 / 691 2244 / 691	11.31 / 10.39 11.50 / 10.39 10.47 / 10.39	SWIR / Visible SWIR / Visible SWIR / Visible
DVI	0.49	3 pairwise bands similar to NDVI's 803 / 488 922 / 488 1790 / 488	… 11.10 / 11.38 11.04 / 11.38 11.56 / 11.38	… NIR / Visible NIR / Visible SWIR / Visible
EVI2	0.55	3 pairwise bands similar to NDVI's 569 / 722 2254 / 488	… 10.84 / 10.60 10.46 / 12.38	… Visible / NIR SWIR / Visible
SR	0.40	Similar to NDVI's	…	…
SAVI	0.55	Similar to NDVI's	…	…
NLI	0.53	681 / 488 1568 / 488 2113 / 498 2254 /498	10.33 / 11.38 11.31 / 11.38 10.78 / 11.35 10.46 / 11.35	NIR / Visible SWIR / Visible SWIR / Visible SWIR / Visible
MNLI	0.53	Similar to NLI's		
MSR	0.52	Similar to SR's		
RDVI	0.51	803 / 488 2184 / 691 2254 / 488	11.10 / 11.38 10.60 / 10.39 10.46 / 11.38	NIR / Visible SWIR / Visible SWIR / Visible
CNDVI	0.62	702 / 752 763 / 590 803 / 590 1104 / 590 1195 / 590	10.46 / 10.71 10.73/ 10.65 11.10 / 10.65 10.97 / 10.65 10.82 / 10.65	NIR / Visible NIR / Visible SWIR / Visible SWIR / Visible SWIR / Visible
CDVI	0.60	Similar to CNDVI's		
CSR	0.61	Similar to CNDVI's		

For each of the 12 VIs, the highest correlation values yielded using NIR or SWIR bands respectively were summarized in second column. From the third to fifth column, the two band and used for yielding high correlations were summarized by means of their band center wavelength, FWHM and spectral region.

In our experiments, we find high correlation value yielded using both NIR bands and

SWIR bands different VIs. Among them, NIR bands at 700-800 nm and SWIR bands 1700-2200 nm generate high correlations with defoliation data. Specifically, the correlation matrices R^2 constructed from SR, EVI2, DVI and MSR have a similar pattern as NDVI, shown in Figure 4.4. The high correlation values were distributed as stripes close to left and bottom of the matrix square. The highest values were constructed from band wavelengths centered at 1568, 1770, 2244 nm in SWIR region. Noticeably more high correlation values were constructed with SWIR bands than NIR bands for NDVI. The SWIR bands were associated with absorption of water, cellulose, starch and sugar (Curran, 1989). The associated visible bands with them belong to yellow-red region with a shorter wavelength and higher frequency than the conventional red band.

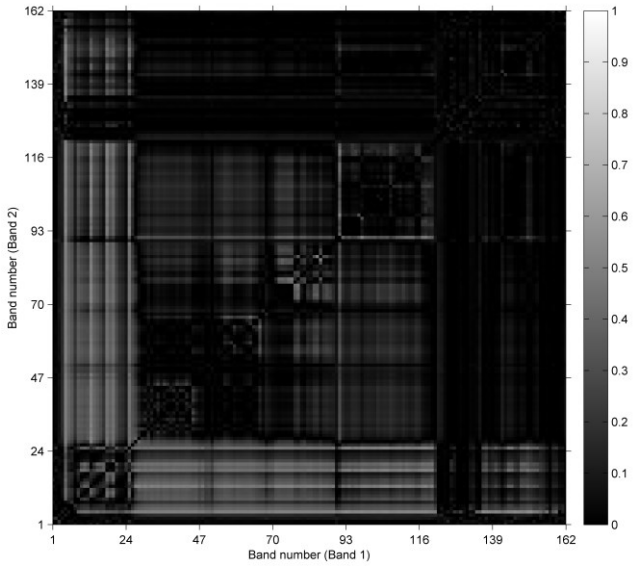

Figure 4.4 Plots for correlation matrix R^2 (from 0 to 1) between defoliation and NDVI calculated using pairwise 162 Hyperion bands 447-2365 nm. Two bands (Band 1 and 2) were used to calculate one NDVI value and generate one correlation coefficient value in the R^2 matrix. NIR bands (band 1-48) and SWIR bands (band 49-162) with high correlation values as illustrated were recommended for estimation of SBW defoliation and summarized in Table 4.2.

The R^2 matrices of NLI and RDVI have their unique patterns as shown in Figure 4.5 and Figure 4.6. The results of NLI and RDVI fail to imply a noticeable increase in correlation compared with NDVI. NLI yields a maximum value 0.53. The associated NIR band resides at 681 nm as a representative of Chlorophyll a while the SWIR bands at 2123 and 2254 nm were close to the bands that absorb starch and protein (Curran, 1989). RDVI yields a maximum value of 0.51. The associated bands were identical or close to the bands introduced in other VIs. The soil adjusted VIs fail to improve their original formula as the highest correlation values keep increasing as we decrease the adjust parameter L from 0.5 to 0. This occurs in both MNLI and SAVI which were soil adjusted versions of NLI and NDVI respectively. This was mainly because of the high density of selected

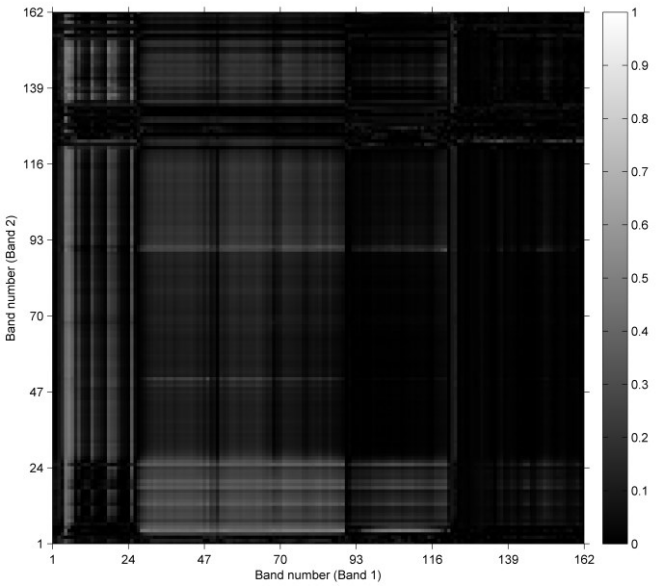

Figure 4.5 Plots for correlation matrix R^2 (from 0 to 1) between defoliation and NLI calculated using pairwise 162 Hyperion bands. For more information refer to Figure 4.4.

samples which contain very little soil component.

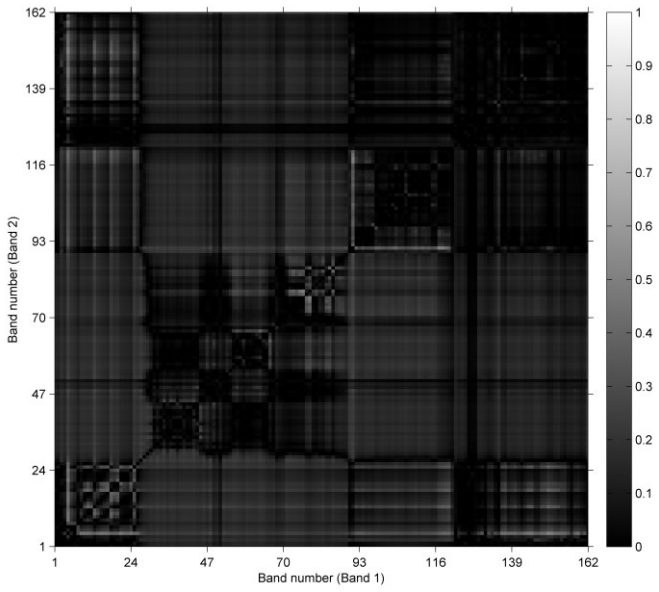

Figure 4.6 Plots for correlation matrix R^2 (from 0 to 1) between defoliation and RDVI calculated using pairwise 162 Hyperion bands. For more information refer to Figure 4.4.

All the three Cosine based indices improved the correlation value of original VIs by considerable amount. Visualization of R^2 matrix constructed using CNDVI was shown in Figure 4.7. The highest correlation value suggests an increase from 0.40 in

original SR to 0.61 in developed CSR.

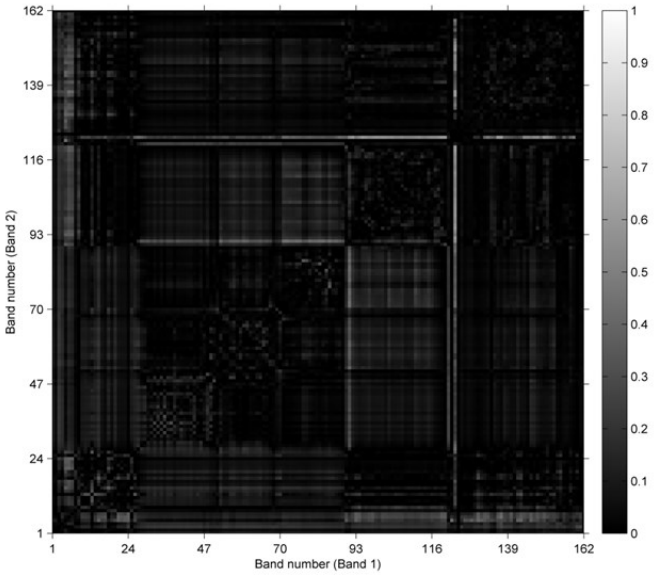

Figure 4.7 Plots for correlation matrix R^2 (from 0 to 1) between defoliation and CNDVI calculated using pairwise 162 Hyperion bands. For more information refer to Figure 4.4.

The highest correlation value suggests an increase from 0.49 in original DVI to 0.60 in CDVI. The highest correlation value suggests an increase from 0.55 in original NDVI to 0.62 in CNDVI. This can due to the use of Cosine function which projected them nonlinearly to reflect relevant characteristics related to SBW defoliation. Especially, the CNDVI constructed with bands at 752 and 702 nm generated the highest correlation value among all the VIs. It was revealed that land-based chlorophyll-producing vegetation has a very strong rise in reflectivity at around 700 nm by a factor of 5 or more (Seager et al., 2005). These bands were close to the red edge which was the name given to the abrupt reflectance change in the 680-740 nm region of vegetation spectra that was caused by the combined effects of strong chlorophyll absorption and leaf internal scattering (Dawson and Curran, 1998). The red edge shifts according to a combined

impact of chlorophyll content, LAI, biomass and hydric status. High chlorophyll content and high LAI make its position shifts toward the longer wavelengths and vice versa. Instead of seeking for an exact or approximate red edge position, the proposed VI construction method makes it possible to capture relevant red edge bands without prior knowledge. Other spectral bands with high correlation with defoliation when applied on CNDVI construction were residing at 763 nm, 803 nm, 1104 nm and 1195 nm. They were controlled by protein, lignin, water, cellulose and starch (Curran, 1989).

As a summary, the NDVI and EVI2 generated the highest correlation coefficient value of 0.55 constructed from the Hyperion hyperspectral bands among existing VIs. Furthermore, the three developed VIs generate higher correlation coefficient than any of that generated by existing VIs. Among them the CNDVI generate the highest correlation coefficient of 0.62. In contrast, the VIs generated using ALI multispectral data only provided correlation coefficients as high as 0. 28.

4.5.3 Mapping SBW defoliation using VIs

NDVI, NLI, RDVI and CNDVI were applied and compared for mapping SBW defoliation in the study site. The mapping results and regions for assessment generated from NDVI, NLI, RDVI and CNDVI were illustrated in Figure 4.8- Figure 4.11 respectively. As a binary classification, each mapping result was displayed as black and white distribution map in which black pixels represent lightly defoliated forest pixels and white pixels represent severely defoliated forest pixels. The whole study site was mapped using NDVI, NLI, RDVI and CNDVI as shown in Figure 4.8(a)- Figure 4.11(a). The

region used for assessment was a part of the study site located at upper right corner and for assessment purpose binary images were shown in Figure 4.8(b)- Figure 4.11(b) respectively. The ground truth map was illustrated in Figure 4.8(c)- Figure 4.11(c).

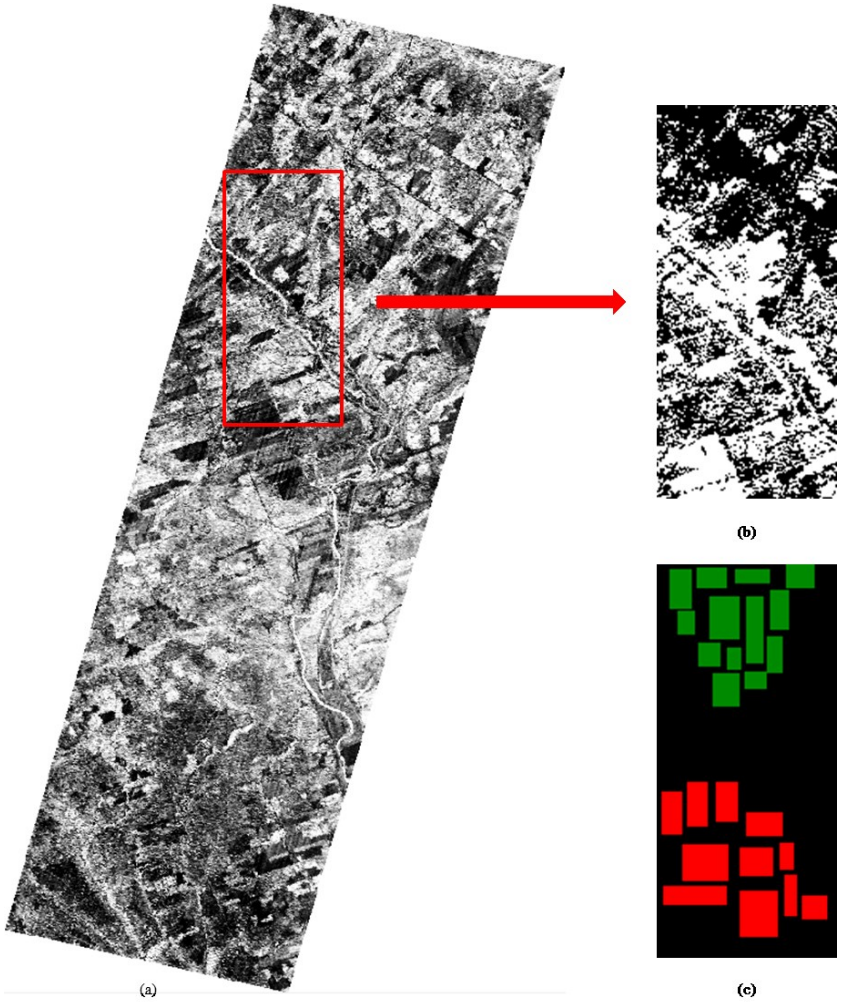

Figure 4.8 Defoliation mapping result using NDVI index of the study site. (a) A grayscale image of the testing area; (b) Defoliation results detected in EO-1 Hyperion image where black pixels indicate light defoliated pixels and white pixels indicate severely defoliated pixels ; (c) Ground truth map of assessment region where green blocks were light defoliated forestry and red blocks were severely defoliated areas.

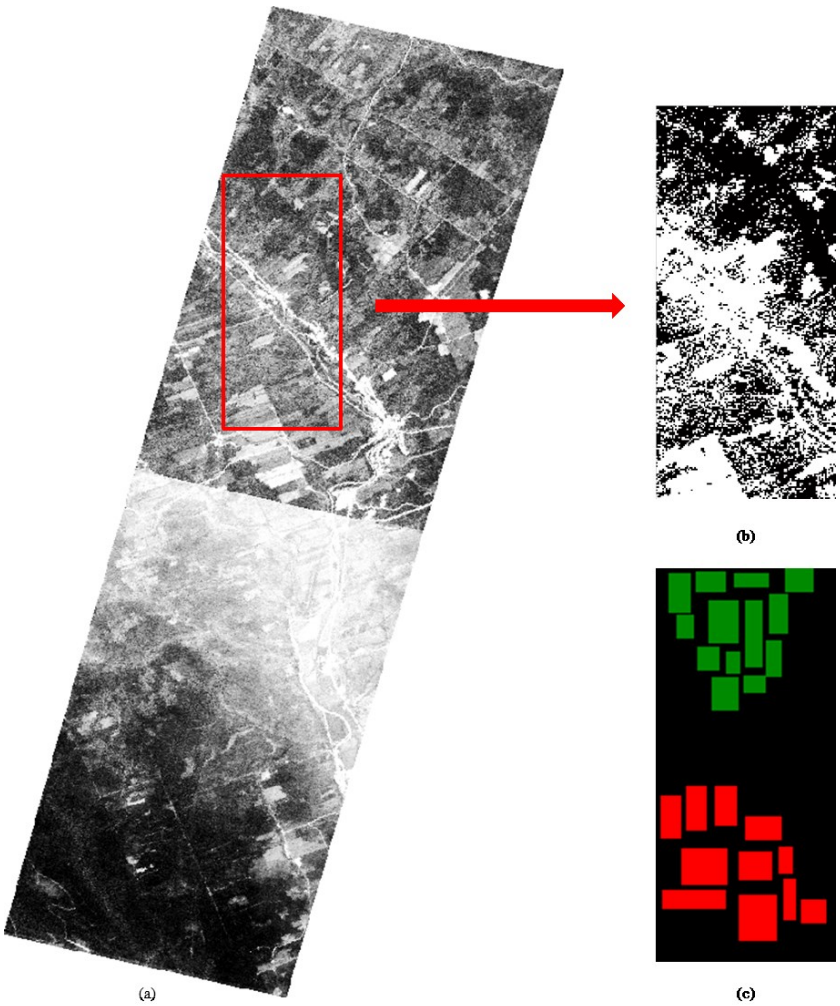

Figure 4.9 Defoliation mapping result using NLI index of the study site. For more information refer to Figure 4.8.

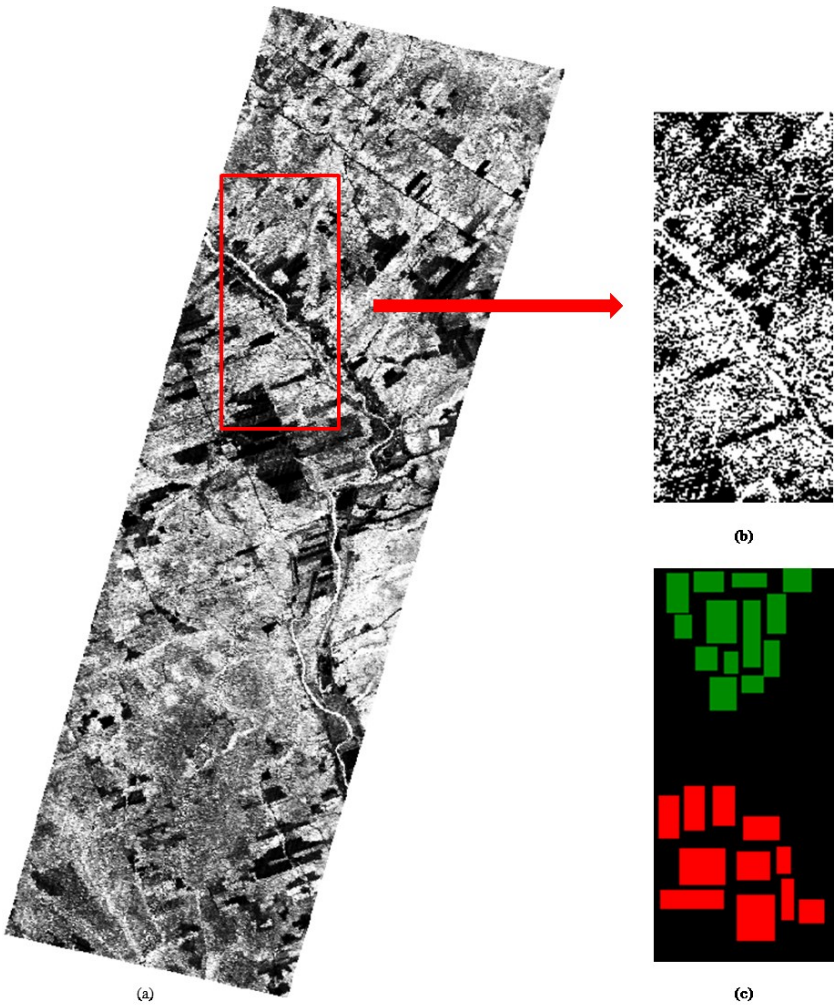

Figure 4.10 Defoliation mapping result using RDVI index of the study site. For more information refer to Figure 4.8.

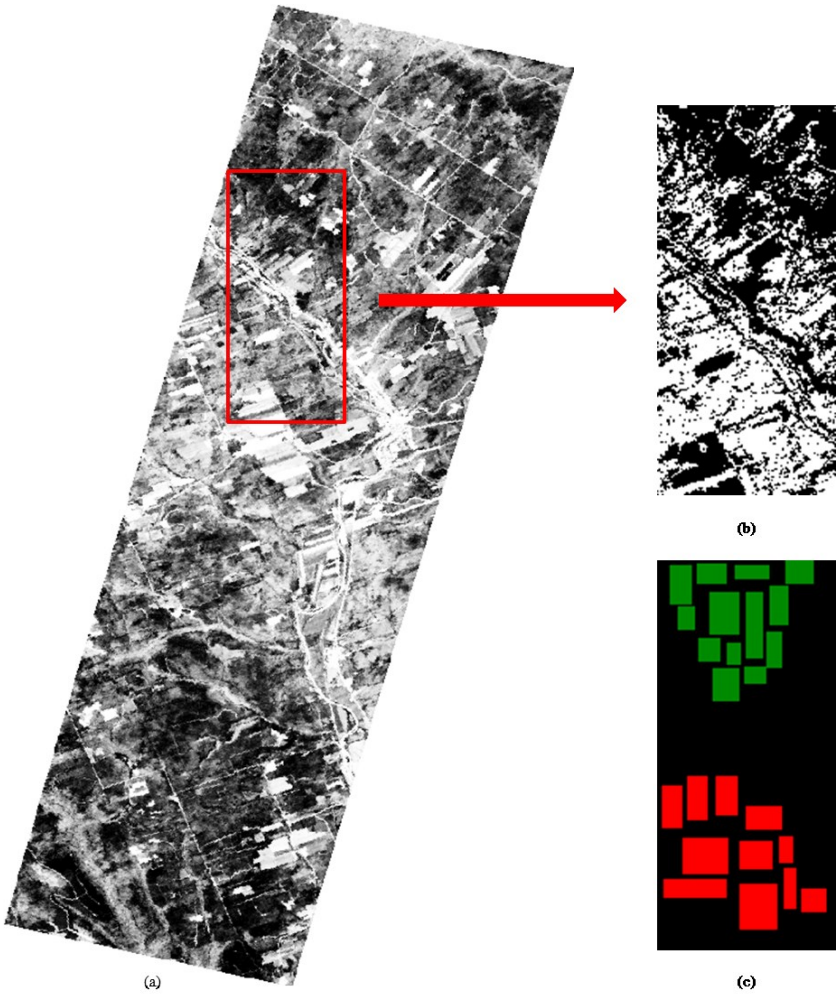

Figure 4.11 Defoliation mapping result using CNDVI index of the study site. For more information refer to Figure 4.8.

It contains two classes shown by red color for severely defoliation pixels, green color for lighted defoliated pixels while black color as background stands for areas without classified information or not being considered as vegetation regions. The NDVI, NLI and CNDVI all have a good performance recognizing the majority of lighted defoliated pixels on the upper left corner while the mapping result of RDVI generates a relatively blurred scene instead of clean delineation. For the defoliated region, large block of white color can be seen from the CNDVI mapping result, followed by NIL and NDVI in which more

pixels were wrongly identified as lighted defoliation. Again, the RDVI fails to generate a satisfactory mapping result.

The mapping results were compared with the ground truth map pixel by pixel to calculate producer's, user's and overall accuracies as well as kappa coefficient for accuracy assessment, as shown in Table 4.3. The developed CNDVI suggests considerable better performances over existing NDVI on mapping both several and slight defoliated forestry regions. Accuracy assessment quantified how well different defoliation magnitude levels were mapped by using NDVI and CNDVI. CNDVI produced the producer's, user's accuracies of 83%, 76% for severe level and 74%, 73% for slight level, respectively. It obtains an overall accuracy of 78% and kappa coefficient of 0.43 which indicated a moderate agreement. Compared with mapping accuracies of NDVI, the CNDVI has made a larger improvement on mapping severe defoliation regions. The reason for this was two-folded: the developed index has better simulated the responses from defoliated forest spectra and moreover it can also due to the change of defoliation magnitude by time as the annual aerial survey report was used. The number of defoliated pixels was also estimated in the regions without ground truth providing more accountable information on their distribution.

Table 4.3 Comparison of accuracies using NDVI and CNDVI for mapping SBW defoliations

Accuracies	NDVI	NLI	RDVI	**CNDVI**
Producer's (Severe/Light)	79% / 61%	78% / 60%	67% / 59%	**83% / 74%**
User's (Severe/Light)	56% / 82%	54% / 82%	62% / 64%	**76% / 81%**
Overall	68%	67%	63%	**78%**
Kappa	0.37	0.35	0.26	**0.56**

ρ_1 and ρ_2 at wavelength 1568 nm and 691nm were used for NDVI, 488 nm and 1568 nm for NLI, 2254 nm and 448 nm for RDVI, 702 nm and 752nm were used for CNDVI.

The mapping results suggest a correspondence with the correlation results yielded using VIs constructed in this study, as the CNDVI constructed from highest correlated bands generate the best mapping results. It further demonstrates the advantage of spectrally correlation analysis using remotely sensed hyperspectral data. The investigation provide more spectrally accurate and specific estimation on SBW defoliation by involvement of all 162 available Hyperion bands and 12 VIs. As a summary, the developed CNDVI is15% more accurate for mapping SBW defoliation in the study site than existing NDVI.

4.6 Conclusion

In this study, we investigated the potential of 9 existing vegetation indices (VIs) and 3 new VIs developed in this study for the estimation of spruce budworm defoliation in Quebec region, Canada, using Hyperion data. Suitable two spectral bands were selected from 162 available Hyperion hyperspectral bands for VI calculations. The VIs

include linear, nonlinear and soil adjusted models. The assessments on the performance of all tested 12 VIs were based on their correlation with defoliation data provided by airborne survey on the same site and mapping results. In our experiments, we noticed the soil adjusted model fail to improve neither linear VIs nor nonlinear VIs. Existing nonlinear VIs fail to improve the correlation results with given data in comparison with their linear correspondence. While the developed Cosine function based VIs suggested outperformances the existing VIs in our experiments.

With same methodology applied, the Hyperion hyperspectral image achieved considerably better estimation results compared with ALI multispectral image. A possible reason was that Huang et al. applied 162 bands of Hyperion hyperspectral data that had much more bands with much higher spectral resolution, while this study applied only nine bands of ALI multispectral data. Hyperspectral data having a large number of bands with narrow spectral interval provide almost continuous spectra of targets and natural backgrounds, and this may increase the discrimination capability of subpixel size targets. Furthermore, the VIs analysis was statistic based. The increase of the number of bands improved the spectral information from the image that involved in the correlation analysis. Consequently, spruce budworm defoliation could be better identified from Hyperion hyperspectral data.

Finally, NIR bands at 600-800 nm and SWIR bands 1700-2200 nm were identified to be more relevant to defoliation estimation. NDVI together with developed CSR, CDVI, and CNDVI were recommended for estimation of SBW defoliation in regions similar to our study site.

Acknowledgement

This research was funded by the Canada Research Chair Program. The authors would like to thank NASA for collecting the Hyperion images of the testing areas, Dr. David MacLean and his research team for the support in field investigation, and Dr. Brigitte Leblon and her student in spectral measurements of the infected spruce and balsam branches.

References

Alfredo Huete, Chris Justice, Wim van Leeuwen, a. (1999). Modis Vegetation Index Algorithm Theoretical Basis. *Environmental Sciences*, (Mod 13), 129.

Beck, R. (2003). EO-1 User Guide v. 2.3, 74. Retrieved from http://eo1.usgs.gov/documents/EO1userguidev2pt320030715UC.pdf

Blackburn, G. A. (1998). Quantifying Chlorophylls and Caroteniods at Leaf and Canopy Scales. *Remote Sensing of Environment*, *66*(98), 273–285. doi:10.1016/S0034-4257(98)00059-5

Chen, J. M. (1996). Evaluation of Vegetation Indices and a Modified Simple Ratio for Boreal Applications. *Canadian Journal of Remote Sensing*, *22*(3), 229–242. doi:10.1080/07038992.1996.10855178

Curran, P. J. (1989). Remote sensing of foliar chemistry, *278*, 271–278. doi:10.1016/0034-4257(89)90069-2

Datt, B., McVicar, T. R., Van Niel, T. G., Jupp, D. L. B., & Pearlman, J. S. (2003). Preprocessing EO-1 Hyperion hyperspectral data to support the application of agricultural indexes. *IEEE Transactions on Geoscience and Remote Sensing*, *41*(6), 1246–1259. doi:10.1109/TGRS.2003.813206

Dawson, T. P., & Curran, P. (1998). A new technique for interpolating the reflectance red edge position [technical note], (April 2015), 37–41. doi:10.1080/014311698214910

De Beurs, K. M., & Townsend, P. A. (2008). Estimating the effect of gypsy moth defoliation using MODIS. *Remote Sensing of Environment*, *112*, 3983–3990. doi:10.1016/j.rse.2008.07.008

Goel, N. S., & Qin, W. (1994). Influences of canopy architecture on relationships between various vegetation indices and LAI and Fpar: A computer simulation. *Remote Sensing Reviews*, *10*(4), 309–347. doi:10.1080/02757259409532252

Gong, P., Pu, R., Biging, G. S., & Larrieu, M. R. (2003). Estimation of forest leaf area index using vegetation indices derived from Hyperion hyperspectral data. *Geoscience and Remote Sensing, IEEE Transactions on*, *41*(6), 1355–1362.

Goodenough, D. G., Dyk, A., Niemann, K. O., Pearlman, J. S., Chen, H., Han, T., … West, C. (2003). Processing Hyperion and ALI for forest classification. *IEEE Transactions on Geoscience and Remote Sensing*, *41*(6), 1321–1331. doi:10.1109/TGRS.2003.813214

Gray, D. R., Régnière, J., & Boulet, B. (2000). Analysis and use of historical patterns of spruce budworm defoliation to forecast outbreak patterns in Quebec. Forest ecology and management, 127(1), 217-231.

Griffin, M. K., May-Hsu, S., Burke, H. K., Orloff, S. M., & Upham, C. A. (2005). Examples of EO-1 Hyperion data analysis. *Lincoln Laboratory Journal*, *15*(2), 271–298.

Han, T., Goodenough, D. G., Dyk, a., & Love, J. (2002). Detection and correction of abnormal pixels in Hyperion images. *IEEE International Geoscience and Remote Sensing Symposium*, *3*(C), 1327–1330. doi:10.1109/IGARSS.2002.1026105

Huete, a. . (1988). A soil-adjusted vegetation index (SAVI). *Remote Sensing of Environment*, *25*, 295–309. doi:10.1016/0034-4257(88)90106-X

ITT Visual Information Systems (2006). "ENVI FLAASH Module User's Guide (2006 Edition)." [Online] September 21, 2012: ftp://popo.jpl.nasa.gov/pub/ENVI_Installers/ENVI_Documentation/docs/FLAASH_Module.pdf.

Jiang, Z., Huete, A. R., Didan, K., & Miura, T. (2008). Development of a two-band enhanced vegetation index without a blue band. *Remote Sensing of Environment*, *112*, 3833–3845. doi:10.1016/j.rse.2008.06.006

Jupp, D.L.B., Datt, B., McVicar, T.R., Van Niel, T.G., Pearlman, J.S., Lovell, J.L. and King, E. A. (2003). Improving the Analysis of Hyperion Red-Edge Index from an Agricultural area. *Image Processing and Pattern Recognition in Remote Sensing*, *4898*(October 2002), 1–15. doi:10.1117/12.472696

Ministère des Forêt, de la Faune et des Parcs (MFFP). (2014). Aires infestées par la tordeuse des bourgeons de l'épinette au Québec en 2014. Version 1.0 [Online] September 2014: http://www.mffp.gouv.qc.ca/publications/forets/fimaq/insectes/tordeuse/TBE_2014_P.pdf

Qi, J., Chehbouni, a., Huete, a. R., Kerr, Y. H., & Sorooshian, S. (1994). A modified soil adjusted vegetation index. *Remote Sensing of Environment*, *48*, 119–126. doi:10.1016/0034-4257(94)90134-1

Roujean, J. L., & Breon, F. M. (1995). Estimating PAR absorbed by vegetation from bidirectional reflectance measurements. *Remote Sensing of Environment*, *51*(December 1994), 375–384. doi:10.1016/0034-4257(94)00114-3

Rullan-Silva, C. D., Olthoff, a. E., Delgado De la Mata, J. A., & Pajares-Alonso, J. A. (2013). Remote monitoring of forest insect defoliation. A review. *Instituto National de Investigacion Y Tecnologia Agraria Y Alimentaria (INIA)*, *22*(3), 377–391. doi:10.5424/fs/2013223-04417

Seager, S., Turner, E. L., Schafer, J., & Ford, E. B. (2005). Vegetation's red edge: a possible spectroscopic biosignature of extraterrestrial plants. *Astrobiology*, *5*(3), 372–390. doi:10.1089/ast.2005.5.372

Smith, P., Reid, D. B., Environment, C., Palo, L., Alto, P., & Smith, P. L. (1979). A Threshold Selection Method from Gray-Level Histograms. *IEEE Transactions on Systems, Man, and Cybernetics*, *9*(1), 62–66. doi:10.1109/TSMC.1979.4310076

Spruce, J. P., Sader, S., Ryan, R. E., Smoot, J., Kuper, P., Ross, K., … Hargrove, W. (2011). Assessment of MODIS NDVI time series data products for detecting forest defoliation by gypsy moth outbreaks. *Remote Sensing of Environment*, *115*(2), 427–437. doi:10.1016/j.rse.2010.09.013

Taylor, S. L., & MacLean, D. A. (2008). Validation of spruce budworm outbreak history developed from aerial sketch mapping of defoliation in New Brunswick. Northern Journal of Applied Forestry, 25(3), 139-145.

Thenkabail, P. S., Smith, R. B., & De Pauw, E. (2000). Hyperspectral vegetation indices and their relationships with agricultural crop characteristics. *Remote Sensing of Environment*, *71*(99), 158–182. doi:10.1016/S0034-4257(99)00067-X

Tucker, C. J. (1979). Red and photographic infrared linear combinations for monitoring vegetation, *150*, 127–150. doi:10.1016/0034-4257(79)90013-0

Ungar, S. G., Pearlman, J. S., Mendenhall, J. A., & Reuter, D. (2003). Overview of the Earth Observing One (EO-1) mission. *IEEE Transactions on Geoscience and Remote Sensing*, *41*(6), 1149–1159. doi:10.1109/TGRS.2003.815999

Vogelmann, J. E. (1990). Comparison between two vegetation indices for measuring different types of forest damage in the north-eastern United States. *TitleREMOTE SENSING*, *11*(12), 2281–2297.

5 CHAPTER 5

EXPLOITING SPECTRAL AND SPATIAL INFORMATION FOR MAPPING SPRUCE BUDWORM DEFOLIATION USING HYPERION HYPERSPECTRAL DATA

Abstract

As an indirect surveying method, remote sensing technique has special advantages on monitoring and mapping the forestry properties that caused by external damages. The spruce budworm (SBW) defoliates dramatically the spruce and balsam fir forests in eastern Canada. Timely and accurate mapping of the defoliation will provide crucial support to mitigate the socio-economic impact on vulnerable forests. In this study, we provide a method for mapping SBW defoliation for a study site in the province of Quebec, Canada using remotely sensed Hyperion hyperspectral data. The Hyperion data provide fine spectral resolution among a wide range of spectral wavelengths which allows for spectral information extraction. However, its spatial resolution was relatively coarse (30m) which results in dominant mixed pixels especially in homogenous forestry regions. Such condition makes conventional mapping methods that need pre-located and labeled endmembers very difficult to use or even inapplicable. In this study, we propose a mapping method that exploits both spectral and spatial information from hyperspectral data. The method requires no pre-labeled endmembers and uses an unsupervised K-

means classifier to map the defoliation. As relevant features were exploited, the classifier performs better than applied on original high dimensional data or other dimensionality reduction method such as Minimum Noise Fraction (MNF) Transform.

Keywords: Hyperspectral image processing, spruce budworm defoliation, feature extraction.

5.1 Introduction

Remote sensing has become an invaluable tool in mapping nature disturbance in forests. Linked with spatial and spectral properties, the biophysical of forests can be identified in remotely sensed imagery. Moreover, the indirect survey makes remote sensing more suitable for investigation on inaccessible forestry areas with considerable size. Specifically, remote sensing techniques have been applied for mapping the defoliation in spruce and fir forests in Quebec, Canada caused by spruce budworm, one of their most harmful inhibited inserts (Gray and Re, 2000). Conventional Strategies to eliminate or slow the spread of these destructive pests such like pesticide spraying can be costly, time consuming and less effective when accurate estimation of defoliated regions was not available. Using remote sensing techniques, especially satellite images, provide spatially unlimited and wide coverage for investigation. Researches have been conducted on mapping forests defoliation caused by SBW or other insects using remote sensing data, such like Landsat (Thomas et al., 2007) and MODIS(de Beurs and Townsend, 2008). However, little evidence has been found on using hyperspectral imagery for

mapping SBW defoliation. Especially, the Hyperion hyperspectral data obtained from EO-1 satellite were used in this study. The imagery was obtained from NASA free of charge. The Hyperion data provide hundreds of channels with spectral interval of around 10 nm provide almost continuous spectra for field observations. The forests biophysical properties can be therefore identified on responses from relevant spectral bands. In order to derive useful information from those bands, narrow band vegetation indices (VIs) can be constructed using available Hyperion bands. Compared with broad band VIs constructed using multispectral bands, narrow-band VIs have advantages in identifying more accurate spectral information.

Research conducted on mapping or classification using hyperspectral data can take advantage of its wealthy spectral information. The increase of dimensionality in hyperspectral data was expected to increase the abilities of classifying objects in remote sensing scenes. However, the classification methods that have been successfully applied to multispectral data in the past were not as effective as to hyperspectral data. The major cause was that the size of training data set does not adapt to the increasing dimensionality of hyperspectral data (Science, 2001). As the dimensionality increases with the number of bands, the number of training samples needed for training a specific classifier should be increased exponentially, which was usually not available. This will result in overfitting of the training data and poor generalization capabilities of the classifier. Moreover, in many objects, their reflectance or absorption characteristics only appear at a very narrow spectral range. The correlation between the bands was also quite strong (Su et al., 2008). All these properties make hyperspectral data redundant in its data volume and

classification accuracies can be affected by irrelevant bands. Thus dimensional reduction by means of feature extraction in hyperspectral data was usually useful. The feature extraction was considered as a data mapping procedure which will reduce the dimensionality of data, especially considered as the number of bands in hyperspectral data, to an appropriate dimension. The resultant data contain less number of bands while preserve critical spectral information. Existing methods, such like Minimum Noise Fraction (MNF) Transform (Boardman, 1993) reduces the spectral dimension by applying a linear transformation on the image bands and retaining only the significant components for further processing. Although these approaches were sufficient for reducing data volume, they do not emphasize individual spectral classes or signatures of interest (Harsanyi and Chang, 1994). For example, the first principal component image contains the most spectral information, but it was generally a linear combination of information from different spectral classes. Especially in homogeneous forest areas, the spectral information was still highly mixed after the transformation. Thus the MNF transformation may not necessarily help separate spectral classes in specific applications.

In this study, we aim to extract feature from Hyperion hyperspectral imagery readily for mapping SBW defoliation. Less or no training samples will be needed. Moreover, the feature will be suitable for existing classifiers and achieve better performance. A Spectral- Spatial based mapping method (SSM) was developed focusing at hyperspectral feature extraction for mapping SBW defoliation. The designed feature extraction consists of two phases: spectral information extraction and spatial information extraction. Instead of applying principle analysis, the proposed method derives spectral

information and reduces the data volume by replacing the original Hyperion bands with constructed VI bands. Research on the performances of difference Hyperion bands and the vegetation indices yielded from them has been conducted in (Gong et al., 2003). Thus the developed VIs constructed with most relevant Hyperion bands were used to extract spectral information for mapping purpose.

Recent studies suggest the advantage of integrate spatial information in hyperspectral classifications. Spectral–spatial classification aims at assigning each image pixel to one class using a feature vector based on the following: 1) its own spectral value (the spectral information) and 2) information extracted from its neighborhood (referred to as the spatial information) (Tarabalka et al., 2009). In this study, a histogram based method was applied to extract spatial information on derived spectral bands. The method was developed with the consideration that neighborhood of similar incident pixel should have similar spatial character identified by their respective histograms. Those histograms were then combined as features integrated both spectral and spatial information. Finally the constructed features as a substitution to the original Hyperion bands were put into a k-means classifier (MacQueen, 1967)attempting to classify and mapping different forest status, i.e., the extent of SBW defoliation in our study site.

5.2 Study Site and Materials

5.2.1 Study site

The study site used in this study for mapping SBW defoliation was shown in Figure 5.1. We established several campaigns for Hyperion data acquisition during June,

July and August, 2014 on a selected site centered at 48°09’54’’S/67 °19’21’’W near the Causapscal city, across the Bas-Saint-Laurent region which located along the south shore of the lower Saint Lawrence River in the Quebec Province, Canada. One footprint of the Hyperion stripes was shown in Figure 5.1. Our study site locates at the upper right corner of the stripe as illustrated.

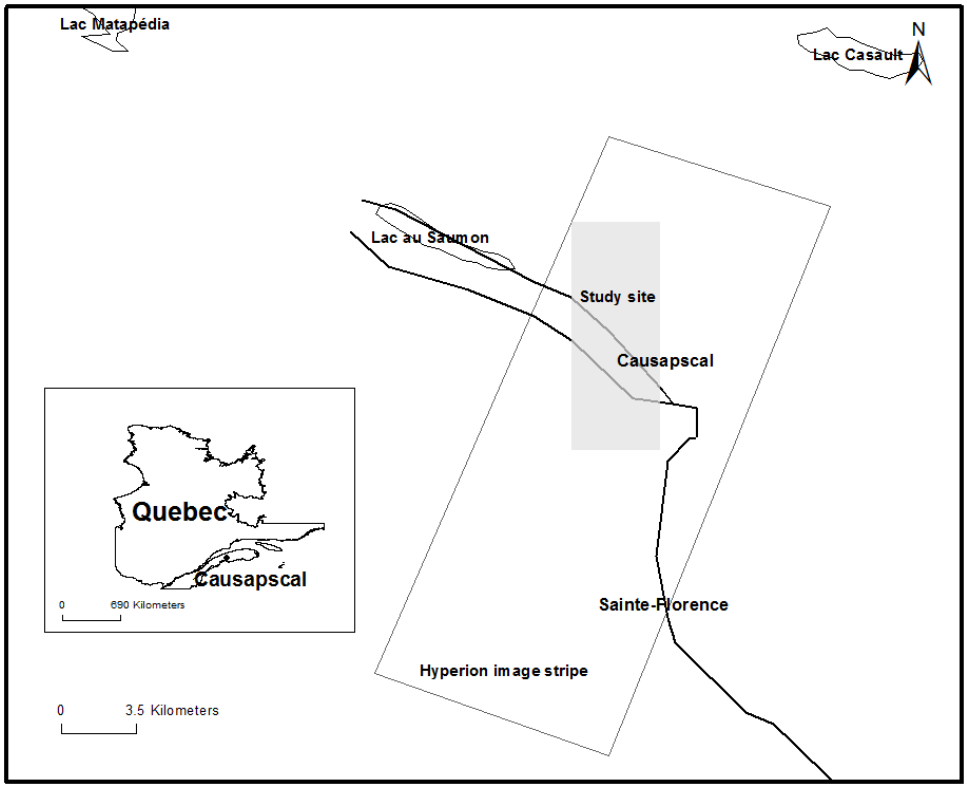

Figure 5.1 Study site

The study on mapping SBW defoliation not only provides novel research approaches but also provides critical information potentially help eliminate spread of SBW. According to the aerial survey report “Infested areas of spruce budworm in Quebec

in 2014" (Quebec, November 2014), the Bas-Saint-Laurent region was one of the most dominant infested areas by spruce budworm in Quebec, totaled 316,103 hectares. It was a relatively homogeneous rural area mostly covered by spruce and fir. The area affected by SBW continues to rise significantly in the province. In 2014, they totaled 4,275,065 hectares compared to 3,200,348 hectares in 2013.

5.2.2 Materials

Interpretation ground truth of SBW infested fields was provided by the Quebec government report (MFFP, 2014). The aerial survey of damage caused by major forest pests was carried out annually since 1967 by the Ministry of Forests, Fauna and Parks (Ministère des Forêt, de la Faune et des Parcs, MFFP). The aerial survey scans natural disturbances observed from the air in real time. The aircraft flies at an altitude of about 240 meters, at a speed of 160 km / h, keeping a distance of 4.5 kilometers between flight lines. The survey reports three levels of defoliation in Quebec, namely slight, moderate and serious, containing the study site mentioned above. According to the study of Dr. Taylor and Dr. MacLean in 2008 (Taylor & MacLean, 2008), from 1985 to 1993, 85% of 332 cases were correctly classified by aerial estimate. They concluded that aerial surveys provide a reasonable estimate of defoliation.

The EO-1 Hyperion hyperspectral image stripe applied in this study was acquired on July 19, 2014, around 10:20 A.M. local time, it was cropped from the same imagery used in Chapter 4. The selection of image stripes was determined by both the image quality which heavily affected by the cloud condition and the acquisition date which

should reflect most infested areas. The selection of study site for mapping in this study was based on observation of airborne report. Even though the report provides across province survey results, the distribution map was relatively coarse. So the study site was selected at a region where two pieces of forests with different levels of defoliations were separated by roads. The image was at level L1R processing, meaning that it was only radiometrically corrected and with no geometrically correction applied (Beck, 2003).

5.3 Methodology

5.3.1 Data Pre-processing

Hyperion data contain 242 spectral bands in total, 44 ones of which were not calibrated because they were intentionally not illuminated or correspond to areas of low sensitivity of the spectrometer materials (Datt et al., 2003). In addition, two more zero bands were identified in our data of use, which were band 80 and 81. In addition, atmospheric water vapor bands which absorb almost the entire incident and reflected solar radiation and the bands that have very severe vertical stripping also need to be removed (Beck, 2003). Thus, the subset of 162 selected bands (bands 10-57, 77-79, 82-119, 134-165, and 181-221 within 447-2365 nm) were applied in this study.

For the subset of 162 selected bands, abnormal pixels that have lower DN values as compared to their neighboring pixels were corrected by replacing their DN values with the average DN values of their immediate left and right neighboring pixels (Han et al., 2002). Vertical stripes were removed using the “SPEAR Vertical Stripe Removal” in the ENVI software (ITT Visual Information Systems, 2006) (Datt et al., 2003). The "smile

effects" that refer to an across-track wavelength shift from center wavelength due to the change of dispersion angle with field position (Goodenough et al., 2003) were removed using the procedure of "Cross-Track Illumination Correction" (Jupp et al., 2003) in the ENVI software (ITT Visual Information Systems, 2006). This study uses the Fast Line-of-sight Atmospheric Analysis of Spectral Hypercubes (FLAASH), an atmospheric correction module implemented in the ENVI to calibrate the at-sensor radiance data to land surface reflectance (Beck, 2003).

The ground truth of study site was derived from one thematic map covering our study site was provided by the aerial survey report. In the ground truth, two levels of defoliations present on two separated pieces of forests: slight (loss of foliage in the upper third of the tops of some trees) and severe (loss of foliage on the entire length of the top of most trees). As illustrated in Figure 5.6(d), slight defoliation areas were marked by green color while severe ones were marked by red color. The black back ground illustrates uninvestigated areas from aerial survey. Both the ground truth map and the Hyperion data were geometrically corrected using the ENVI “Image to Map Registration” process. They were first projected to datum WGS 84 and the “Geographic lat/lon” projection was selected. The latitude and longitude of selected ground control points were matched on Google Earth. An overall root mean square error (RMSE) of 0.39 pixel was achieved.

5.3.2 Exploit Spectral Information

The proposed SSM method starts with extraction of relevant spectral information concerning SBW defoliation. Hyperspectral data contains rich spectral information for feature extraction. The spectral feature extraction should serve to preserve the information of interest for a special application or problem. In our case, the extracted spectral feature should be able to distinguish regions with different conditions in defoliated magnitudes. Construction of vegetation indices was effectively applied to relate forestry biophysical condition to remotely sensed image data. Meanwhile the increase of number of spectral bands in hyperspectral data makes it possible to construct narrow-band VIs, which allows for obtaining more specific and precise VIs that highly correlated with defoliation status. Those VIs were described by a function whose output varies with the input spectral bands. The study on the selection of the function as well as accompanied spectral bands were studied in (Huang, 2015). So in this study, we reduce the dimensionality of Hyperion data by replacing the original hyperspectral bands with constructed vegetation indices bands, as shown in Figure 5.2(a)-(b). The applied vegetation index was

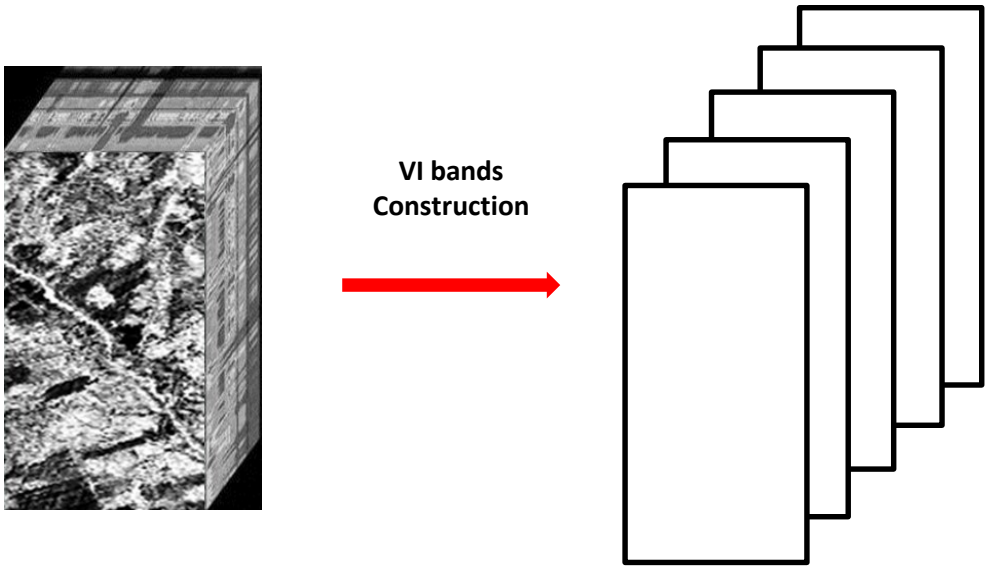

Figure 5.2 Extract spectral information from original Hyperion data as shown in (a) by constructing 5 vegetation index bands as shown in (b).

developed in (Huang, 2015) by applying a Cosine function on conventional normalized difference vegetation index (NDVI). Narrow-band VIs were constructed using this index. Based on their results, the applied Hyperion bands for constructing the vegetation indices bands were summarized in Table 5.1. Unlike conventional dimensional reduction methods that derive spectral information by considering spectral significance in general, the narrow band VIs used in our study contains most relevant spectral information for identifying SBW defoliations. This was supported by researches and experiments conducted in (Huang, 2015) where VIs and associated Hyperion bands with highest correlation with defoliation data were reported. After the VI band construction, only five

bands were used for mapping and classifying defoliation status in our study site.

Table 5.1 Construction of VI bands used for spectral information extraction

VI band	Formulas (subscripts shown applied Hyperion bands)	Wavelengths
1	$\cos\frac{\rho_{40}-\rho_{35}}{\rho_{40}+\rho_{35}}$	752 nm / 702 nm
2	$\cos\frac{\rho_{15}-\rho_{41}}{\rho_{15}+\rho_{41}}$	590 nm / 763 nm
3	$\cos\frac{\rho_{15}-\rho_{45}}{\rho_{15}+\rho_{45}}$	590 nm / 803 nm
4	$\cos\frac{\rho_{15}-\rho_{96}}{\rho_{15}+\rho_{96}}$	590 nm / 1104nm
5	$\cos\frac{\rho_{15}-\rho_{105}}{\rho_{15}+\rho_{105}}$	590 nm / 1195nm

Details on VIs construction and their relationship with SBW defoliation can be referred to (Huang, 2015).

As mentioned, existing methods for hyperspectral dimensional reduction, such like MNF transformation, was also widely applied in spectral information extraction. Therefore in this study we compare our method with conventional MNF method to demonstrate the efficiency of proposed spectral extraction method.

5.3.3 Exploit Spatial Information

The second phase of proposed SSM method was about exploiting spatial information to enhance the efficiency of extracted feature. Exploit spatial information in a hyperspectral scene can increase the robustness of feature and make different objects more distinguishable. In proposed method, this process was done by integration of information from neighboring pixels of one incident pixel. As pixels on an image were highly correlated, i.e. the pixels in the immediate neighborhood possess nearly the same feature data. Therefore, the spatial relationship of neighboring pixels was an important characteristic that can be of great aid in imaging classification. The combination of neighboring information was implemented by using histogram. A histogram was a graphical representation of the distribution of data. In images, the histograms serve as a statistic summary of pixel values. The summary can be applied on local neighborhood of each incident pixel as well, considered as local histogram (Figure 5.3(a)). Local image histograms contain a great deal of information useful for applications in image processing and computer vision. Making use of such information could help distinguish spectral classes that can be hardly classified if only one pair of incident pixels was compared. With neighborhood of each pixel taken in to account in homogenous forestry region in hyperspectral scenes, the classified regions tend to form blocks instead of discrete points which was more close to reality.

In order to integrate spatial information to construct features, we first define a neighborhood surrounding each incident pixel on each VI band image. A histogram was extract for each pixel location based on its neighborhood. The process was illustrated in

Figure 5.3(a)- (c). Depending on the size of neighborhood, the pixels near the boundary of each VI band will not get sufficient neighbors, so we generate a solution in this study by applying a symmetric padding around the original VI band image, as illustrated in Figure 5.4. An original VI band image was defined inside the black outlines. First, an outside boundary was defined in order to make room for neighborhood generation. Given a neighborhood with size $w \times w$, the four outside boundary was located by extending the each original boundary of the VI band image with a width of r, where $r = (w-1)/2,$ i.e. if the distance r of a pixel was close enough to its closest boundary that not greater half of the neighborhood size, it will be copied to generate a new

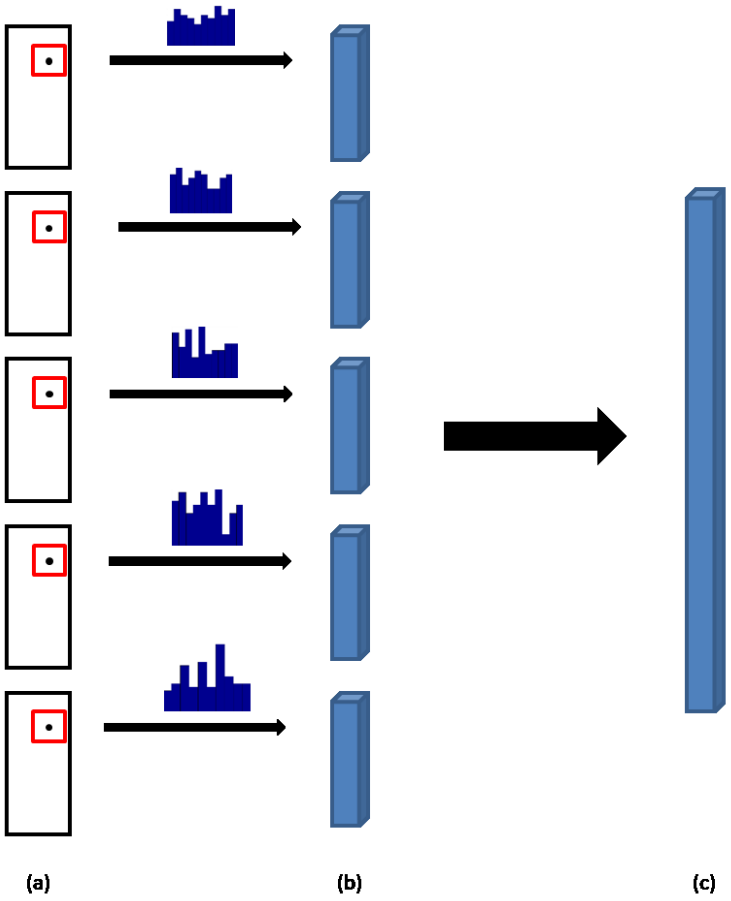

Figure 5.3 Process of exploiting spatial information by extracting histogram vectors (b) from each VI band (a) and stacking into a single feature vector (c) for each pixel location.

point outside the original boundary with the same pixel value by means of point or line symmetry. The pixels inside the red squares on the four corners of the original image will be copied to the four corners of the new boundaries by means of point symmetry. Pixels within other colored blocks will be copied to outside blocks in new boundaries with the same colors.

This was to provide neighborhood for all the pixels on the original VI bands to calculate the histograms. Each histogram was saved as a vector with its dimension equals to the bin used in histograms. Finally the histogram generated from each VI band for one

pixel will be stacked one after another into one feature vector and put in classifier for classification and mapping.

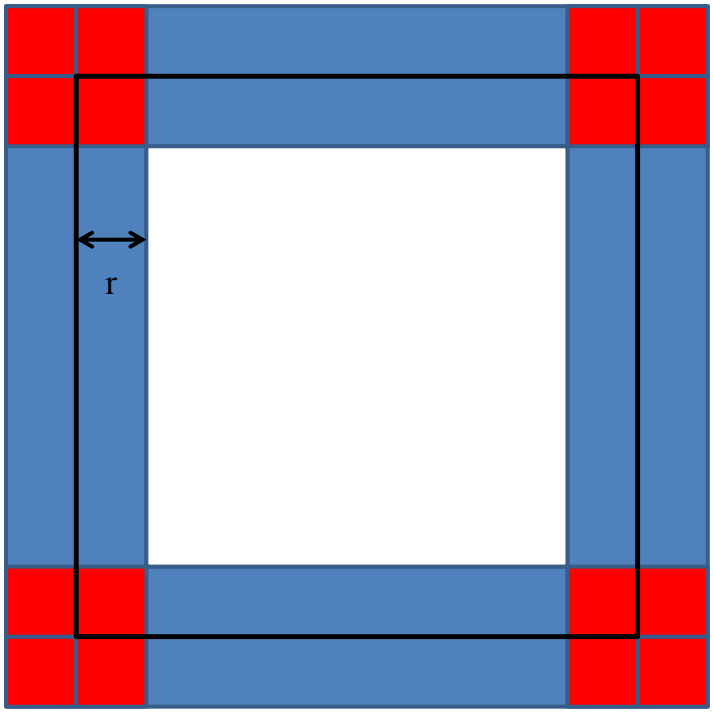

Figure 5.4 Illustration of symmetric padding method used in neighborhood construction. The original VI band image was defined inside the black outlines. The blue and red blocks outside the black outlines were generated based on line or point symmetry based on their respective locations.

5.3.4 Classification and mapping SBW defoliation

The final step of proposed method was to apply a classifier on constructed features to generate classified mapping results. An unsupervised k-means classifier was applied in this study, meaning that we didn't provide the classifier any training samples of SBW defoliation data. This will further demonstrate the efficiency of our spectral-spatial feature. k-means classifier was an algorithm developed to partition the n

observations $\mathbf{x} = \{x_1, x_2, ..., x_k\}$ into k (≤ n) sets $\mathbf{S} = \{S_1, S_2, ..., S_k\}$ so as to minimize the within-cluster sum of squares (WCSS):

$$\arg\min_{\mathbf{S}} \sum_{i=1}^{k} \sum_{\mathbf{x} \in S_i} \| \mathbf{x} - \mu_i \|^2,$$

where μ_i was the mean of the points in set S_i.

In our particular case, we aim to mapping the SBW defoliation by classifying into two sets in which relatively light defoliated pixels and severely defoliated pixels can be presented. Thus k =2 in our experiments. Three types of data will be put into k-means classifier for comparison, namely the original Hyperion data, MNF bands and feature bands constructed using proposed method. Their performances will be compared and analyzed in next section.

5.4 Experimental Results and Assessment

5.4.1 Comparison of mapping results

The reflectance image obtained from pre-processing of used Hyperion data was used for mapping task. The reflectance data has 162 spectral bands. For comparison of the mapping results, three different input data were applied with the same k-means classifier, namely, the original reflectance data, with each data point a dimension of 162, the MNF bands, with each data point a dimension of 5 and the developed spectral-spatial feature, with each data point a dimension of 5**h**, where **h** stands for the number of bins used in histogram extraction.

The MNF transformation which derives principle components from the original bands will result in a sequence of MNF bands with decreasing significance in terms of spectral information derived. Thus in order to compare the performance of using MNF bands with our method, same number of five bands were selected from MNF bands by using the first five bands, as shown in Figure 5.5. The five bands contain different spectral information though there's no control or knowledge on which aspect of information has been extracted by each MNF band. For instance, the first band appears to extract brightness of the scene while the rest appears to have more information concern the landscape of scene while features like edges and shapes were still randomly spread among the bands.

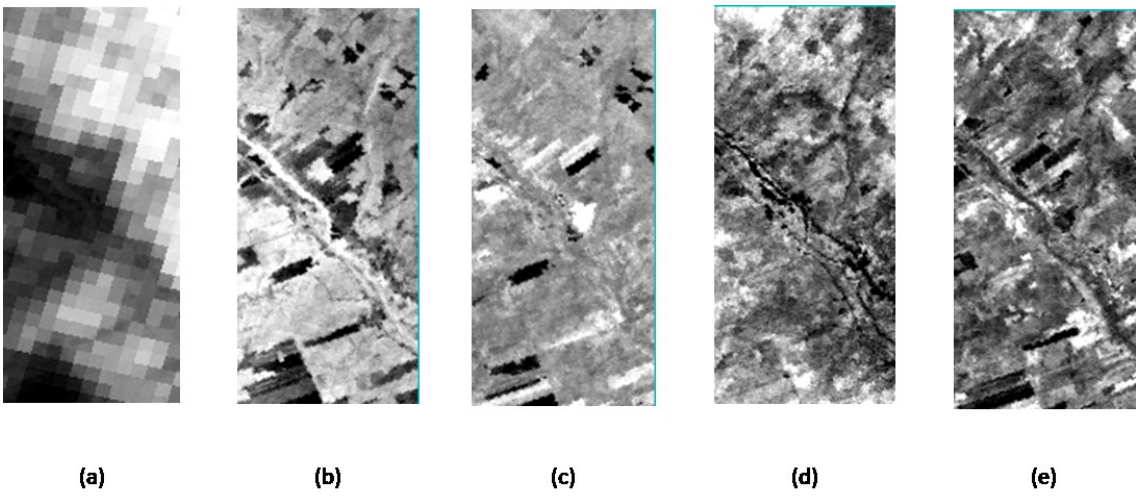

Figure 5.5 MNF bands 1-5 as shown in (a)-(e) were used for comparison in mapping SBW defoliation.

For proposed Spectral- Spatial based mapping method (SSM), a neighborhood size of 15×15 with a bin of 15 was applied for the histogram. The mapping results of

using three different inputs with the same k –means classifier were shown in Figure 5.6. As a binary classification was applied, the cluster number of the k –means classifier was set to be 2 for all the experiments. Then the classified results were displayed with black and while colors. As shown in the mapping results Figure 5.6(a)-(c), the white pixels represent severely defoliated regions while the black pixels were classified as light defoliated regions. The ground truth derived from the airborne survey was displayed in Figure 5.6(d) in which red blocks represent severely defoliated regions and green blocks represent light defoliated regions. Visually, one can find the SSM mapping result displayed in Figure 5.6(a) has the best result and dominant performance compared with the rest two. Most classified regions have precise match with the ground truth. In addition the mapped regions turn to be more homogeneous just like the real case in defoliated forests. The mapping result using MNF bands displayed in Figure 5.6(b) has also generate a relatively satisfying result for the light defoliated regions as compared with severely defoliation regions. As one find easily find large blocks at the lower right corner have been detected as light defoliated regions while they were mostly severely defoliated in real case. It was noteworthy that the mapping result also generated relatively homogeneous regions for both defoliated conditions. However, the zigzag artifacts were also very obvious. The original hyperspectral data, with the highest data volume in terms of dimension, fails to generate a satisfying result. The result turns to provide little discrimination between different defoliation magnitudes.

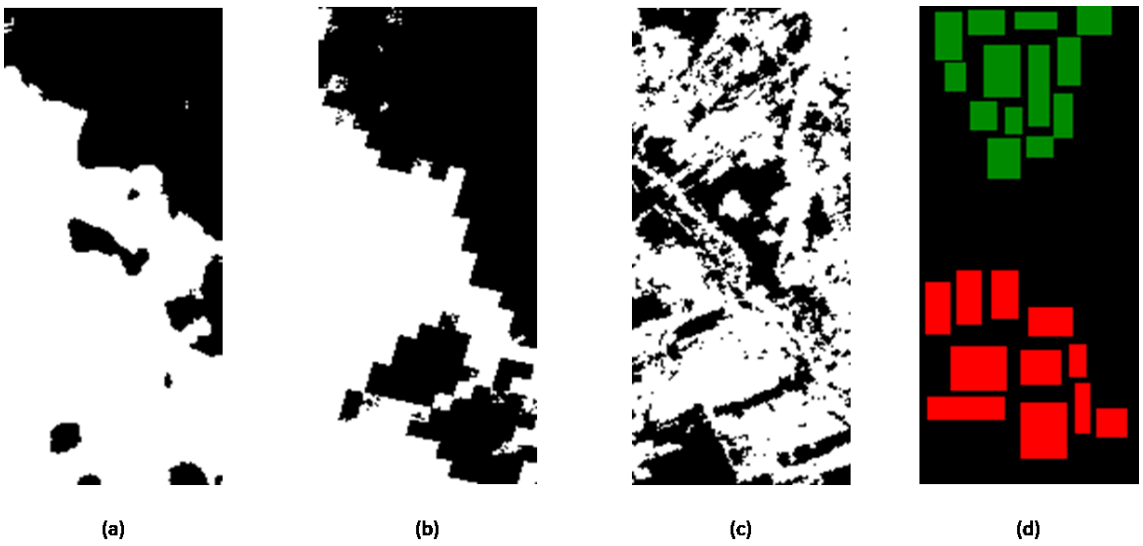

Figure 5.6 Mapping result for SBW defoliation condition of study site. (a) Mapping result by using proposed SSM method; (b) Mapping result by using MNF; (c) Mapping result by using original Hyperion reflectance data; (d) Ground truth map of assessment region where green blocks were light defoliated areas and red blocks were severely defoliated areas.

The mapping results were also evaluated with standard accuracy assessment as summarized in Table 5.2. SSM performs the best among the three in terms of Producer's, User's and Overall Accuracies and a strongest agreement suggested by high Kappa coefficient. As a binary classification, a successful classified result should have high accuracy detecting both classes. This explains why SSM has the best performance as all accuracies achieved for both classes were near or above 90%. This also explains why the other two classification results were not satisfactory though they sometimes detected very well on one class which was however a result of overcompensating the detection on the other. Thus this kind of biased classification result should not be considered as accurate

or useful.

Table 5.2 Comparison of accuracies using NDVI and CNDVI for mapping SBW defoliations

Accuracies	SSM	MNF	Original
Producer's (Severe/Slight)	91.8% / 99.7%	95.1% / 64.0%	59.5% / 60.7%
User's (Severe/Slight)	99.7% / 89.5%	54.0% / 96.7%	80.8% / 35.0%
Overall	95.1%	73.6%	59.8%
Kappa	0.90	0.49	0.16

Both SSM and MNF used 5 bands as input while the original Hyperion data used 162 bands as input.

As SSM extracts more relevant information from hyperspectral data and uses them as features, it shows clear advantage over conventional spectral feature extraction method MNF. Noticeably, directly applying k-means classifier on original Hyperion data shows its incompetence in classifying the high dimensional data for our mapping purpose. The high dimensional data contains considerable noise that can mislead the classifier to wrong directions.

5.4.2 Parameter Adjustments

As mentioned above, two parameters need to be adjusted for proposed SSM method to generate best results, namely the neighborhood size w and the bin size h for the histograms. Mutual tests on these two parameters concerning the mapping accuracies were conducted. First the bin size h was set to be 12 to seek for best performance given a

range of w. Then the w was fixed to seek for a best h. The user's, producer's and overall accuracies together with kappa coefficients when running these mutual tests were shown in Figure 5.7 and Figure 5.8. The results in Figure 5.7 suggest both overall accuracy and Kappa coefficient increase from smaller size neighborhood until reached maximum at w = 15 then decreases. So w = 15 was used to seek for an optimal bin size h. As shown in Fig. 8 the overall accuracies had a slight increasing with increments of w while slight fluctuations can be identified with associated Kappa coefficients. This was because k-means algorithm uses random initialization points which may end up in slight different classification results in each execution, but generally we consider the factor h has a less impact on our experiments as compared with w.

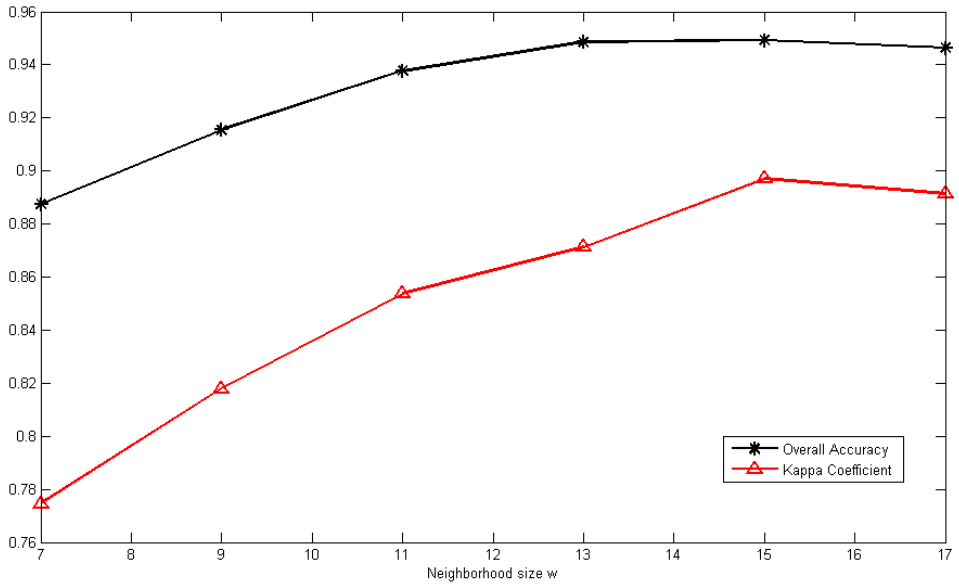

Figure 5.7 Overall accuracies and Kappa coefficients with a range of neighborhood size w being used for experiments. The bin size of histograms **h** was set to be 12.

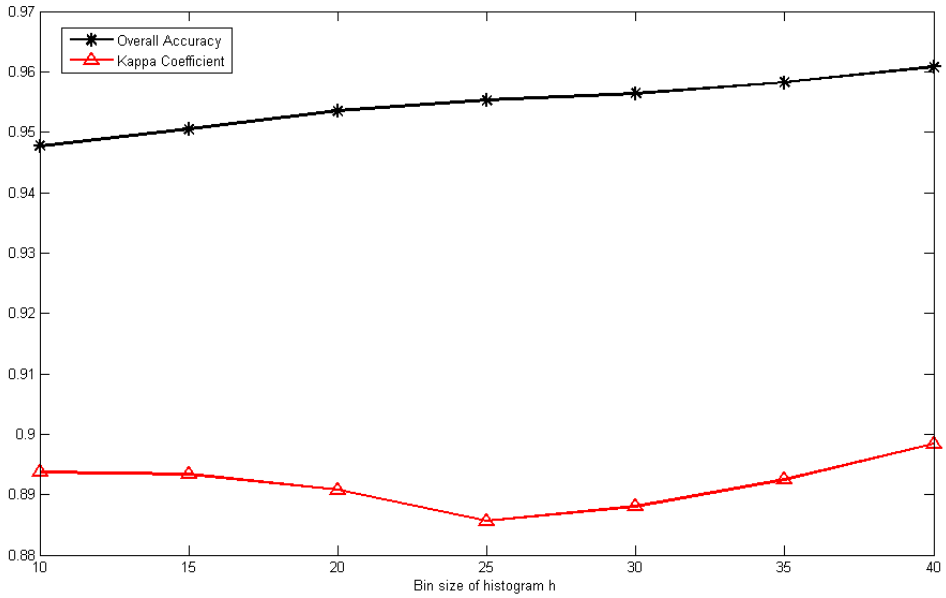

Figure 5.8 Overall accuracies and Kappa coefficients with a range of histogram bin size h being used for experiments. The neighborhood size w was set to be 15.

5.5 Conclusion

In this study, we proposed a spectral-spatial based method for mapping the defoliation caused by spruce budworm in a study site in Quebec, Canada using Hyperion hyperspectral data. The spectral information were derived from vegetation index bands. Those bands were proven to be most relevant to defoliation status. As only 5 bands were used, the proposed method can be considered a new approach for hyperspectral dimensional reduction. Moreover, the proposed method integrates the spatial information from used VI bands by extracting histograms from neighborhood of each incident pixel. Thus spectral-spatial features can be extracted from hyperspectral data. The efficiency of constructed feature was examined in mapping experiments. The experimental results

suggests noticeable advantage of applying proposed feature in an unsupervised k-means classifier for mapping SBW defoliation than conventional spectral feature extraction method MNF or method without feature extraction.

Acknowledgement

This research was funded by the Canada Research Chair Program. The authors would like to thank NASA for collecting the Hyperion images of the testing areas.

References

Beck, R. (2003). EO-1 User Guide v. 2.3, 74. Retrieved from http://eo1.usgs.gov/documents/EO1userguidev2pt320030715UC.pdf

Boardman, J. W. (1993). Automating spectral unmixing of AVIRIS data using convex geometry concepts. *4th JPL Airborne Geoscience Workshop (Washington, D.C.). JPL, Pasadena, Calif.*, 11–14.

Datt, B., McVicar, T. R., Van Niel, T. G., Jupp, D. L. B., & Pearlman, J. S. (2003). Preprocessing EO-1 Hyperion hyperspectral data to support the application of agricultural indexes. *IEEE Transactions on Geoscience and Remote Sensing*, *41*(6), 1246–1259. doi:10.1109/TGRS.2003.813206

De Beurs, K. M., & Townsend, P. A. (2008). Estimating the effect of gypsy moth defoliation using MODIS. *Remote Sensing of Environment*, *112*, 3983–3990. doi:10.1016/j.rse.2008.07.008

Gong, P., Pu, R., Biging, G. S., & Larrieu, M. R. (2003). Estimation of forest leaf area index using vegetation indices derived from Hyperion hyperspectral data. *Geoscience and Remote Sensing, IEEE Transactions on*, *41*(6), 1355–1362.

Goodenough, D. G., Dyk, A., Niemann, K. O., Pearlman, J. S., Chen, H., Han, T., … West, C. (2003). Processing Hyperion and ALI for forest classification. *IEEE Transactions on Geoscience and Remote Sensing*, *41*(6), 1321–1331. doi:10.1109/TGRS.2003.813214

Gray, D. R., Régnière, J., & Boulet, B. (2000). Analysis and use of historical patterns of spruce budworm defoliation to forecast outbreak patterns in Quebec. Forest ecology and management, 127(1), 217-231.

Han, T., Goodenough, D. G., Dyk, a., & Love, J. (2002). Detection and correction of abnormal pixels in Hyperion images. *IEEE International Geoscience and Remote Sensing Symposium*, *3*(C), 1327–1330. doi:10.1109/IGARSS.2002.1026105

Harsanyi, J. C., & Chang, C. I. (1994). Hyperspectral image classification and dimensionality reduction: An orthogonal subspace projection approach. *IEEE Transactions on Geoscience and Remote Sensing*, *32*(4), 779–785. doi:10.1109/36.298007

Huang, Z. (2015). Chapter 4: Estimation and Mapping of Spruce Budworm Defoliation Using Vegetation Indices Derived From Hyperion Hyperspectral Data.

ITT Visual Information Systems (2006). "ENVI FLAASH Module User's Guide (2006 Edition)." [Online] September 21, 2012: ftp://popo.jpl.nasa.gov/pub/ENVI_Installers/ENVI_Documentation/docs/FLAASH_Module.pdf.

Jupp, D.L.B., Datt, B., McVicar, T.R., Van Niel, T.G., Pearlman, J.S., Lovell, J.L. and King, E. A. (2003). Improving the Analysis of Hyperion Red-Edge Index from an Agricultural area. *Image Processing and Pattern Recognition in Remote Sensing*, *4898*(October 2002), 1–15. doi:10.1117/12.472696

MacQueen, J. B. (1967). Kmeans Some Methods for classification and Analysis of Multivariate Observations. *5th Berkeley Symposium on Mathematical Statistics and Probability 1967*, *1*(233), 281–297. doi:citeulike-article-id:6083430

Ministère des Forêt, de la Faune et des Parcs (MFFP). (2014). Aires infestées par la tordeuse des bourgeons de l'épinette au Québec en 2014. Version 1.0 [Online] September 2014: http://www.mffp.gouv.qc.ca/publications/forets/fimaq/insectes/tordeuse/TBE_2014_P.pdf

Science, N. (2001). Feature Extraction of Hyperspectral Images Using Matching Pursuit, (200).

Su, L., Liu, X., Wang, X., & Jiang, N. (2008). Dimensional Reduction in Hyperspectral Images By Danger Theory Based Artificial Immune System. *The International Archives of the Photogrammetry, Remote Sensing and Spatial Information Sciences.*, *XXXVII.*(Part B7.).

Taylor, S. L., & MacLean, D. A. (2008). Validation of spruce budworm outbreak history developed from aerial sketch mapping of defoliation in New Brunswick. Northern Journal of Applied Forestry, 25(3), 139-145.

Tarabalka, Y., Benediktsson, J., & Chanussot, J. (2009). Spectral–Spatial Classification of Hyperspectral Imagery Based on Partitional Clustering Techniques. *IEEE Trans. on Geoscience and Remote Sensing*, *47*(8), 2973–2987. doi:10.1109/TGRS.2009.2016214

Thomas, S. J., Deschamps, A., Landry, R., van der Sanden, J. J., & Hall, R. J. (2007). Mapping insect defoliation using multi-temporal Landsat data. Proceedings: Our common borders–safety, security, and the environment through remote sensing, October 28–November 1, Ottawa, Ontario, Canada.

6 CHAPTER 6

CONCLUSIONS AND RECOMMENDATIONS

This chapter summarized this MScE research that aimed to achieve the objective of monitoring the spruce budworm defoliation by means of estimating and mapping using remotely sensed satellite images. Then, the contributions of this research were highlighted. Finally, several recommendations were outlined for future studies.

6.1 Summary of the Research

In Chapter 1, the thesis introduced the problem of spruce budworm defoliation in Quebec, Canada. The significant amount of forest areas affected and the aggravating situation highlighted the necessity of the timely monitoring of spruce budworm defoliation through remote sensing. The literature review of remote sensing of spruce budworm defoliation identified an important and urgent research problem: how to estimate and map the spruce budworm defoliation by taking advantage of the rich spectral information provided by spaceborne hyperspectral sensor? Therefore, this thesis aimed to find a way to monitor effectively the spruce budworm defoliation in Quebec, Canada from EO-1 Hyperion hyperspectral data. The investigation attempted to explore the possibility of extending the vegetation indices study on defoliation to narrowband level which constructed with nearly continuous hyperspectral bands.

Taking EO-1 Advanced Land Imager (ALI) data as an example, Chapter 2 demonstrated that moderate spatial resolution multispectral data could not provide acceptable estimation or mapping results for spruce budworm defoliation.

In Chapter 3, the potential of using existing form of VIs constructed with Hyperion data for monitoring spruce budworm defoliation were investigated. The study site was centered to the east of the Sainte-Florence village, west of Lac Humqui, at the southern part of the Bas-Saint-Laurent region in Quebec, Canada. Two multi-temporal images were applied for VIs based change detection in order to find the VIs with significant response during the defoliation. Based on the yielded change rates, narrowband VIs were chosen from different aspects of forest health regarding greenness, canopy water content and light use efficiency. Forest health analysis was conducted based on those VIs to provide a forest stress map.

Although the VIs based forest health analysis can delineate the forest stress with considerable visually correlate with the spruce budworm defoliation, more specific and accurate estimation was still needed. Hence, Chapter 4 designed a thorough investigation on the potential of existing and new narrowband vegetation indices (VIs) constructed with 162 available Hyperion hyperspectral bands on estimating and mapping SBW defoliation. The selection of VIs was based on a correlation analysis between the VIs and defoliation magnitude. Nine existing and three developed non-linear two-band VIs were investigated. Compared with conventional NDVI, the developed CNDVI constructed with suitable Hyperion bands achieved 15% of accuracy improvement in general in estimation and mapping SBW defoliation.

The accurate classification of defoliation magnitude or intensities was considered a long challenging problem. Chapter 5 attempted to find a solution to it. The exploration of spectral information within hyperspectral data enhanced the ability of VIs for estimating SBW defoliation. The constructed VIs bands can be considered as a process of exploiting spectral information. Meanwhile, to generate a robust feature with considerable ability to differentiate different level of defoliation, the thesis also exploited the spatial information within the hyperspectral scenes. Based on the assumption that the defoliation intensities should have a homogeneous distribution within the scene as neighboring pixels should have effect on the center pixel, a local histogram was applied to derive the feature. A high accurate classification result was achieved by applying the constructed spectral-spatial feature to an unsupervised classifier.

Chapter 4 and 5 used the same study site located close to the Causapscal city, across the Bas-Saint-Laurent region in Quebec, Canada. All of Chapters 3-5 applied EO-1 Hyperion hyperspectral data.

6.2 Contributions of the Research

The major contributions of this thesis was that the exploration of using hyperspectral data for estimating and mapping spruce budworm defoliation. The estimation was mainly achieved by taking advantage of the fine spectral resolution provided by hyperspectral sensor and thorough analysis on the spectral domain by means of vegetation indices analysis. The mapping and classification of spruce budworm

defoliation was mainly achieved by integrating exploited spectral and spatial information from the hyperspectral scene.

The studies on defoliation caused by spruce budworm or other insects through remote sensing highlight the role of vegetation indices constructed using reflectance from relevant spectral regions. This thesis extended the studies in this area to hyperspectral level, i.e., more specific narrowbands were used to construct VIs instead of using the broadband VIs constructed with multispectral images. The study starts with approaches similar to that used in multispectral VIs studies for defoliations and visually satisfactory results were achieved. Furthermore, the study breaks the fixed form of conventional VIs that specified spectral bands were used to calculate each VI. 162 available Hyperion bands were used to calculate VIs through 12 forms of VIs, this amount to 1944 different combinations. The aim was then to find the suitable combination of VI as well as the bands that were used for estimating defoliation magnitude. To the knowledge of the author, this thesis was the first study attempting to reveal the most relevant narrowband VIs with SBW defoliation using satellite hyperspectral imagery. Furthermore, the non-linear Cosine based VIs developed in this thesis was discovered to be highly correlated with the spruce budworm defoliation in the study site.

The classification of SBW defoliation intensities was solved in the thesis. Even though hyperspectral data provide more spectral information than data from any other sensors, the high dimensionality and redundancy were making the process of hyperspectral images more difficult and less efficient unless suitable feature extraction method was applied. This thesis proved the possibility of applying local histogram on

derived VIs bands as features for hyperspectral data. The proposed classification method achieved high accuracy for classifying the defoliation intensities in the study site.

To the authors' knowledge, there was little evidence that aerial and/or satellite hyperspectral data have been used to monitor spruce budworm defoliation in previous studies. This thesis employed spaceborne EO-1 Hyperion hyperspectral imagery. The Hyperion imagery was free of charge. This makes it possible to cover the widely distributed spruce and fir forests in Canada. In contrast, high spatial resolution satellite imagery and aerial hyperspectral data with high spatial resolution were too expensive for this developing country if without financial aids.

6.3 Recommendations for Furthermore Research

Remote sensing has been increasingly being used in forest health monitoring of insect defoliation. However the research in this field was still at an early stage. Remote sensing of defoliation was a complex and multifactorial task, dependent on several factors such as physiographic conditions or host and pest phenologies (Rullan-Silva et al., 2013). Such conditions make it harder to relate the reflectance values captured from sensors to the real phenomenon. Furthermore, it can be extremely hard to relate data captured by satellite sensors to defoliations happened close to ground, considering the distances and phenomenon occurred in between which can affect dramatically the results. This calls for evolution of the satellite sensors but more importantly high accuracy of correction of the satellite imagery.

Forest defoliation does not mean a simple change in foliage condition, so each case should be treated as unique, testing different sensors and combining different techniques that may produce the best results. For example, mounted on the same satellite EO-1, the multispectral sensor ALI provides multispectral images and panchromatic images simultaneously as Hyperion images were acquired. The panchromatic images have a higher resolution of 10m which help identify better the changes occurred in spatial scenes. The image fusion between hyperspectral images or multispectral images and panchromatic images can produce images with higher spatial resolution and meanwhile remains a good spectral resolution. The airborne and field captured imagery or spectral data can be potentially integrated with satellite hyperspectral data by means of correlation. The ground based spectroradiometric measurements can be also used to improve the retrieved reflectance for each pixel on the satellite hyperspectral image (Gong et al., 2003).

It has been revealed the climate warming trends may provide favorable environmental conditions for endemic spruce budworm outbreaks. It then becomes relevant and meaningful to synthesize the information from sources other than direct monitoring of the forests, e.g., the climate monitoring satellite nowadays can provide real time weather data.

Finally, the methods developed in this study focused at the study sites in Quebec, Canada. It was still meaningful to check if it can be successfully applied for other regions or other insects' outbreaks. Therefore, if groudtruth data obtained from field or airborne surveys were available in other regions, further testing if this sensor under the different

conditions noted would be very useful in assessing the applicability of this approach to different regions.

References

Gong, P., Pu, R., Biging, G. S., & Larrieu, M. R. (2003). Estimation of forest leaf area index using vegetation indices derived from Hyperion hyperspectral data. *Geoscience and Remote Sensing, IEEE Transactions on*, *41*(6), 1355–1362.

Rullan-Silva, C. D., Olthoff, a. E., Delgado De la Mata, J. A., & Pajares-Alonso, J. A. (2013). Remote monitoring of forest insect defoliation. A review. *Instituto National de Investigacion Y Tecnologia Agraria Y Alimentaria (INIA)*, *22*(3), 377–391. doi:10.5424/fs/2013223-04417

1

CURRICULUM VITAE

Candidate's full name: Zhongwei Huang

Universities attended:

Beihang University, Beijing, China, 2009-2013, B.Sc. in Mathematics and Systems

Publications:

*Paper 1 (peer reviewed):

Huang, Z.W., Y. Zhang (2015) "Remote Sensing of Spruce Budworm Defoliation Using Eo-1 Hyperion Hyperspectral Data: An Example in Quebec, Canada." *9th Symposium of the International Society for Digital Earth (ISDE)*, 5-9 October, 2015, Halifax, Nova Scotia, Canada.

Paper 2 (peer reviewed):

Huang, Z.W., Shi, Z.W., Y. Zhang (2014) "An Inner-Product-Based Discriminative IRLS Algorithm for Sparse Hyperspectral Detection." *Selected Topics in Applied Earth Observations and Remote Sensing, IEEE Journal of*, vol.7, no.6, pp.2383, 2392, June 2014

Paper 3 (peer reviewed):

Huang, Z.W., Shi, Z.W., Y. Shuo (2013) "Nonlocal Similarity Regularized Sparsity Model for Hyperspectral Target Detection." *Geoscience and Remote Sensing Letters, IEEE*, vol.10, no.6, pp.1532, 1536, Nov. 2013

Paper 4 (peer reviewed):

*Paper 1 was included in this thesis.

Huang, Z.W., Shi, Z.W., Q. Zhen (2013) “Convex relaxation based sparse algorithm for hyperspectral target detection." *Optik - International Journal for Light and Electron Optics,* Volume 124, Issue 24, December 2013, Pages 6594-6598

*Paper 1 was included in this thesis.